



QUILL Quarterly Report

November 18 - January 2019

Name:	Marian Borucki		
Supervisor(s):	Dr Peter Nockemann, Dr Stephen Glover & Dr Małgorzata Swadźba-Kwaśny		
Position:	PGR Student		
Start date:	01.2018	Anticipated end date:	2021
Funding body:	Bryden Centre, Horiba Mira		

Lithium ion batteries degradation study using spectroscopy techniques

Background

Lithium ion batteries (LIB) are a secondary (rechargeable) batteries that are currently the main energy storage device. LIB are applied in various applications as in portable devices, grid energy storage, grid current regulation as well as in hybrid- and electric vehicles. Energy harvested by the renewable energies is often environmental dependent, what results in discontinuous energy supply. In order to store energy that have been over generated during less energy consuming times of a day, energy storage stations based on LIB are used. The other, yet not less important, application is one where LIB are replacing the fossil fuel by storing the energy for transport sector, namely in hybrid (HEV) and electric vehicles (EV). The trend of replacing the fossil fuels both in energy sector by supplementing them with renewable energy power plants as well as by supporting the market of HEV, EV and fuel-cell vehicles (FCEV) is growing. New policies of EV30@30 and New Policy Scenario are the programmes that are aimed in expanding the market of HEV, EV and FCEV, thus the supply for lithium ion batteries will grow. Yet, for the market to growth the research, ones that solve current issues, are needed. Automotive council UK in their roadmap report for the lithium ion batteries have gathered up the issues that are needed to be addressed if the automotive of EV, HEV and FCEV is to grow. Such an issues are based on the need of improving the safety of battery usage, lowering the costs of the batteries, researching a new materials for the batteries that will allow to store more energy and provide more power, thus be fast chargeable, issues concerning the battery pack and modules combination, one that will allow to minimize the losses related to cell joining, as well as their thermal management, increasing the lifespan of the batteries as well as increase their recyclability, eventually the research on the next gen batteries is needed.

In order to meet all the requirements a thrill study of the current batteries as well as the development of a new chemistries is needed. Lifespan as well as the safety of the battery is nowadays ones of the most important factor when it comes to the battery application in the transportation market. Battery life is limited by the degradation mechanism, ones that occur inside the cell. Currently there are known number of such mechanism occurring, even though the proper investigating technique allowing *in operando* study have not been developed yet. Moreover, the degradation is highly chemistry dependent so whenever the new chemistry is tested for the battery the new degradation mechanism could occur. On the other hand the safety of the battery is limited by the usage of the organic based electrolyte, which is highly flammable and might lead to battery explosion. Proper electrolyte, non-toxic, environmental friendly, non-flammable as well as of high performance should be developed. With developing the new electrolyte, often the development of



the electrodes is needed as the electrolyte stability as well as the energy density of the battery highly depends on them.

Objective of this work

The aim of the PhD programme is focused on investigating the lithium ion battery (LIB) degradation processes occurring inside the cell during its operation. In order to achieve the goal a development of an experimental method basing on the spectroscopy analysis techniques will be needed. A proper method would allow to observe and measure the changes that occur *in operando* inside the lithium ion battery. During the PhD programme an analytical data of LIB degradation will be acquired, using various analytical techniques including electrode surface examination, electrolyte composition. Acquired spectroscopy data will be linked with the rest of the data gathered in order to develop the sensing method. Eventually, batteries of a different cell chemistries will be investigated.

Progress to date

Laboratory preparation with new equipment and its installation was needed in order to initiate the study. Equipment as glove box, CVD furnace, pressured electrode coater, coin cell crimping machine, electrode punching machine as well as battery testers were bought and prepared for the functioning. Graphite and NMC based electrodes as well as commercial organic based electrolyte solution were obtained. Meanwhile the literature research as well as workshops participation was the main responsibility of mine. Initial studies of the coin lithium ion cells have been undertaken. CR2032 coin cell batteries based on the graphite and NMC electrodes as well as organic electrolyte has been prepared and the initial electrochemical studies had been undertaken.

Whole process of the coin cell preparation can be summarized in a few points:

1. Preparation of electrodes
2. Preparation of electrolyte
3. Coin cell assembly

During my study I have focused on coin cell assembly as the electrodes and electrolyte have been bought from the external supplier, in order to manufacture and test most commercial setup as possible. The assembling process is needed to be performed inside the inert atmosphere (Ar based) and with low concentration of water and oxygen (less than 0.1 ppm) due to the use of an organic electrolyte. . The process of CR2032 coin cell assembly is not unified so a different ways to perform it have been implemented, varying on number of separators, number of spacers, volume of electrolyte, addition of electrolyte layer as well as the pressure of crimping. The most efficient coin cell assembly process have been picked and it is shown on Figure 1.

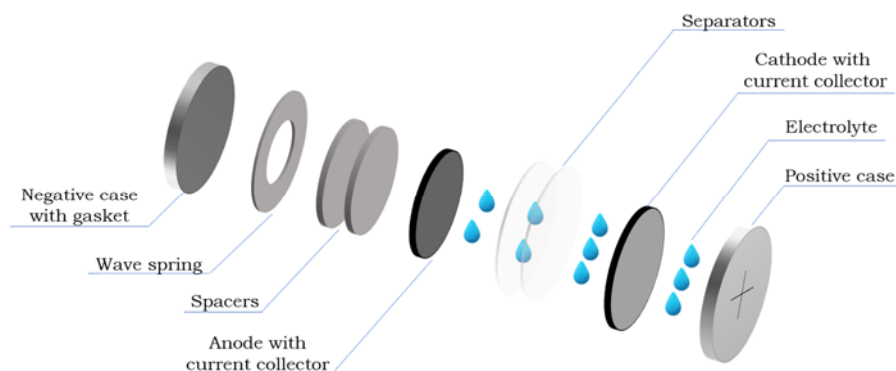


Figure 1. CR2032 Coin cell assembly process.

After the CR2032 cell coin assembly it testing was needed. There have been four procedures implemented in order to fully test one battery, such procedures include:

1. Three charge-discharge at theoretical 0.1 C current rate (establishing capacity of the battery system)
2. Series of constant current discharge of different C rates (capacity stability check).
3. Peak power tests (needed as DTS and FUDS cycles depends on peak power)
4. DST / FUDS driving cycle implementation

Firstly, the calculations of theoretical capacity of active materials as well as electrodes of fixed diameter has been performed as well as the current of various C-rates has been established.

Beside the procedures undertaken on the battery tester system, an electrochemical studies as LSV, CV, EIS using potentiostat station has been performed in order to establish the initial performance of an electrolyte in non-aged battery cells.

Conclusions and future work

Ageing tests of the manufactured batteries will be undertaken for the duration of up to 11 months in order of determining the degradation mechanism occurring. During the ageing study part of the cycled batteries will be disassembled depending on the charge-discharge cycles number. *Ex situ* microscopic, crystallographic as well as spectroscopic studies will be performed in favour of obtaining the information about the severity of each degradation mechanisms. Both degradation mechanisms of losses in lithium inventory (LLI) as well as losses in active material (LAM) will be investigated. Meanwhile the methodology of *in situ* spectroscopic study of the cell will be developed. Data gathered through *ex situ* studies will be used to determine the level of degradation for the lithium ion cells monitored through *in situ in operando* technique.

Moreover the electrochemical systems of different electrolytes and electrodes setups will be assembled and further studied according to the previous mentioned methodology. The planned studied setups includes carbon, silica and carbon-silica based anodes as well as the pure and semi-solid ionic liquid electrolytes. The studies of their stability as well as overall performance will be undertaken.



QUILL Quarterly Report

July 2018 – March 2019

Name:	Robert Boyd		
Supervisor(s):	Peter Nockemann, Martin Atkins		
Position:	PhD student		
Start date:	October 2016	Anticipated end date:	October 2019
Funding body:	DEL		

Organic Redox Flow Electrolytes

Background

Cheap, safe and efficient energy storage is essential in developing practical and sustainable energy strategies necessary for maintaining a balanced, efficient and reliable electric grid system based on both conventional electricity generation industries and the integration of intermittent renewable energy sources.

Batteries for large-scale grid storage must satisfy a different set of variables compared to many conventional rechargeable batteries. Such batteries must be; durable, maintain efficiency over a large number of charge/discharge cycles, have high round-trip efficiency, able to respond instantly to changes in load or input, and have reasonable capital costs². Redox flow batteries are able to meet much of this criterion hence there has been significant interest in the optimisation of redox flow batteries for large-scale energy storage over the last few decades.

The all vanadium RFB was and remains the 'flagship' for redox flow batteries. It has a higher energy efficiency, longer operational lifetime and lower cost compared with other redox batteries (zinc bromide, sodium sulfur and lead acid)³. It remains the only RFB to have been sold in significant numbers due in part to being the only RFB to make use of the same metal species in both half-cells, avoiding cross-contamination issues.

Flow batteries incorporating organic molecules as the charge carriers are experiencing significant interest for large scale energy storage. Engineering the structure of organic molecules can deliver low cost redox active molecules with favourable potentials, increased solubility and greater stability. Both quinones and N-heterocycles are currently experiencing extensive investigation for application in flow batteries.

Objective of this work

Design and synthesise new flow electrolytes with superior properties compared to the all vanadium electrolyte.

Progress to date

Ionic Liquid Electrolyte

A series of ionic liquids including 1-butyl-3-methylimidazolium (C_4mim), 1-butyl-1-methylpyrrolidinium (BMP) and trihexyltetradecylphosphonium (P_{66614}) featuring the bis(trifluoromethylsulfonyl)imide anion were analysed electrochemically with a range of inorganic metal salts.

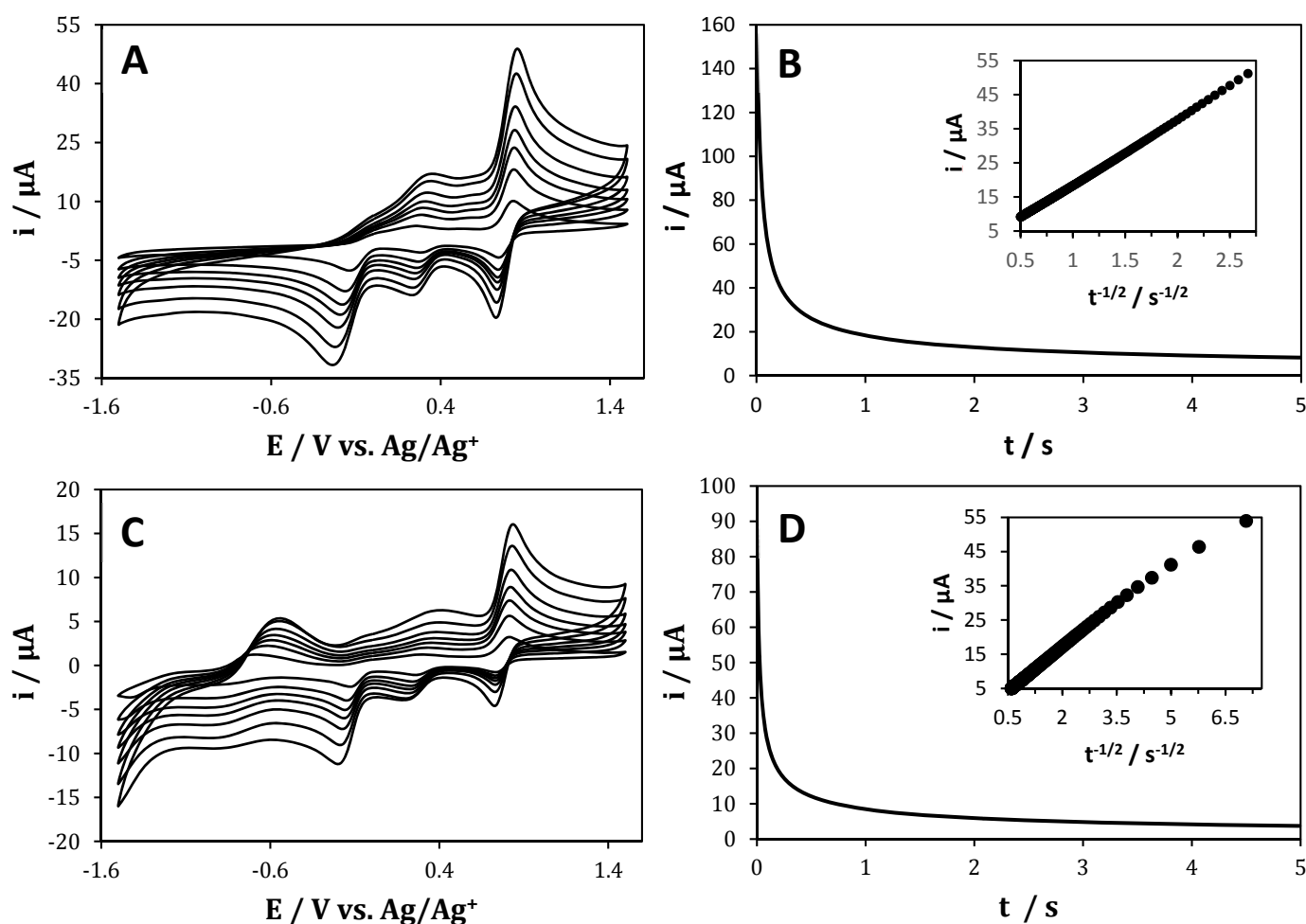


Figure 1: (A) CVs recorded at a 5 mm diameter GC disk electrode in $0.01 M Mn(acac)_3$ in $[BMP][NTf_2]$ at (from top to bottom) $0.2 V s^{-1}$, $0.15 V s^{-1}$, $0.1 V s^{-1}$, $0.07 V s^{-1}$, $0.05 V s^{-1}$, $0.03 V s^{-1}$ and $0.01 V s^{-1}$. (B) Chronoamperogram recorded using recorded at a 5 mm diameter GC disk electrode in $0.01 M Mn(acac)_3$ in $[BMP][NTf_2]$. The potential was stepped from $0.5 V$ to $1.1 V$ and held for $1 s$. The inset shows the plot of i vs. $t^{1/2}$. (C) CVs recorded at a 3 mm diameter Pt electrode in $0.01 M Mn(acac)_3$ in $[BMP][NTf_2]$ at (from top to bottom) $0.2 V s^{-1}$, $0.15 V s^{-1}$, $0.1 V s^{-1}$, $0.07 V s^{-1}$, $0.05 V s^{-1}$, $0.03 V s^{-1}$ and $0.01 V s^{-1}$. (D) Chronoamperogram recorded using recorded at a 3 mm diameter Pt electrode in $0.01 M Mn(acac)_3$ in $[BMP][NTf_2]$. The potential was stepped from $0.6 V$ to $1 V$ and held for $1 s$.

Manganese displayed reversible redox active behaviour however the narrow distance between the oxidation and reduction potentials prevents $\text{Mn}(\text{acac})_3$ being used in a single metal flow battery.

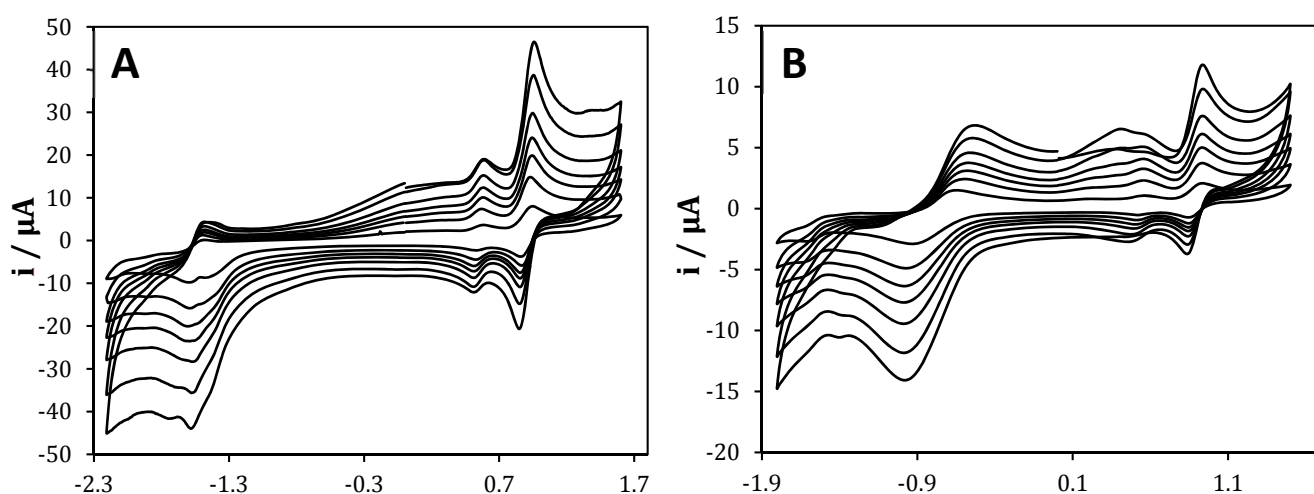


Figure 2: (A) CVs recorded at a 5 mm diameter GC disk electrode in 0.01 M $\text{VO}(\text{acac})_2$ in $[\text{BMP}][\text{NTf}_2]$ at (from top to bottom) 0.2 V s^{-1} , 0.15 V s^{-1} , 0.1 V s^{-1} , 0.07 V s^{-1} , 0.05 V s^{-1} , 0.03 V s^{-1} and 0.01 V s^{-1} . (B) CVs recorded at a 3 mm diameter Pt disk electrode in 0.01 M $\text{VO}(\text{acac})_2$ in $[\text{BMP}][\text{NTf}_2]$ at (from top to bottom) 0.2 V s^{-1} , 0.15 V s^{-1} , 0.1 V s^{-1} , 0.07 V s^{-1} , 0.05 V s^{-1} , 0.03 V s^{-1} and 0.01 V s^{-1} .

TEMPO Anion

Compounds featuring the TEMPO anion were synthesised forming red room temperature, redox active, active ionic liquids.

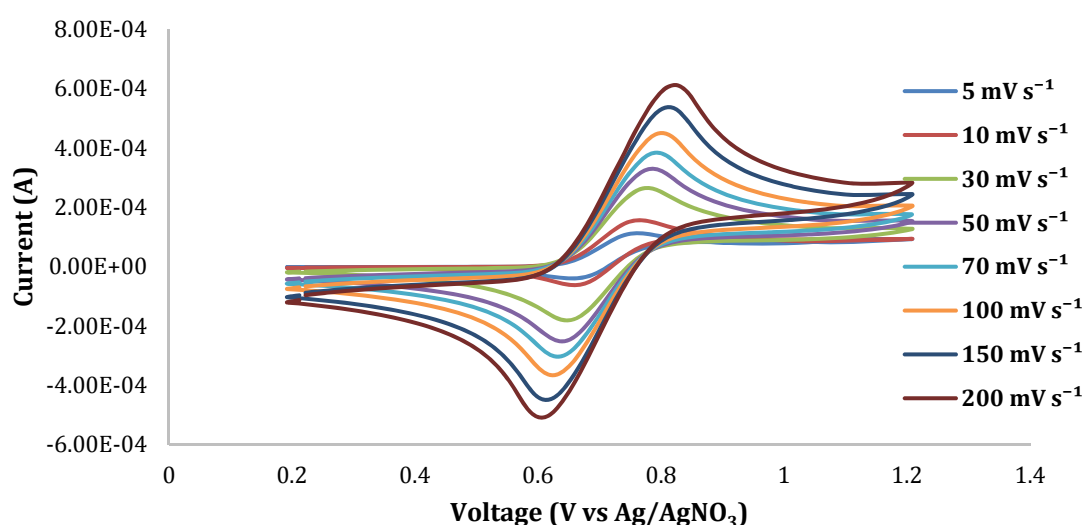


Figure 3: CV of $[\text{C}_4\text{mim}][\text{TEMPO}]$ (0.005 M) in acetonitrile with $[\text{NBu}_4][\text{BF}_4]$ (0.1 M).



A single electron was reversibly stored over the N-O unit delivering a relatively light weight metal-free species for energy storage.

Converting TEMPO to the cation again increased the redox potential by 0.2 V widening the theoretical cell potential.

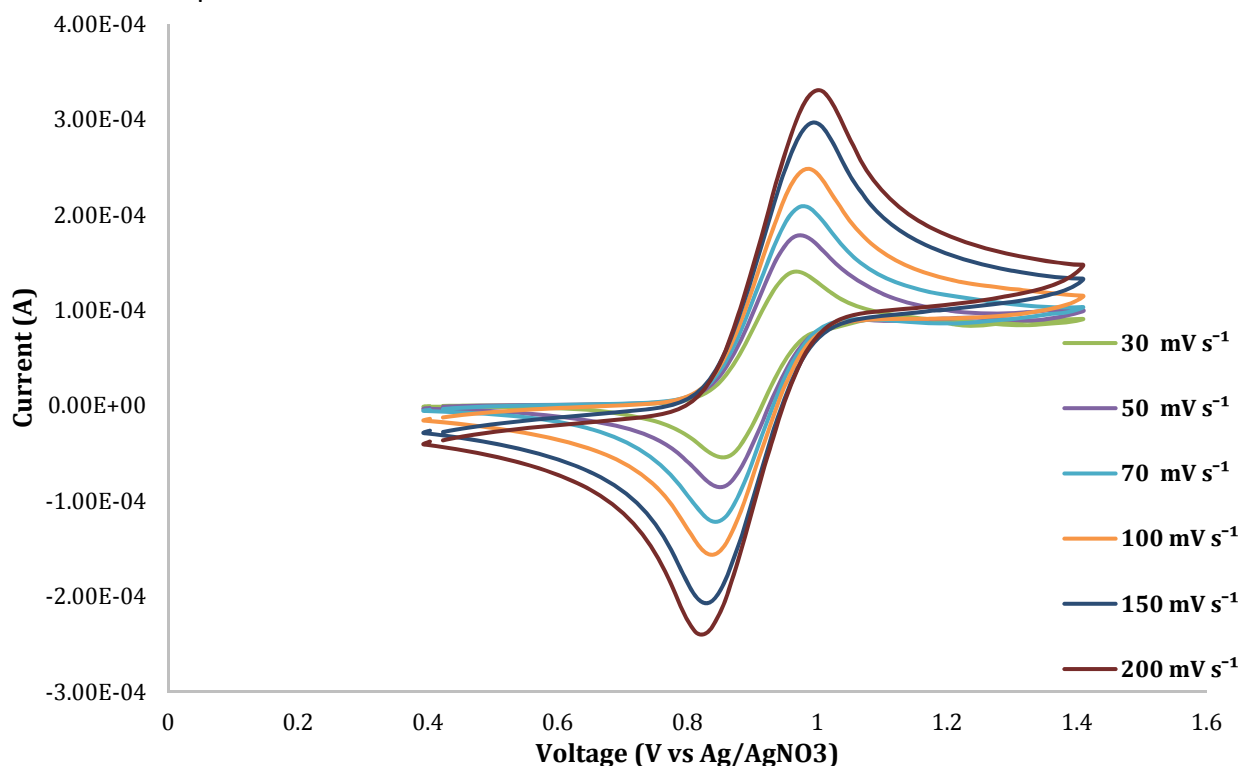


Figure 4: CV of $[\text{NR}_3\text{TEMPO}][\text{NTf}_2]$ (0.005 M) in acetonitrile with $[\text{NBu}_4][\text{BF}_4]$ (0.1 M).

Greater cell potentials can lead to more efficient, energy dense batteries improving their applicability for both large and small scale energy storage.

Conclusions

All compounds synthesised displayed reversible redox behaviour and good solubility in organic electrolytes. Transferring to organic electrolytes removes the 1.4 V aqueous voltage limitation enabling greater cell potentials to be realised in order to increase the efficiency and energy density.

Future Work

Cyclic voltammetry - electrochemically analyse all anthraquinone ([Ch], [C₂mim], [C₄mim], and [P₆₆₆₁₄]), hydroquinone ([Ch], [C₂mim], [C₄mim], and [P₆₆₆₁₄]) and TEMPO salts synthesised under proper experimental conditions (gas purged, 3 cycles, no bubbling during measurement).

H-cell – determine the charge and discharge capabilities of synthesised redox couples.



QUILL Quarterly Report

November 2018 – January 2019

Name:	Lucy Brown		
Supervisor(s):	Gosia Swadzba-Kwasny		
Position:	PhD student		
Start date:	October 2015	Anticipated end date:	April 2019
Funding body:	EPSRC		

Developing Borenium Ionic Liquids

Background

Frustrated Lewis pairs (FLPs) are combinations of Lewis acids and Lewis bases which are unable to form adducts.¹ This is typically achieved by steric hindrance. Whilst not able to quench each other, the reactivity of the system can be utilised for the splitting of small molecules, such as H₂ and CO₂.² Whilst the mechanism of this is understood to be analogous to that of transition metals, FLPs offer an alternative to traditional hydrogen activation. Since the discovery in 2006 of this mechanism the wealth of reactions utilising it has grown enormously, with 1499 papers published on the topic in just 12 years. More generally work by Wagner and colleagues has demonstrated the use of an intramolecular FLP capable of trapping a huge variety of small molecules, from N₂O to CCl₄ (with cleavage of the C-Cl bond).³ Highlights over the past year demonstrate the breadth of the reactions this approach is applied to, for example the use of gold nanoparticles which form an active FLP site on their surface in the hydrogenation of alkynes to cis-alkenes,⁴ to the emergence of increasingly water tolerant systems, with Fasano *et al.* demonstrating water tolerant reductive aminations via FLPs.⁵

Borenium ionic liquids have been developed from the need for Lewis acidic ionic liquids with Lewis acidity located on the cation. Typical chlorometallate ionic liquids, which form the bulk of research on Lewis acidic ionic liquids, have their Lewis acidity on the anion, which is an electron rich species. In a sense this is surprising, but borenium ionic liquids, where the acidity is centered on a BX₂L species, have demonstrated immense acidity, with the highest Gutmann acceptor number reported in the literature.⁶ Their acidity has been exploited in classic Lewis acid catalyzed reactions successfully used in both the Diels-Alder reaction and for dypnone synthesis via Aldol condensation.

7

Objective of this work

By developing novel boron complexes and borenium ionic liquids the ambition of this work is to develop new species which may be used in frustrated Lewis pair catalysis. By including a bidentate ligand (catechol) onto the boron centre disassociation to BCl₃ can be discouraged and using non-acidic anions is anticipated to reduce the number of species with which a base can react.

Progress to date

The first stage of this work focused on developing a borenium centre with a bidentate ligand. Catechol is a ligand which has been used in the formation of borenium cations in previous work and



the synthesis of B-chlorocatecholborane is readily achieved using a similar synthetic method as for the synthesis of BX_3L complexes.⁸ The catechol interacts with the boron centre through both the oxygens forming a tricoordinate boron complex. To this L-donor ligands may be added, in this work the following ligands are being explored as L-donors to these complexes – methylimidazole, triethylamine, trioctylphosphine, tri-*tert*-butyl phosphine, shown in Figure 1. The synthesis of these complexes was discussed in the previous QUILL report.

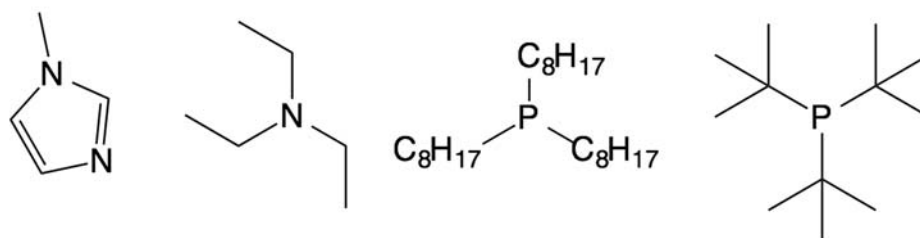


Figure 1. Ligands discussed in this work (l-r methylimidazole, triethylamine, trioctylphosphine and tri-*tert*-butyl phosphine)

These complexes exist in a range of physical states which are dependent on the ligand added, from a fine white powder (in the case of P^tBu_3) to a liquid (in the case of trioctylphosphine). As an addition to the work from the previous report, the ligand trioctylphosphine oxide has been used as this was found to also form a liquid and provides an oxygen donor for studying. Oxygen donors are not compatible with chlorometallate ionic liquids as they coordinate too well with the metal centre, promoting the formation of BCl_3 , however it is hoped that in a system without chlorometallate anions these donors might be effective.

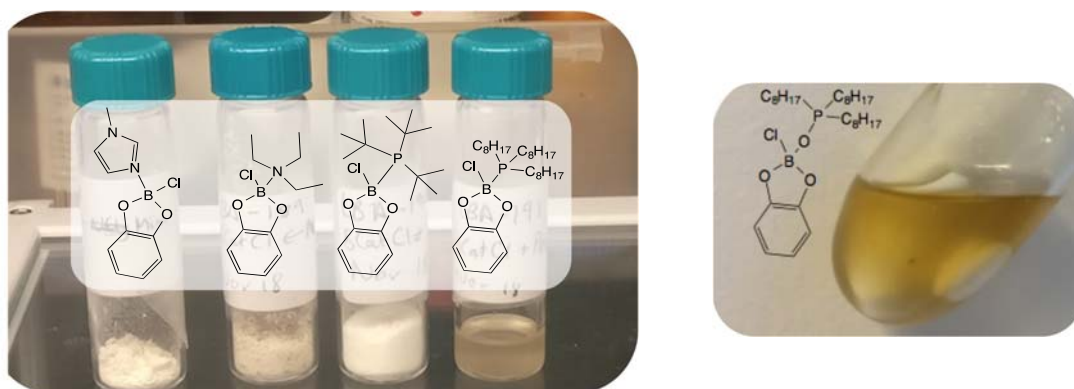


Figure 2. Physical appearance of boron complexes and their structures showing $BCatCIL$ where L = l-r methylimidazole, triethylamine, tri-*tert*-butyl phosphine, trioctylphosphine and trioctylphosphine oxide.

Combinations of these liquids with different anions has been explored in this work as a potential opportunity to avoid chlorinated Lewis acidic ionic liquids, preventing the formation of HCl by-products in catalytic applications. The anions used in this work so far have been bistriflimide and triflate, the structures of which are given below.

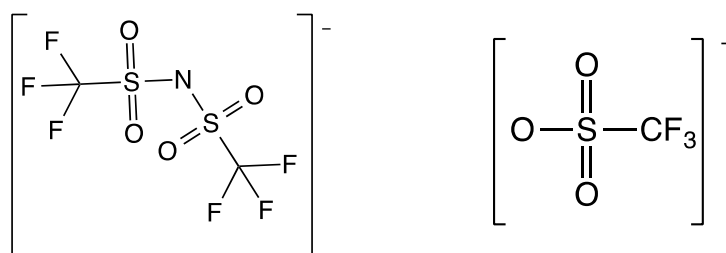










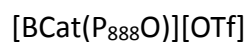
Figure 3. The structure of (l) bistriflimide and (r) triflate anions



These anions were selected because they are relatively non-coordinating, do not contain aromatic groups which could increase melting point with π - π stacking and are commercially available in complexes which can be used in halide abstraction, N-methyl bistriflimide (MeNTf₂) and trimethylsilyl triflate (TMSOTf) respectively. The formation of ionic liquids is a relatively straightforward procedure, with the boron complex dissolved in a small volume of dichloromethane and an equimolar amount of halide abstracting agent was added dropwise in the glovebox. Following stirring and heating to 50 °C, the solvent and volatile by-products (methyl chloride and trimethylsilyl chloride) were removed *in vacuo*. The appearance of the products varied with the different ligands and this is summarised in Table 1 below.

Table 1. Description of the appearance of the ionic liquid synthesised in this work.

Compound Name	Appearance	Photo
[BCat(Mim)][NTf ₂]	Did not form liquid, with intense heating formed purple liquid	
[BCat(NEt ₃)][NTf ₂]	Brown liquid	
[BCat(P ^t Bu ₃)][NTf ₂]	Light brown liquid on heating to 50 °C	
[BCat(P ₈₈₈)][NTf ₂]	Colourless liquid	
[BCat(P ₈₈₈ O)][NTf ₂]	Golden liquid	
[BCat(NEt ₃)][OTf]	Very light brown crystalline structure, liquid at 50 °C	
[BCat(P ^t Bu ₃)][OTf]	Fine white powder	
[BCat(P ₈₈₈)][OTf]	Colourless liquid	



Light brown liquid



Following the synthesis with methyl bistriflimide, it was decided to discontinue studying compositions with a methylimidazole ligand as these did not form a liquid before decomposing. Of the compositions where a liquid did form, analysing these liquids by NMR spectroscopy has provided information on their speciation and the temperature dependence. It is known from previous work on borenium ionic liquids that tetra-coordinate boron peaks will emerge at around 0-10 ppm with borenium ions emerging at higher chemical shifts in ^{11}B NMR spectroscopy.

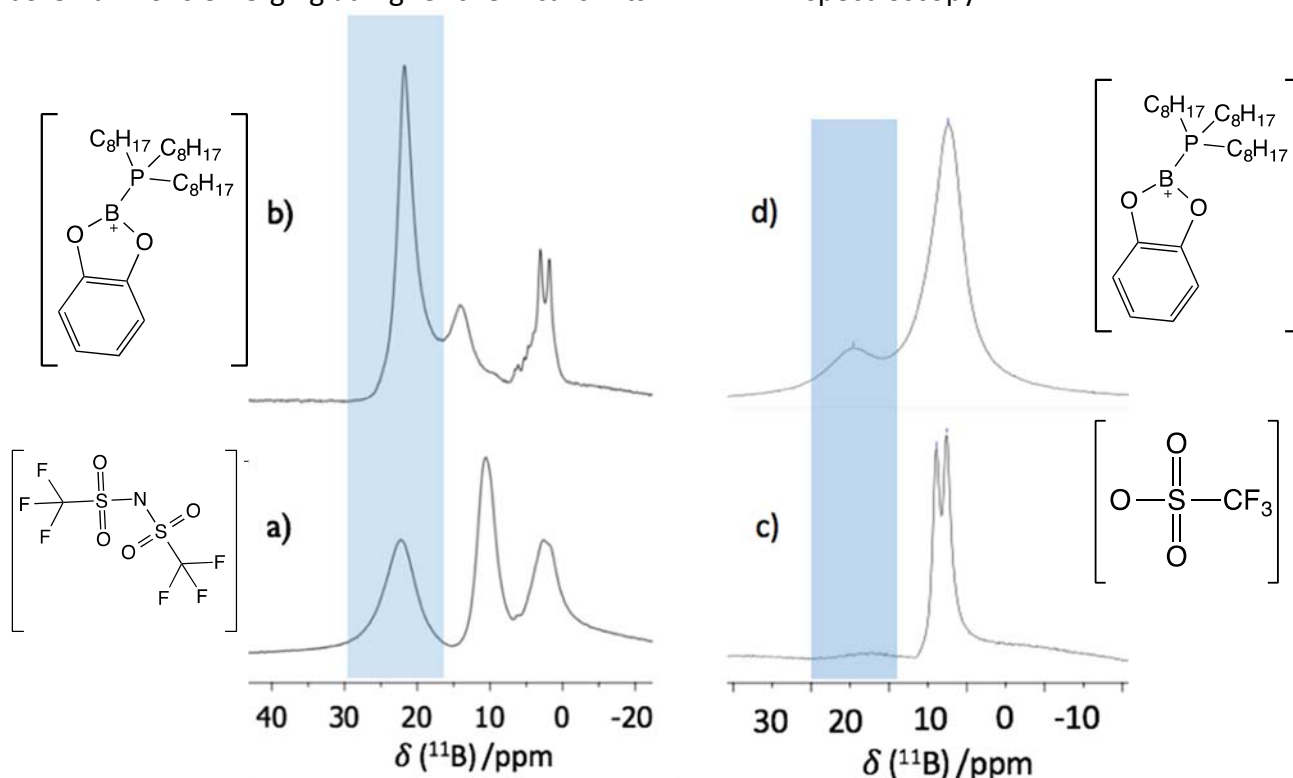


Figure 4. Effect of heating on ^{11}B NMR spectra for (l) $[\text{BCatP}_{88}][\text{NTf}_2]$ and (r) $[\text{BCatP}_{88}][\text{OTf}]$ where a and c) are at room temperature and b and d) are at 77 °C.

It can be seen from Figure 4 that on heating the proportion of boron which is at a higher, tricoordinate, chemical shift increases. This suggests that the naked borenium ion exists at higher temperatures and is a trend which is seen across all species measured in this work. It is important to note that on cooling the NMR spectra show the same peak distribution as before heating, showing that this effect is not the formation of side products. The naked cation was reached at lower temperatures with bistriflimide anions, this is not surprising as this is a bulkier anion and is not so easily coordinated as the triflate anion.



While the speciation changes with temperature, the capability of the boron to react with a base is not affected as the interaction between anion and cation is weak. This is exemplified by Gutmann Acceptor Number measurements, which show that across the temperature range the acidity does not change, indicating that it is the same interaction between the borenium ionic liquid and TEPO probe molecule occurring at all temperatures. The range of ANs recorded is given in Table 2 below.

Table 2. Gutmann Acceptor Numbers recorded for borenium ionic liquids.

Species	Acceptor Number
[BCatNEt ₃][NTf ₂]	105.1
[BCatP ^t Bu ₃][NTf ₂]	113.1
[BCatP ₈₈₈][NTf ₂]	94.6
[BCatNEt ₃][OTf]	No value
[BCatP ^t Bu ₃][OTf]	98.7
[BCatP ₈₈₈][OTf]	106.5

From Table 2 the high acidity of these borenium ionic liquids can be seen. Compared to chlorometallate borenium ionic liquids, which gave measurements of over 150 for several systems, these are less acidic, however the acidity is still very high, with 100 representing a superacidic species.⁶

Conclusions and future work

In this work expansion of the family of borenium ionic liquids has been demonstrated. The use of non-chlorometallate anions prevents an equilibrium being set up between borenium cations and the Lewis acidic BCl₃. Furthermore, the high Lewis acidity of these ionic liquids, with Gutmann acceptor numbers greater than 100, has been demonstrated but without chloride groups, meaning that the formation of HCl is avoided. This suggests that they have the potential to be used as catalysts for industrial applications. An area of interest for these ionic liquids is in frustrated Lewis pair type reactions as the boron centre is capable reacting with small molecules whilst being sterically hindered from interaction with larger bases.

This work should be further characterised by thermal measurements, such as thermal gravimetric analysis (TGA) and differential scanning calorimetry (DSC). A stated advantage of other Lewis acidic liquids, such as liquid coordination temperatures, is their stability at higher temperatures, above 250 °C, therefore it is important to characterise these systems in comparison with other similar liquids.

References

- 1 D. W. Stephan, G. C. Welch, R. San Juan and J. D. Masuda, *Science*, 2006, **314**, 1121–1124.
- 2 G. C. Welch and D. W. Stephan, *J. Am. Chem. Soc.*, 2007, **129**, 1880–1881.



- 3 K. Samigullin, I. Georg, M. Bolte, H.-W. Lerner and M. Wagner, *Chem. Eur. J.*, 2016, **22**, 3478–3484.
- 4 J. L. Fiorio, N. López and L. M. Rossi, *ACS Catal.*, 2017, **7**, 2973–2980.
- 5 V. Fasano and M. J. Ingleson, *Chem. Eur. J.*, 2017, **23**, 2217–2224.
- 6 S. Coffie, J. M. Hogg, L. Cailler, A. Ferrer-Ugalde, R. W. Murphy, J. D. Holbrey, F. Coleman and M. Swadźba-Kwaśny, *Angew. Chem.*, 2015, **127**, 15183–15186.
- 7 K. Matuszek, S. Coffie, A. Chrobok and M. Swadźba-Kwaśny, *Catalysis Science & Technology*, 2017, **7**, 1045–1049.
- 8 A. Del Grosso, P. J. Singleton, C. A. Muryn and M. J. Ingleson, *Angew. Chem. Int. Ed.*, 2011, **50**, 2102–2106.



QUILL Quarterly Report

November 2018 – January 2019

Name:	Emily Byrne		
Supervisor(s):	Dr. Małgorzata Swadźba-Kwaśny and Dr. John Holbrey		
Position:	PhD student		
Start date:	October 2017	Anticipated end date:	October 2020
Funding body:	DfE (Department for the Economy)		

Physical characterisation of functional liquids

Background

It is proposed that deep eutectic solvents 'DES' are a chemical component mixture composed of hydrogen bond donors and acceptors which have intermolecular interactions that result in a freezing point which is lower than that of the isolated individual components of the system with no interactions between each other.¹ They are asymmetric species which, due to their orbitals' inability to overlap well and thus, pack into a regular lattice arrangement, have low lattice energy and so do not require a large amount of energy in order to exist as a liquid and as a result tend to have low melting points.

The most common and well renowned DES are those prepared with the combination of organic salts such as choline chloride, which act as a hydrogen bond acceptor and carboxylic acids or alcohols with a hydrogen bond donating role.^{2–5} However, these solvents are generally miscible with water and so their application is quite limited. Therefore, work was undertaken by van Osch *et al.* which led to the publication of the first hydrophobic deep eutectic solvent using a carboxylic acid hydrogen bond donor and a long chain quaternary ammonium salt in 2015.⁶ In addition to this, DES have since been formed using alcohols and fatty acid hydrogen bond donors in combination with organic salts to form deep eutectic solvents which can be used for extraction of metals⁷ and natural products^{8,9}. In addition to this, in an attempt to reduce the viscosity associated with these charged DES species, Ribeiro *et al.* developed DES systems using D-menthol and carboxylic acid hydrogen bond donors where the individual components used are non-ionic species.¹⁰ More recently, DES made with the combination of trioctylphosphine oxide (TOPO) and phenol have been published and its use as a uranyl extractant shown.¹¹

TOPO has a number of uses such as capping agents^{12–16} in nanoparticle synthesis, metals^{17,18}, organic acids^{19–22} and phenolics^{23–26} extraction and so a number of DES will be prepared using a range of hydrogen bond donors most suited to the potential application.

Objective of this work

In this work a number of hydrogen bond donors such as levulinic acid and malonic acid have been combined with TOPO to form a eutectic. They have been combined across the whole compositional range in increments of 0.1 from $\chi_{\text{TOPO}} = 0.1$ -1.0 and mixtures at $\chi_{\text{TOPO}} = 0.33$, 0.55 and 0.67 have also

been included. The physical properties of the mixtures have been characterised and they will be applied to an industrial application.

Progress to date

Following on from previous reports where I showed a TOPO:Malonic acid eutectic in a 2:1 ratio was used to extract gallium from an acidic chloride source with a LogD_{Ga} approximately 3 times greater than that of the literature benchmark¹⁷ when conditions were replicated. This led to an interest in finding out more about the physical characteristics of this 2:1 TOPO:Malonic acid extractant. Therefore, physical properties such as thermal decomposition, a phase diagram and density measurements were carried out along with tracking of the TOPO phosphorus peak in ^{31}P NMR with an increasing malonic acid proportion in the liquid samples. Levulinic acid is also of interest as it has many uses, such as a precursor to biofuel and so these physical characterisation techniques were also repeated for TOPO:levulinic samples; with future work on this system looking at extracting levulinic acid from biomass waste streams, however, the physical characterisation on this system has not been included in this report.

To begin this section of work, TOPO:Malonic acid samples were made across the whole compositional range $\chi_{\text{TOPO}} = 0.1-1.0$ including $\chi_{\text{TOPO}} = 0.33$ and 0.67 . Thermal decomposition of the samples was first of interest and so TGA pans were prepared for each of the samples. The results of thermal decomposition of these samples are shown in Figure 1.

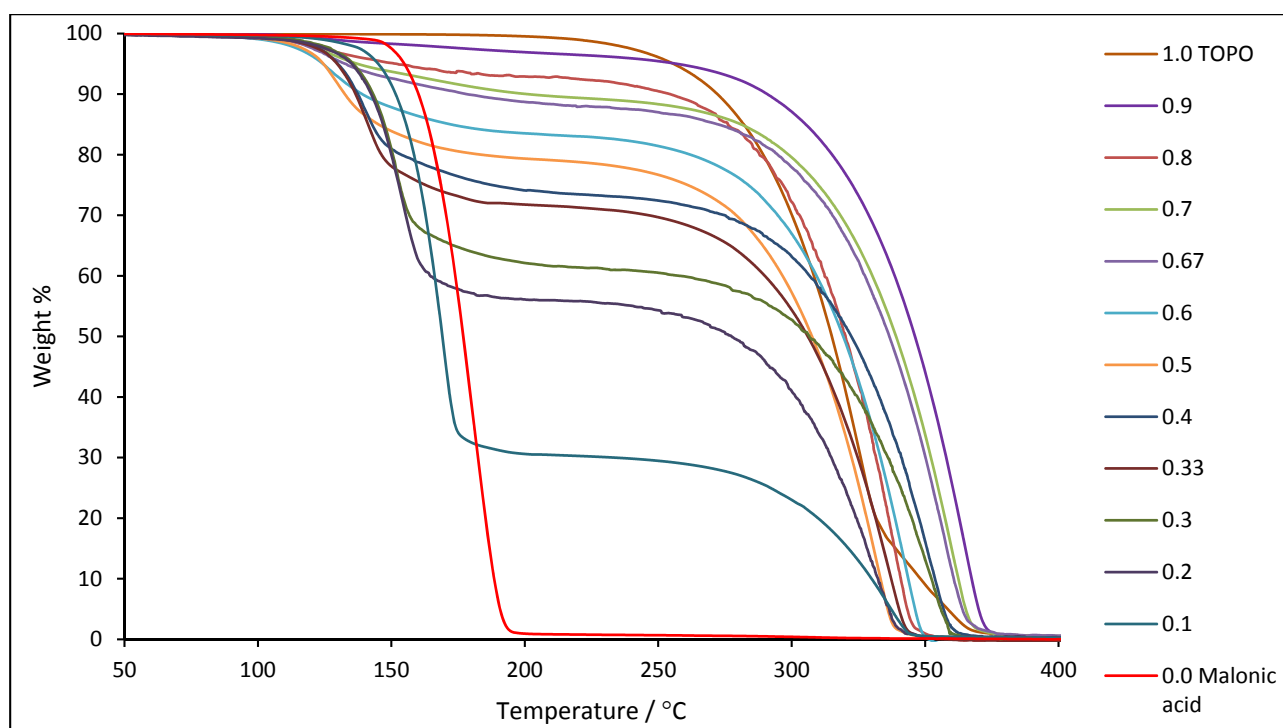


Figure 1. Thermal decomposition of TOPO:malonic acid mixtures and individual components as a function of temperature

It is observed that thermal decomposition of these TOPO:malonic acid mixtures as a function of temperature occurs in a 2 step event, losing malonic acid first. Initial decomposition begins between 102-117 °C for $\chi_{\text{TOPO}} = 0.1-0.2$ and 0.9 , i.e. the mixtures at the extremes of the range which are most

similar to their starting materials and between 89-99 °C for the mixtures mid-range between $\chi_{\text{TOPO}} = 0.3-0.8$. This malonic acid loss is typically complete by approximately 200 °C in all samples. This is then followed by the loss of TOPO at temperatures greater than approximately 250 °C. The thermal decomposition temperatures for all mixtures is complete between 340-375 °C within the range $\chi_{\text{TOPO}} = 0.1-0.9$, however, the temperature of decomposition for these mixtures is defined as the temperature corresponding to the onset of mass loss.

Each χ_{TOPO} sample was then prepared for DSC and solid liquid cell (SLC) apparatus to understand the phase behaviour of the samples at varying χ_{TOPO} values and the temperature recorded for a thermal event. The results were reported as the mid-point of the line on the DSC due to relatively broad peaks in comparison to that of crystalline structures. DSC samples were not run above 80 °C due to reaching the limit of decomposition and so not all melting points were acquired through DSC analysis, therefore further requiring SLC analysis. It was thought that there was another phase present in these samples between $\chi_{\text{TOPO}} = 0.5-0.1$ which melts above 70 °C. This is confirmed by observational recording of melting point by solid-liquid cell apparatus, taking the temperature of the sample above 70 °C until melting is observed, recording the point at which the sample becomes colourless or clear yellow if decomposition occurs. The results of this are shown below in Figure 2. Phase behaviour of TOPO:malonic acid mixtures at varying χ_{TOPO} values as a function of temperature and χ_{TOPO}

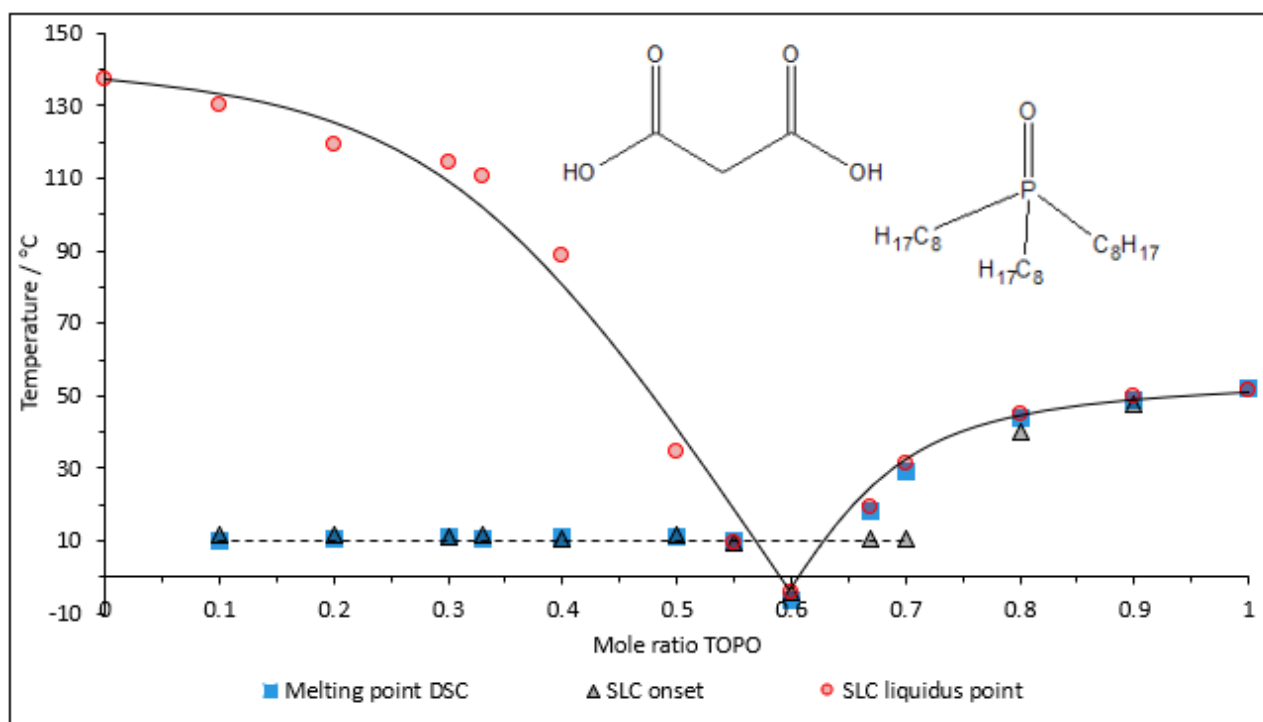


Figure 2. Phase behaviour of TOPO:malonic acid mixtures at varying χ_{TOPO} values as a function of temperature and χ_{TOPO}

Figure 2. Phase behaviour of TOPO:malonic acid mixtures at varying χ_{TOPO} values as a function of temperature and χ_{TOPO} 2 above highlights two regions of interest, that of onset melting corresponding to the formation of the eutectic component of the mixtures as shown by the horizontal line in the diagram and the liquidus point of the sample at each χ_{TOPO} value. Discolouration of the sample occurs with melting in $\chi_{\text{TOPO}} = 0.33-0.1$ and so it is noted that they



decompose upon melting. Observational solid-liquid cell analysis of these samples confirms the presence of another phase.

Tracing the liquidus point line shows that with increasing χ_{TOPO} values from 0.0 (i.e. pure malonic acid), there is a depression melting point from +137 °C to -6 °C at its minimum at $\chi_{\text{TOPO}} = 0.6$. This point at $\chi_{\text{TOPO}} = 0.6$, however, appears to exhibit supercooling as it is below the horizontal line produced by the other samples which corresponds to a eutectic component in these mixtures. When using SLC apparatus, the $\chi_{\text{TOPO}} = 0.6$ sample was a glassy species and therefore, only the onset of stirrer bar movement could be recorded. With further increase in χ_{TOPO} , there is an increase in melting point of the samples until $\chi_{\text{TOPO}} = 1.0$ (i.e. pure TOPO). This is in agreement with observational assessment of the sample phases in their corresponding vials. Between $\chi_{\text{TOPO}} = 0.1 - 0.5$, samples have both a solid and liquid component, with the liquid component proportion increasing as the χ_{TOPO} composition increases where $\chi_{\text{TOPO}} = 0.1$ appears solid to the eye, however must possess a small liquid proportion, $\chi_{\text{TOPO}} = 0.2$ is mostly solid with some liquid and $\chi_{\text{TOPO}} = 0.5$ is mostly liquid with some solid, but not transparent. Transparent liquids were formed at $\chi_{\text{TOPO}} = 0.60$ and 0.67. At $\chi_{\text{TOPO}} = 0.7$, initially the sample consisted of a transparent liquid with a small amount of solid suspension, however, this eventually formed a solid over the course of 2 weeks. Finally, between the range $\chi_{\text{TOPO}} = 0.8-0.9$, white solids were formed.

The lowest melting point within this phase diagram is $\chi_{\text{TOPO}} = 0.6$ and not $\chi_{\text{TOPO}} = 0.5$ as co-crystal formation would suggest due to the formation of 2 hydrogen bonding interactions between phosphorus and the hydrogen bond donor.²⁷ This suggests that there is a dynamic switching in TOPO co-ordination in the liquid phase between $\chi_{\text{TOPO}} = 0.67$ and $\chi_{\text{TOPO}} = 0.5$ where the number of hydrogen bonds associated with each phosphorus entity changes between 1 and 2 respectively. This increase the extent of disruption when considering the packing of species into a lattice and further destabilises the system; allowing a greater ease of liquid formation at $\chi_{\text{TOPO}} = 0.6$.

NMR studies were then performed on the 4 liquid samples $\chi_{\text{TOPO}} = 0.5-0.67$ in order to track how addition of malonic acid effects the acidity of the phosphorus environment on TOPO. NMR of the liquid samples were carried out neat with the presence of a d- H_3PO_4 capillary, locking onto D_2O and referencing the spectra to H_3PO_4 ($\delta^{31}\text{P} = 0$). The results of this is shown in Figure 3 below.

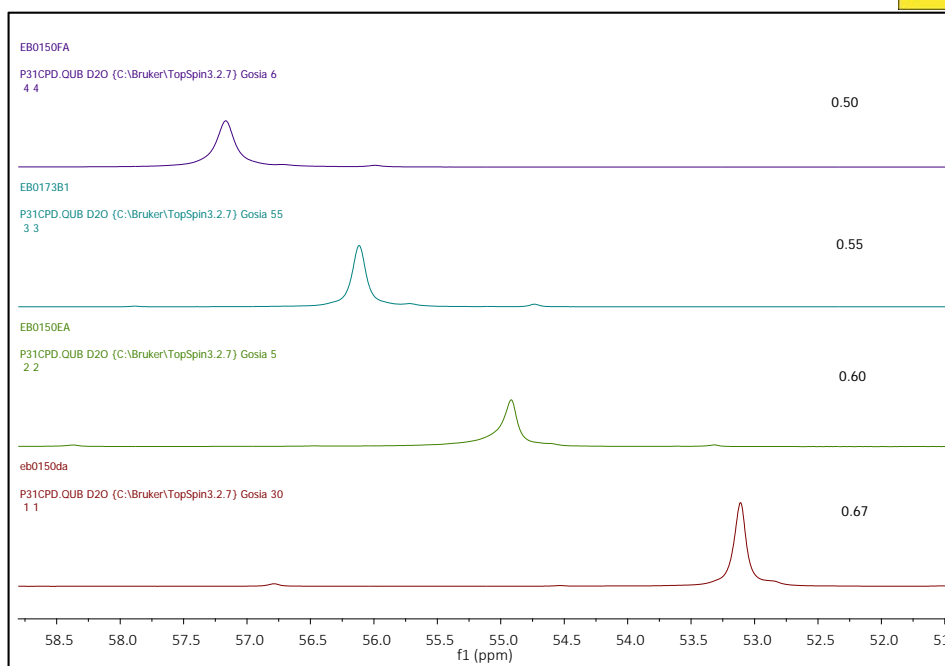


Figure 3. ^{31}P NMR comparison between TOPO:Malonic acid mixtures

The $\delta^{31}\text{P}$ shifts of the TOPO component of the mixtures are as follows: $\chi_{\text{TOPO}} = 0.67$ ($\delta^{31}\text{P} = 53.11$ ppm), $\chi_{\text{TOPO}} = 0.60$ ($\delta^{31}\text{P} = 54.92$ ppm), $\chi_{\text{TOPO}} = 0.55$ ($\delta^{31}\text{P} = 56.12$ ppm) and $\chi_{\text{TOPO}} = 0.50$ ($\delta^{31}\text{P} = 57.17$ ppm) as shown in Table 1. $\delta^{31}\text{P}$ Shifts associated with χ_{TOPO} mixtures

χ_{TOPO}	$\delta^{31}\text{P} / \text{ppm}$
0.67	53.11
0.60	54.92
0.55	56.12
0.50	57.17

Table 1. $\delta^{31}\text{P}$ Shifts associated with χ_{TOPO} mixtures

With a decreasing TOPO component in the mixture, ^{31}P signals shift downfield as the proportion of malonic acid present increases. This suggests, that the acidity of the phosphorus environment of the TOPO molecule is increasing. Similar to work conducted by Gilmore et al.¹¹ studying a TOPO:phenol system, the $\Delta\delta^{31}\text{P}$ remains constant at approximately constant with $\Delta\delta = 2$ ppm between each subsequent χ_{TOPO} mixture, suggesting that it is the malonic acid is directly affecting the acidity of the phosphorus environment.

The chemical shifts associated with these TOPO:malonic acid mixtures, however, are further downfield (more acidic) than the TOPO:phenol mixtures reported¹¹ at the same molar ratio of TOPO as $\chi_{\text{TOPO}} = 0.60$ ($\delta^{31}\text{P} = 54.92$ ppm) and $\chi_{\text{TOPO}} = 0.50$ ($\delta^{31}\text{P} = 57.17$ ppm) for TOPO:malonic acid mixtures, however $\chi_{\text{TOPO}} = 0.60$ ($\delta^{31}\text{P} = 49.1$ ppm) and $\chi_{\text{TOPO}} = 0.50$ ($\delta^{31}\text{P} = 50.1$ ppm) for TOPO:phenol mixtures; a $\Delta\delta = 5.82$ and 7.07 ppm respectively. The values for $\delta^{31}\text{P}$ in these TOPO:malonic acid mixtures, and in $\chi_{\text{TOPO}} = 0.67$ ($\delta^{31}\text{P} = 53.11$ ppm) are comparable, however, to $\delta^{31}\text{P}$ values for TOPO:phenol mixtures in the range $\chi_{\text{TOPO}} = 0.4$ - 0.2 .¹¹

As Gilmore *et al.* suggest that the likely eutectic minimum for their system is $\chi_{\text{TOPO}} = 0.33$, comparable to $\delta^{31}\text{P}$ of $\chi_{\text{TOPO}} = 0.6$ for the TOPO:malonic acid system, which has two hydrogen bond donors in comparison to one hydrogen bond donor in a phenol system; it is thought that there is a

dynamic speciation of malonic acid's hydrogen bond donating sites switching between two and one hydrogen bond formation with phosphorus in TOPO. Finally, density was also measured for each of the liquid samples formed and the results shown in Figure 4 below.

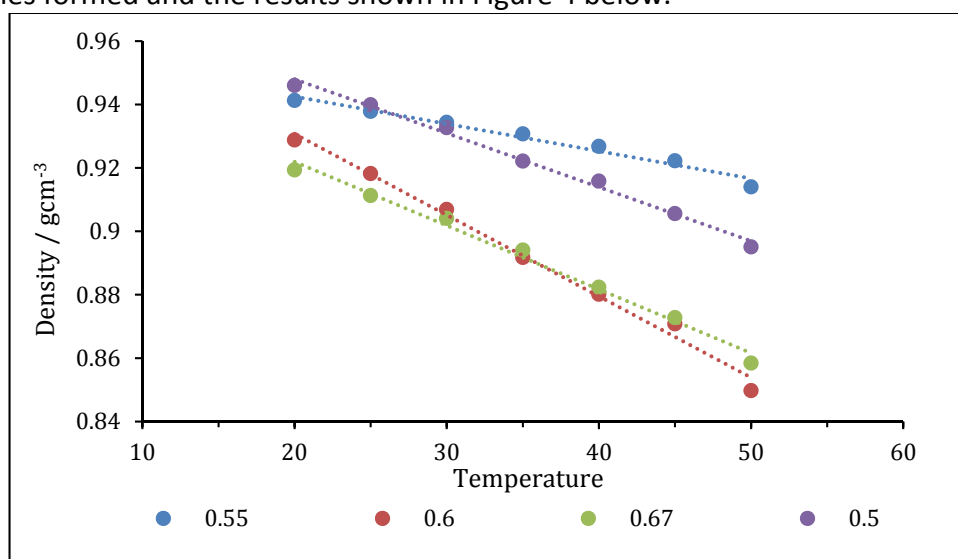


Figure 4. Comparison of density with changing χ_{TOPO} as a function of temperature

Results from this study show that density decreases with an increasing χ_{TOPO} mole ratio as expected due to TOPO being less dense than malonic acid (0.861 g cm^{-3} and 1.62 g cm^{-3} respectively) and also that density of each liquid sample decreases with increasing temperature as expected.

Conclusions and future work

To conclude, TOPO:Malonic acid mixtures were prepared across the whole compositional range from $\chi_{\text{TOPO}} = 0.1$ -1.0 with thermal gravimetric analysis to determine thermal stability performed and a phase diagram produced using both differential scanning calorimetry and solid liquid cell observational analysis. This phase diagram shows that the eutectic point occurs at $\chi_{\text{TOPO}} = 0.6$ and thus indicates that there is a competitive equilibrium between TOPO's phosphorus bound to one hydrogen bond and 2 hydrogen bonds which destabilises the lattice; increasing the ease with which a liquid can form at $\chi_{\text{TOPO}} = 0.6$. NMR studies of the liquid samples were performed and highlighted that malonic acid contributes directly to the acidity of the phosphorus environment experienced by the phosphorus on TOPO. These studies also highlighted that the eutectic point shown by the phase diagram at $\chi_{\text{TOPO}} = 0.6$ has a chemical shift of a comparable value to that of the eutectic point of the recently published work on TOPO:phenol mixtures.¹¹ Therefore, perhaps a $\delta^{31}\text{P} = 54.92 \text{ ppm}$ (i.e. that of $\chi_{\text{TOPO}} = 0.6$) is indicative of the eutectic point for TOPO mixtures with a range of carboxylic acids and alcohols.

In the near future, phase diagrams for TOPO:Levulinic acid will also be reported by recording the temperature at which onset melting and liquidus points occur visually using a solid-liquid cell and the results compared with DSC results. TGA, DSC and SLC of mixtures made with these mixtures and the physical properties such as density will be studied. Application for these eutectics will then be applied. In addition to this, species which allow proton hopping for the use in non-aqueous electrolytes will also be physically characterised.

References

- 1 A. P. Abbott, G. Capper, D. L. Davies, H. L. Munro, R. K. Rasheed and V. Tambyrajah, *Chem. Commun.*, 2001, 2010–2011.
- 2 Q. Zhang, K. De Oliveira Vigier, S. Royer and F. Jérôme, *Chem. Soc. Rev.*, 2012, **41**, 7108.
- 3 M. C. Kroon, M. Francisco, A. Van Den Bruinhorst and M. C. Kroon, 2013, **2012**, 3074–3085.
- 4 E. L. Smith, A. P. Abbott and K. S. Ryder, *Chem. Rev.*, 2014, **114**, 11060–11082.
- 5 A. P. Abbott, D. Boothby, G. Capper, D. L. Davies and R. K. Rasheed, *J. Am. Chem. Soc.*, 2004, **126**, 9142–9147.
- 6 D. J. G. P. van Osch, L. F. Zubeir, A. van den Bruinhorst, M. A. A. Rocha and M. C. Kroon, *Green Chem.*, 2015, **17**, 4518–4521.
- 7 D. J. G. P. van Osch, D. Parmentier, C. H. J. T. Dietz, A. van den Bruinhorst, R. Tuinier and M. C. Kroon, *Chem. Commun.*, 2016, **52**, 11987–11990.
- 8 J. Cao, M. Yang, F. Cao, J. Wang and E. Su, *ACS Sustain. Chem. Eng.*, 2017, **5**, 3270–3278.
- 9 J. . Cao, L. . Chen, M. . Li, F. . Cao, L. . Zhao and E. Su, *Green Chem.*, 2018, **20**, 1879–1886.
- 10 B. D. Ribeiro, C. Florindo, L. C. Iff, M. A. Z. Coelho and I. M. Marrucho, *ACS Sustain. Chem. Eng.*, 2015, **3**, 2469–2477.
- 11 M. Gilmore, E. N. Mccourt, F. Connolly, P. Nockemann and J. D. Holbrey, *ACS Sustain. Chem. Eng.*, 2018, **6**, 17323–17332.
- 12 I. Mekis, D. V Talapin, A. Kornowski, M. Haase and H. Weller, *J. Phys. Chem.*, 2003, **107**, 7454–7462.
- 13 F. V Mikulec, M. Kuno, M. Bennati, D. A. Hall, R. G. Griffin and M. G. Bawendi, *J. Am. Chem. Soc.*, 2000, **122**, 2532–2540.
- 14 T. Cassagneau, T. E. Mallouk and J. H. Fendler, *J. Am. Chem. Soc.*, 1998, **120**, 7848–7859.
- 15 T. Trindade and P. O. Brien, *Chem Mater*, 1997, **9**, 523–530.
- 16 A. A. Guzelian, J. E. B. Katari, A. V Kadavanich, U. Banin, K. Hamad, E. Juban, A. P. Alivisatos, R. H. Wolters, C. C. Arnold and J. R. Heath, *J. Phys. Chem.*, 1996, **100**, 7212–7219.
- 17 T. Sato, T. Nakamura and S. Ishikawa, *Solvent Extr. Ion Exch.*, 1984, **2**, 201–212.
- 18 E. K. Watson and W. A. Rickelton, *Solvent Extr. Ion Exch.*, 1992, **10**, 879–889.
- 19 P. O. . Saboe, L. P. . Manker, W. E. . Michener, D. J. . Peterson, D. G. . Brandner, S. P. . Deutch, M. . Kumar, R. M. . Cywar, B. G. T.; and E. M. Karp, *Green Chem.*, 2018, **20**, 1791–1804.
- 20 T. Brouwer, M. Blahusiak, K. Babic and B. Schuur, *Sep. Purif. Technol.*, 2017, **185**, 186–195.
- 21 G. Kim, S. Park and B. Um, *Ind. Crop. Prod.*, 2016, **89**, 34–44.
- 22 S. Uenoyama, T. Hano, M. Hirata and S. Miura, *J. Chem. Technol. Biotechnol.*, 1996, **67**, 260–264.
- 23 P. Praveen and K. C. Loh, *Chem. Eng. J.*, 2014, **255**, 641–649.
- 24 P. Praveen and K. Loh, *Chemosphere*, 2016, **153**, 405–413.
- 25 P. Praveen and K. Loh, *J. Memb. Sci.*, 2013, **437**, 1–6.
- 26 P. Taylor, E. K. Watson, W. A. Rickelton, A. J. Robertson and T. J. Brown, *Solvent Extr. Ion Exch.*, 1988, **6**, 207–220.
- 27 E. Y. Tupikina, M. Bodensteiner, P. M. Tolstoy, G. S. Denisov and I. G. Shenderovich, *J. Phys. Chem. C*, 2018, **122**, 1711–1720.

QUILL Quarterly Report

November 2018 – January 2019

Name:	Miriam de Miguel		
Supervisor(s):	Dr. Małgorzata Swadźba-Kwaśny		
Position:	Lab technician student		
Start date:	November 2018	Anticipated end date:	May 2019
Funding body:	DfE (Department for the Economy)		

Physical characterisation of functional liquids

Background

It is proposed that deep eutectic solvents 'DES' are a chemical component mixture composed of hydrogen bond donors and acceptors which have intermolecular interactions that result in a freezing point which is lower than that of the isolated individual components of the system with no interactions between each other.¹ They are asymmetric species which, due to their orbitals' inability to overlap well and thus, pack into a regular lattice arrangement, have low lattice energy and so do not require a large amount of energy in order to exist as a liquid and as a result tend to have low melting points.

The most common and well renowned DES are those prepared with the combination of organic salts such as choline chloride, which act as a hydrogen bond acceptor and carboxylic acids or alcohols with a hydrogen bond donating role.^{2–5} However, these solvents are generally miscible with water and so their application is quite limited. Therefore, work was undertaken by van Osch *et al.* which led to the publication of the first hydrophobic deep eutectic solvent using a carboxylic acid hydrogen bond donor and a long chain quaternary ammonium salt in 2015.⁶ In addition to this, DES have since been formed using alcohols and fatty acid hydrogen bond donors in combination with organic salts to form deep eutectic solvents which can be used for extraction of metals⁷ and natural products^{8,9}. In addition to this, in an attempt to reduce the viscosity associated with these charged DES species, Ribeiro *et al.* developed DES systems using D-menthol and carboxylic acid hydrogen bond donors where the individual components used are non-ionic species.¹⁰ More recently, DES made with the combination of trioctylphosphine oxide (TOPO) and phenol have been published and its use as a uranyl extractant shown.¹¹

TOPO has a number of uses such as capping agents^{12–16} in nanoparticle synthesis, metals^{17,18}, organic acids^{19–22} and phenolics^{23–26} extraction and so a number of DES will be prepared using a range of hydrogen bond donors most suited to the potential application.

Objective of this work

In this work a number of hydrogen bond donors such as levulinic acid and malonic acid have been combined with TOPO to form a eutectic. They have been combined across the whole compositional range in increments of 0.1 from $\chi_{\text{TOPO}} = 0.1$ -1.0 and mixtures at $\chi_{\text{TOPO}} = 0.33$ and 0.67 have also been included. The physical properties of the mixtures have been characterised and they will be applied to an industrial application.

Progress to date

Following on from previous reports that showed the many uses of Levulinic acid, such as a precursor to biofuel and so these physical characterisation techniques were also repeated for TOPO:levulinic samples; with future work on this system looking at extracting levulinic acid from biomass waste streams.

To begin this section of work, TOPO:Levulinic acid samples were made across the whole compositional range $\chi_{\text{TOPO}} = 0.1$ -1.0 including $\chi_{\text{TOPO}} = 0.33$ and 0.67. Thermal decomposition of the samples was first of interest and so TGA pans were prepared for each of the samples.

Each χ_{TOPO} sample was also prepared for DSC and solid liquid cell (SLC) apparatus to understand the phase behaviour of the samples at varying χ_{TOPO} values and the temperature recorded for a thermal event. The results were reported as the mid-point of the line on the DSC due to relatively broad peaks in comparison to that of crystalline structures. DSC samples were not run above 80 °C due to reaching the limit of decomposition and so not all melting points were acquired through DSC analysis, therefore further requiring SLC analysis.

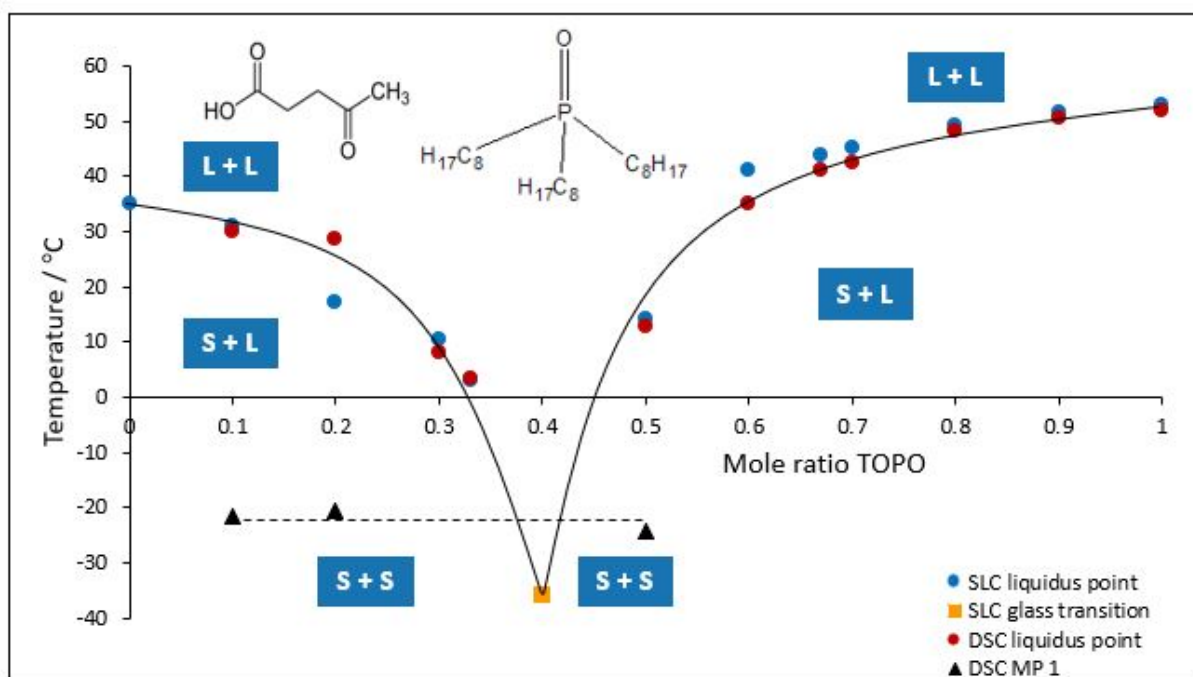


Figure 1. Phase behaviour of TOPO:malonic acid mixtures at varying χ_{TOPO} values as a function of temperature and χ_{TOPO}

Figure 1 above highlights two regions of interest, that of onset melting corresponding to the formation of the eutectic component of the mixtures as shown by the horizontal line in the diagram and the liquidus point of the sample at each χ_{TOPO} value. Observational solid-liquid cell analysis of these samples confirms the presence of another phase.

Tracing the liquidus point line shows that with increasing χ_{TOPO} values from 0.0 (i.e. pure levulinic acid), there is a depression melting point from +35 °C to -38 °C at its minimum at $\chi_{\text{TOPO}} = 0.4$. This point at $\chi_{\text{TOPO}} = 0.4$, however, appears to exhibit supercooling as it is below the horizontal line produced by the other samples which corresponds to a eutectic component in these mixtures. When using SLC apparatus, the $\chi_{\text{TOPO}} = 0.4$ sample was a glassy species and therefore, only the onset of stirrer bar movement could be recorded. With further increase in χ_{TOPO} , there is an increase in melting point of the samples until $\chi_{\text{TOPO}} = 1.0$ (i.e. pure TOPO). This is in agreement with observational assessment of the sample phases in their corresponding vials. Between $\chi_{\text{TOPO}} = 0.9 - 0.5$, samples have both a solid and liquid component, with the liquid component proportion decreasing as the χ_{TOPO} composition increases. Transparent liquids were formed at $\chi_{\text{TOPO}} = 0.1$ and 0.4 and between the range $\chi_{\text{TOPO}} = 0.5-0.9$, white solids were formed.

NMR studies were then performed on the 5 liquid samples $\chi_{\text{TOPO}} = 0.1-0.4$ in order to track how addition of malonic acid effects the acidity of the phosphorus environment on TOPO. NMR of the liquid samples were carried out neat with the presence of a d- H_3PO_4 capillary, locking onto D_2O and referencing the spectra to H_3PO_4 ($\delta^{31\text{P}} = 0$).

Conclusions and future work

To conclude, TOPO:Levulinic acid mixtures were prepared across the whole compositional range from $\chi_{\text{TOPO}} = 0.1$ -1.0 with thermal gravimetric analysis to determine thermal stability performed and a phase diagram produced using both differential scanning calorimetry and solid liquid cell observational analysis. This phase diagram shows that the eutectic point occurs at $\chi_{\text{TOPO}} = 0.4$ and thus indicates that there is a competitive equilibrium between TOPO's phosphorus bound to one hydrogen bond and 2 hydrogen bonds which destabilises the lattice; increasing the ease with which a liquid can form at $\chi_{\text{TOPO}} = 0.4$.

References

- 1 A. P. Abbott, G. Capper, D. L. Davies, H. L. Munro, R. K. Rasheed and V. Tambyrajah, *Chem. Commun.*, 2001, 2010–2011.
- 2 Q. Zhang, K. De Oliveira Vigier, S. Royer and F. Jérôme, *Chem. Soc. Rev.*, 2012, **41**, 7108.
- 3 M. C. Kroon, M. Francisco, A. Van Den Bruinhorst and M. C. Kroon, 2013, **2012**, 3074–3085.
- 4 E. L. Smith, A. P. Abbott and K. S. Ryder, *Chem. Rev.*, 2014, **114**, 11060–11082.
- 5 A. P. Abbott, D. Boothby, G. Capper, D. L. Davies and R. K. Rasheed, *J. Am. Chem. Soc.*, 2004, **126**, 9142–9147.
- 6 D. J. G. P. van Osch, L. F. Zubeir, A. van den Bruinhorst, M. A. A. Rocha and M. C. Kroon, *Green Chem.*, 2015, **17**, 4518–4521.
- 7 D. J. G. P. van Osch, D. Parmentier, C. H. J. T. Dietz, A. van den Bruinhorst, R. Tuinier and M. C. Kroon, *Chem. Commun.*, 2016, **52**, 11987–11990.
- 8 J. Cao, M. Yang, F. Cao, J. Wang and E. Su, *ACS Sustain. Chem. Eng.*, 2017, **5**, 3270–3278.
- 9 J. . Cao, L. . Chen, M. . Li, F. . Cao, L. . Zhao and E. Su, *Green Chem.*, 2018, **20**, 1879–1886.
- 10 B. D. Ribeiro, C. Florindo, L. C. Iff, M. A. Z. Coelho and I. M. Marrucho, *ACS Sustain. Chem. Eng.*, 2015, **3**, 2469–2477.
- 11 M. Gilmore, E. N. Mccourt, F. Connolly, P. Nockemann and J. D. Holbrey, *ACS Sustain. Chem. Eng.*, 2018, **6**, 17323–17332.
- 12 I. Mekis, D. V Talapin, A. Kornowski, M. Haase and H. Weller, *J. Phys. Chem.*, 2003, **107**, 7454–7462.
- 13 F. V Mikulec, M. Kuno, M. Bennati, D. A. Hall, R. G. Griffin and M. G. Bawendi, *J. Am. Chem. Soc.*, 2000, **122**, 2532–2540.
- 14 T. Cassagneau, T. E. Mallouk and J. H. Fendler, *J. Am. Chem. Soc.*, 1998, **120**, 7848–7859.
- 15 T. Trindade and P. O. Brien, *Chem Mater*, 1997, **9**, 523–530.
- 16 A. A. Guzelian, J. E. B. Katari, A. V Kadavanich, U. Banin, K. Hamad, E. Juban, A. P. Alivisatos, R. H. Wolters, C. C. Arnold and J. R. Heath, *J. Phys. Chem.*, 1996, **100**, 7212–7219.
- 17 T. Sato, T. Nakamura and S. Ishikawa, *Solvent Extr. Ion Exch.*, 1984, **2**, 201–212.
- 18 E. K. Watson and W. A. Rickelton, *Solvent Extr. Ion Exch.*, 1992, **10**, 879–889.
- 19 P. O. . Saboe, L. P. . Manker, W. E. . Michener, D. J. . Peterson, D. G. . Brandner, S. P. . Deutch, M. . Kumar, R. M. . Cywar, B. G. T.; and E. M. Karp, *Green Chem.*, 2018, **20**, 1791–1804.
- 20 T. Brouwer, M. Blahusiak, K. Babic and B. Schuur, *Sep. Purif. Technol.*, 2017, **185**, 186–195.
- 21 G. Kim, S. Park and B. Um, *Ind. Crop. Prod.*, 2016, **89**, 34–44.
- 22 S. Uenoyama, T. Hano, M. Hirata and S. Miura, *J. Chem. Technol. Biotechnol.*, 1996, **67**, 260–264.
- 23 P. Praveen and K. C. Loh, *Chem. Eng. J.*, 2014, **255**, 641–649.
- 24 P. Praveen and K. Loh, *Chemosphere*, 2016, **153**, 405–413.
- 25 P. Praveen and K. Loh, *J. Memb. Sci.*, 2013, **437**, 1–6.

- 26 P. Taylor, E. K. Watson, W. A. Rickelton, A. J. Robertson and T. J. Brown, *Solvent Extr. Ion Exch.*, 1988, **6**, 207–220.
- 27 E. Y. Tupikina, M. Bodensteiner, P. M. Tolstoy, G. S. Denisov and I. G. Shenderovich, *J. Phys. Chem. C*, 2018, **122**, 1711–1720.



QUILL Quarterly Report

November 2018 – January 2019

Name:	Martyn J Earle		
Supervisor(s):	Peter Nockemann/Marijana Blesic		
Position:	Senior Research Fellow		
Start date:	Marcj 1995	Anticipated end date:	
Funding body:			

Green Lanthanide Separations using Countercurrent Chromatography and Ionic Liquids

This report described the ongoing work for the clean separation of lanthanide elements by countercurrent chromatography using ionic liquid stationary phases.

Lanthanide nitrate distribution ratios

The following solvent systems: A1, A2, A3 and A4 were prepared using the solvents and ionic liquids in Table 1. The values for D_R in parentheses refers to the distribution ratio in the presence of the metal in parentheses, such that Pr(Er) refers to the DR value of Praseodymium(III) in the presence of Erbium(III).

Table 1, the compositions and absorbances of the solvent system phases used in the lanthanide nitrate separations measured at 50 °C.

Solvent System	Component	Quantity	Density in g cm ⁻³ at 50 °C			MP Absorbance	SP Absorbance	Dr = $\frac{[Ln^{3+}]_{SP}}{[Ln^{3+}]_{MP}}$
			SP	MP	MP-SP			
A1	Water	800 cm ³	0.890	0.972	0.082			Pr 0.116
	Ethyl Ethanoate	200 cm ³						Pr(Er) 0.019
	[P _{6 6 6 14}]Cl	200 cm ³						Er 0.503
	TBPO	0.0 g						Er(Pr) 0.16
A2	Water	800 cm ³	0.894	0.974	0.080			Pr 0.135
	Ethyl Ethanoate	200 cm ³						Pr (Er) 0.062
	[P _{6 6 6 14}]Cl	200 cm ³						Er 0.730
	TBPO	20.0 g						Er(Pr) 0.262
A3	Water	40 cm ³	---	---	---			Pr 0.178
	Ethyl Ethanoate	10 cm ³						Pr(Er) 0.136
	[P _{6 6 6 14}]Cl	10 cm ³						Er 0.920
	TBPO	2.0 g						Er(Pr) 0.676
A4	Water	40 cm ³	---	---	---			Pr 0.232
	Ethyl Ethanoate	10 cm ³						Pr(Er) 0.336
	[P _{6 6 6 14}]Cl	10 cm ³						Er 1.29
	TBPO	3.0 g						Er(Pr) 1.85

[P_{6 6 6 14}]Cl = trihexyltetradecylphosphonium chloride, TBPO = tributylphosphine oxide

For each solvent system A1 – A4, $\text{Ln}(\text{NO}_3)_3 \cdot (\text{H}_2\text{O})_n$ ($n=6$ for Pr, $n=5$ for Er) salts (0.30 g) were dissolved in ca. 0.7 cm^3 of MP (lower aqueous phase) + 0.7 cm^3 of SP (ionic / organic upper phase) at 50°C . Both phases were made up to a volume of 1.00 ml each (total = 2.00 cm^3) in a volumetric flask and the UV-Vis absorbances at 445 nm for $\text{Pr}(\text{NO}_3)_3$ ($\epsilon = 0.983$ (Figure 2)), and 523 nm ($\text{Er}(\text{NO}_3)_3$) ($\epsilon = 0.461$ (Figure 3)) or 652 nm ($\epsilon = 0.207$ (Figure 4)) were measured for each phase (based on peak height) and shown in Figures 1 and Table 1. Also, a mixture of $\text{Pr}(\text{NO}_3)_3 \cdot 6(\text{H}_2\text{O})$ and $\text{Er}(\text{NO}_3)_3 \cdot 5(\text{H}_2\text{O})$ (1.00 : 1.00 ratio by weight) was prepared and dissolved in the solvent systems A1-A4 in order to determine how the metals affect each-others distribution ratio. This data is also shown in Table 1 and Figure 1. Assuming that the extinction coefficients of the absorption peaks of the lanthanide salts were not affected by the solvent system, the distribution ratios were calculated using the formula $\text{Dr}_{(\text{Ln})} = [\text{Ln}^{3+}]_{\text{SP}} / [\text{Ln}^{3+}]_{\text{MP}} = \text{Abs.}(\text{Ln}^{3+}) \text{ in SP} / \text{Abs.}(\text{Ln}^{3+}) \text{ in MP}$. The UV-Vis spectra of 0.30 g of Pr(III), Nd(III) and Er(III) nitrate salts (0.30 g) in water (1.00 cm^3) are shown in Figure 5.

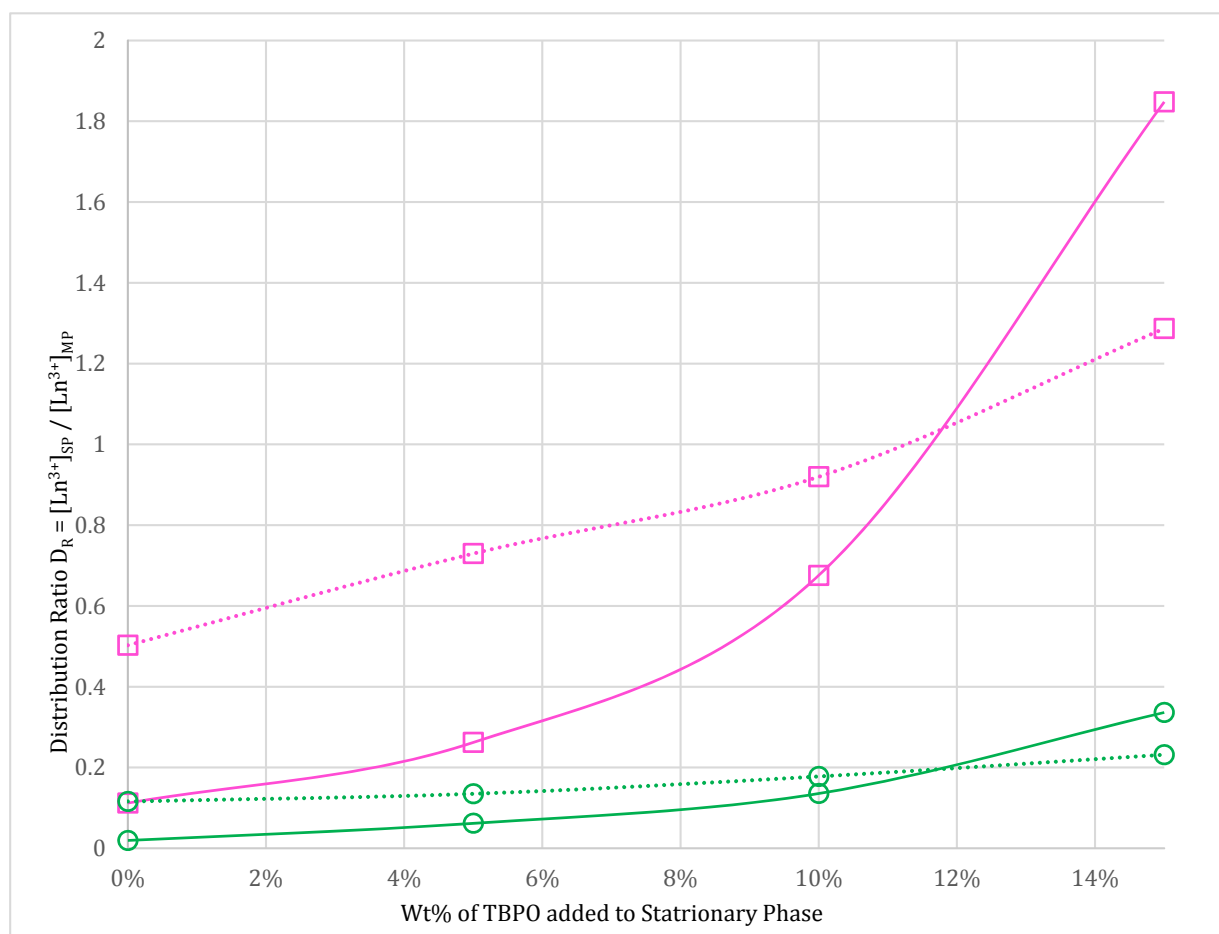


Figure 1, The variation of distribution ratio ($\text{Dr}_{(\text{Ln})} = [\text{Ln}^{3+}]_{\text{SP}} / [\text{Ln}^{3+}]_{\text{MP}}$) of $\text{Ln}(\text{NO}_3)_3 \cdot n(\text{H}_2\text{O})$ ($\text{Ln} = \text{Pr}$, $n = 6$; $\text{Ln} = \text{Er}$, $n = 5$) (0.30 g) dissolved in 2.00 cm^3 of the solvent systems A1, A2, A3 and



A4 (Table 1) (consisting of 1.00 cm^3 of MP + 1.00 cm^3 of SP) at $50\text{ }^\circ\text{C}$. The dotted lines show the Ln^{3+} (Green = Pr^{3+} and Magenta = Er^{3+}) distribution ratio for the individual metals (0.30g) in the solvent systems A1-A4, and the solid lines show the distribution ratios for a 1:1 mixture of Pr^{3+} (0.15g) and Er^{3+} (0.15g). Error in the distribution ratio data points = ± 0.04 .

Extinction Coefficient Calculations for $\text{Ln}(\text{NO}_3)_3$ salts.

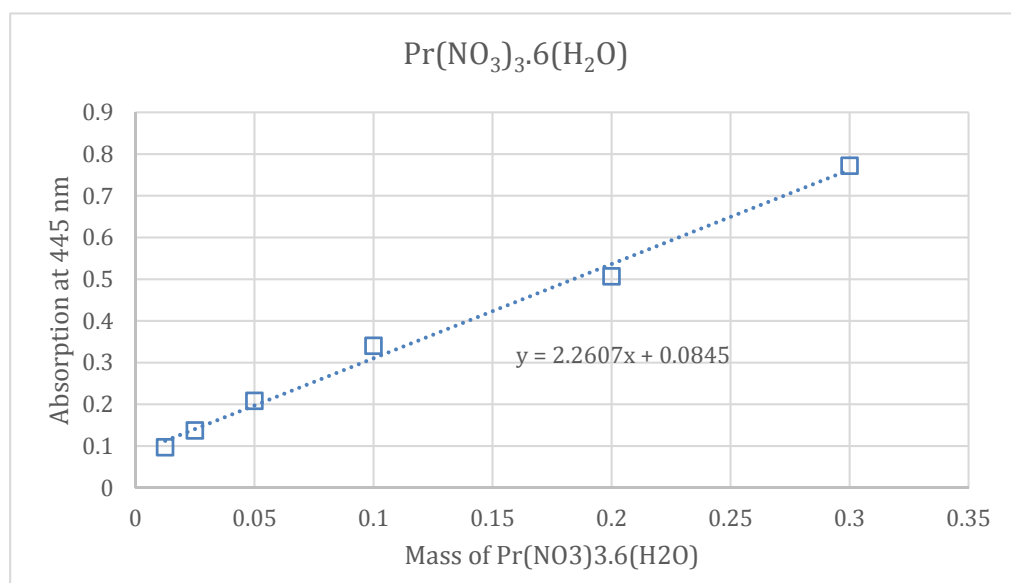


Figure 2. The absorbance of $\text{Pr}(\text{NO}_3)_3 \cdot 6(\text{H}_2\text{O})$ at 445nm by UV-Vis spectroscopy for different masses dissolved in 1.00 cm^3 of water.

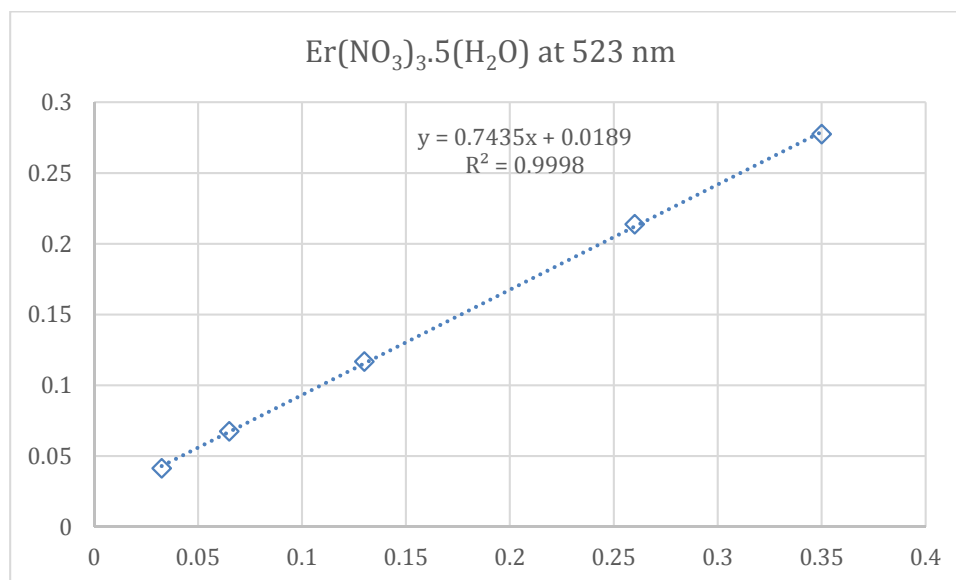


Figure 3. The absorbance of $\text{Er}(\text{NO}_3)_3 \cdot 5(\text{H}_2\text{O})$ at 523nm by UV-Vis spectroscopy for different masses dissolved in 1.00 cm^3 of water.

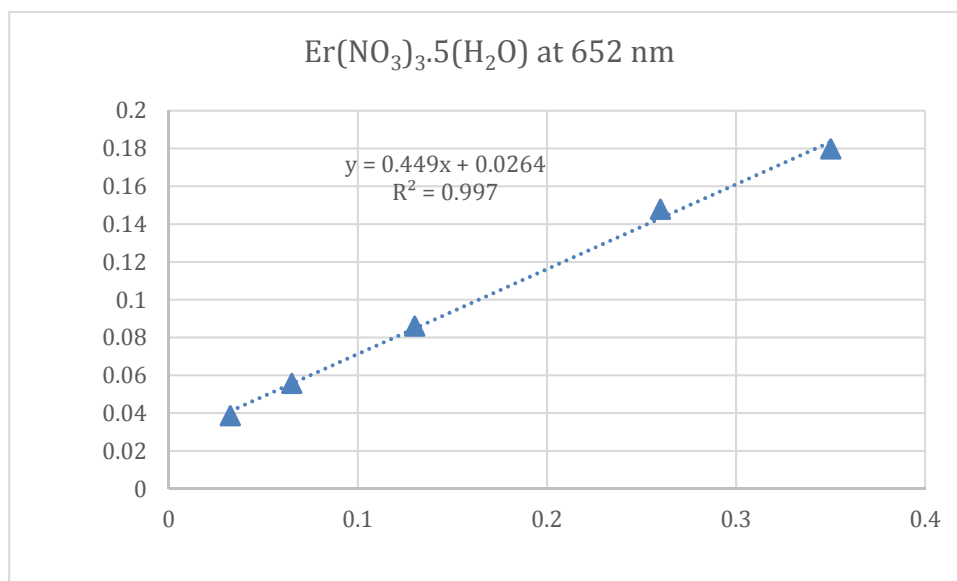


Figure 4. The absorbance of $\text{Er}(\text{NO}_3)_3 \cdot 5(\text{H}_2\text{O})$ at 652nm by UV-Vis spectroscopy for different masses dissolved in 1.00 cm^3 of water.

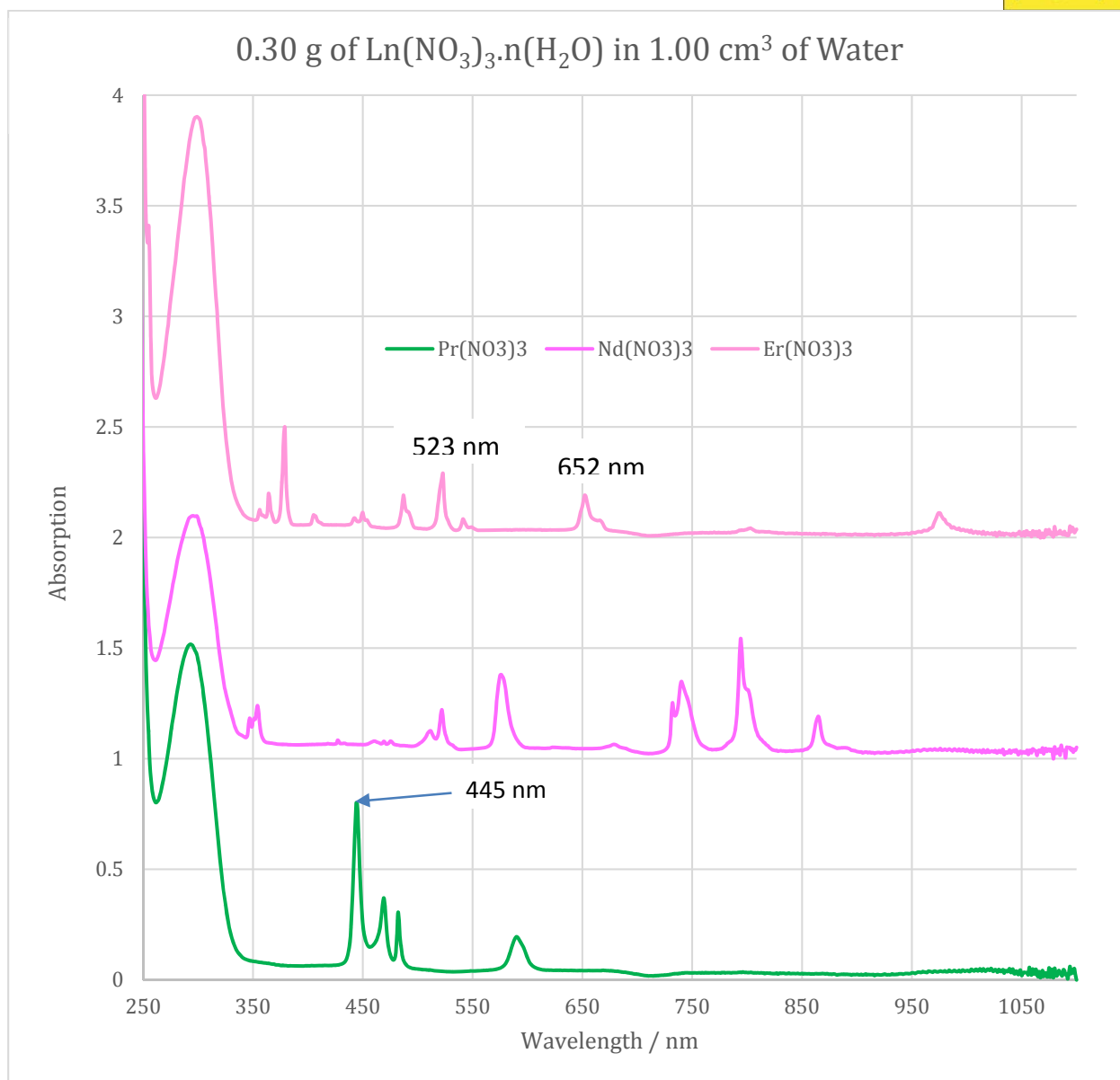


Figure 5, The UV-Vis spectra of $\text{Pr}(\text{III})$, $\text{Nd}(\text{III})$ and $\text{Er}(\text{III})$ nitrate salts (0.30g) in water (1.00cm^3).

Lanthanide Separation Procedure

Stationary Phase Retention Curves

The IL-Prep™ ionic liquid-liquid chromatography (ILLC) machine consists of a J-type centrifuge with four stainless steel (SS) coils, with two coils on each bobbin. Using the apparatus shown in Figure 6, in recirculation mode, the stationary phase retention curves (Figure 7) for six solvent systems (Table 1) used in the lanthanide separations were determined for Coil 2 (133 cm^3 , 2.1 mm internal diameter) at $50\text{ }^\circ\text{C}$ and 890 r.p.m.,¹⁶ using the methodology described in the literature.^{16,17}

The solvent systems with the highest density contrast between the MP and SP (Table 1) have higher stationary phase retentions, and the addition of 5 wt% TBPO to the SP slightly increases the stationary phase retention values. Generally, high stationary phase retention values improve separation performance and reduce the amount of mobile phase required for the separation.²⁶

Previous research on metal separations used ethyl ethanoate as a co-solvent to reduce the viscosity of the $[P_{66614}]Cl$ containing phase,¹⁶ but it was found that separations using 3-pentanone as a co-solvent (Table 1, B1 and B2) gave better separation performance and lower solvent system turbidity. The hexane containing solvent systems C1 and C2, have an increased density contrast between the MP and the SP (Table 1) leading to higher SP retention values, which generally improve the overall separations performance.

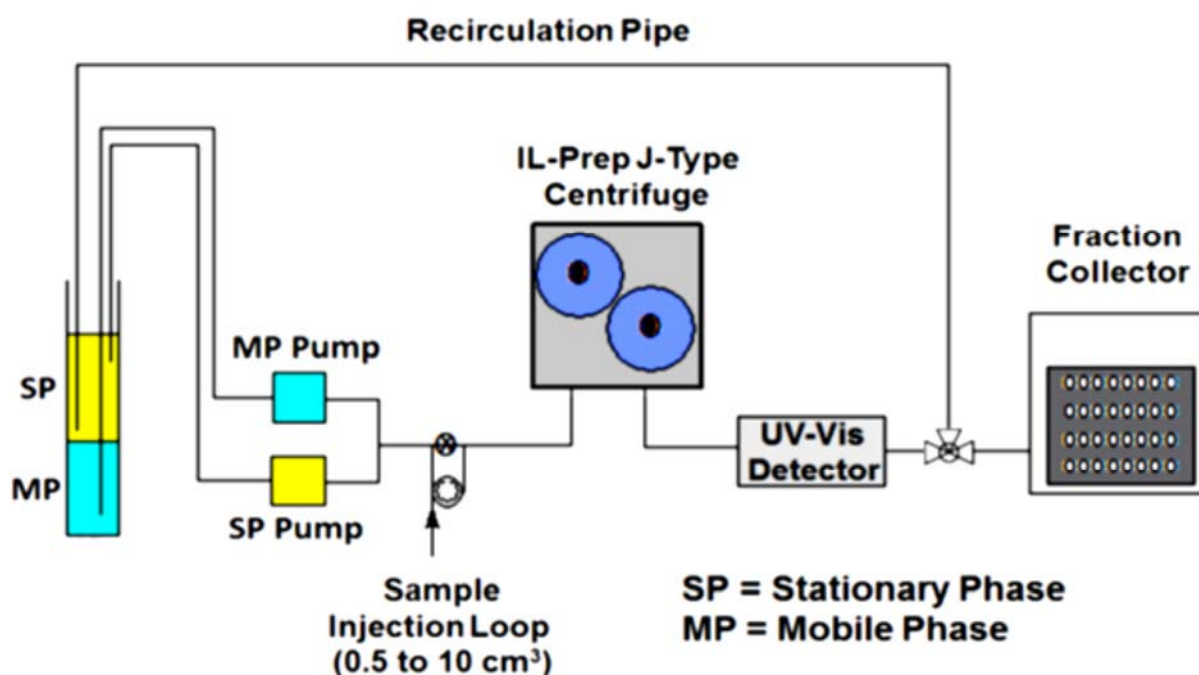


Figure 6. A schematic of the IL-Prep™ CCC instrument, used in the lanthanide separations.

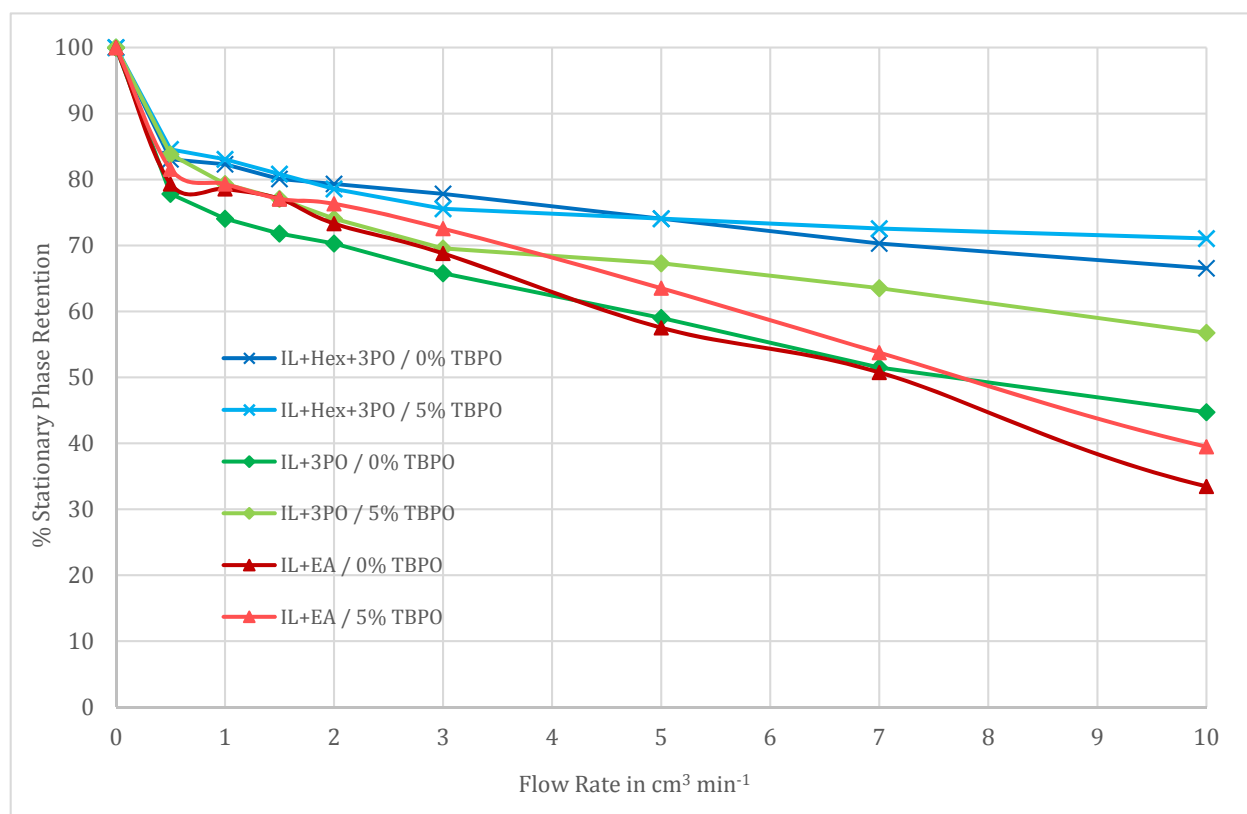


Figure 7. The stationary phase retention curves for six solvent systems used in the lanthanide separations (Table 1, A1, A2, B1, B2, C1 and C2) using Coil 2 at 50 °C and 890 r.p.m.¹⁷ The solvent systems are **Dark Red (A1):** water (800 cm³) / [P_{6 6 6 14}]Cl (200 cm³) + ethyl ethanoate (200 cm³);¹⁷ **Light Red (A2):** water (800 cm³) / [P_{6 6 6 14}]Cl (200 cm³) + ethyl ethanoate (200 cm³) + 5 wt% TBPO in the SP; **Dark Blue (C1):** water (1000 cm³) / [P_{6 6 6 14}]Cl (200 cm³) + hexane (270 cm³) + 3-pentanone (30 cm³); **Light Blue (C2):** water (1000 cm³) / [P_{6 6 6 14}]Cl (200 cm³) + hexane (270 cm³) + 3-pentanone (30 cm³) + 5 wt% TBPO dissolved in the SP; and **Dark Green (B1):** water (800 cm³) / [P_{6 6 6 14}]Cl (200 cm³) + 3-pentanone (200 cm³); **Light Green (B2):** water (800 cm³) / [P_{6 6 6 14}]Cl (200 cm³) 3-pentanone (200 cm³) + 5 wt% TBPO dissolved in the SP. Error in data points = ± 3.0% stationary phase retention.

Solvent Systems

The lanthanide separation chosen for detailed study was the separation of Pr(NO₃)₃·6H₂O from Er(NO₃)₃·5H₂O. These two lanthanide nitrate salts have non-overlapping UV-Vis absorption peaks in the visible part of the electromagnetic spectrum, making observation with the online UV-Vis detector (an ECOM Flash 14 DAD 800 Detector) straightforward and easy to visualise. In half of the separations, tributylphosphine oxide (TBPO) was added to the stationary phase at 5 wt% concentrations, to investigate its effects on separation



performance. In all the experiments, the mobile phase was water (saturated with organic solvents). The SP was not consumed in the separations, and was reused for multiple separations (typically 5-10 times over 1-2 days of experimentation). The SP could be recovered and stored for future use by reverse pumping (in the tail to head direction) it from the ILLC coil using the MP. ^1H , ^{13}C , and ^{31}P NMR analysis of the stationary phase show that it was unchanged after use in 10 consecutive separations.

Lanthanide Separations Procedures

The typical procedure for the separations was as follows: the lanthanide(III) nitrate hexahydrate or pentahydrate salts (0.35 g to 2.0 g of each metal) were dissolved in mobile phase (4.0 cm^3) and loaded into the 5.0 cm^3 sample injection loop using a syringe. Coil 2 of the IL-Prep machine (at $50\text{ }^\circ\text{C}$, 890 r.p.m.) was first filled with stationary phase (tail to head direction), then the mobile phase was pumped into the coil (head to tail direction) at $1.0\text{ cm}^3\text{ min}^{-1}$ faster than the flow rate used in the separation under investigation. The separation was started by switching the sample injection valve to pass through the sample loop (Figure 6), starting the fraction collector (typically 3.2 cm^3 samples) and setting the computer to record the chromatogram, using ECOMAC chromatographic software (Version 1.7.3.0). The absorption peaks measured were 445 nm for praseodymium, and 652 or 523 nm for erbium, and the baseline measurements for the peaks were recorded at 422 (for $\text{Pr}(\text{NO}_3)_3$) and 620 nm (for $\text{Er}(\text{NO}_3)_3$). The baseline signal was subtracted from the lanthanide metal signals to obtain the peak heights and improve the signal to noise ratio of the peak measurements. A typical chromatogram is shown in Figure 8, and was obtained in two different ways. (A) Directly measurement of the metal absorption peaks and baseline signals in the effluent from the coil (Figure 6) without using a lanthanide selective dye.²⁷ The direct measurement simplifies product isolation from the aqueous mobile phase, but can produce noisy chromatograms due to variable turbidity of the mobile phase eluting from the coils, and bubbles of stationary phase passing through the detector cell. The data obtained from the in-line detector was processed using a computer spreadsheet (MS Excel), by subtracting the baseline signal (422 or 620 nm) from the raw lanthanide signal data (445nm for $\text{Pr}(\text{III})$ and 523 or 652nm for $\text{Er}(\text{III})$), smoothing the data using a 10 to 30 second moving average, then applying a linear baseline correction. The spectra were integrated and normalised to give either $\text{Er}(\text{NO}_3)_3 = 100\%$ signal or $\text{Pr}(\text{NO}_3)_3 = 100\%$, and the areas of the $\text{Ln}(\text{III})$ peaks were

scaled to have an area difference of 1.019 : 1.000 (Pr(III) : Er(III)) due to the molar ratio of $\text{Ln}(\text{NO}_3)_3$ salts were injected into the ILLC instrument ($\text{Pr} = 435.01 \text{ g mol}^{-1}$ and $\text{Er} = 443.35 \text{ g mol}^{-1}$). Alternatively, the chromatograms could be constructed by measuring the UV-Vis absorption spectra of the samples in the fraction collector in a standard UV-Vis spectrophotometer using a $0.1 \times 1.0 \text{ cm}$ quartz cell. Figure 8 shows typical chromatograms for a $\text{Pr}(\text{NO}_3)_3 / \text{Er}(\text{NO}_3)_3$ separation (using 0.80 g of each metal) using the C2 solvent system: water (1000 cm^3) / $[\text{P}_{66614}]\text{Cl}$ (200 cm^3) + hexane (270 cm^3) + 3-pentanone (30 cm^3) solvent system, containing 5 wt% TBPO dissolved in the stationary phase. The solid lines (Figure 8) represent the chromatograms obtained using the in-line detector measured at 445 nm for Pr and 523 nm for Er. The dashed lines show the chromatogram obtained from the samples collected in the fraction collector. Of the two methods, the in-line detector data in Figure 8 should be preferred, due to its better temporal resolution (*ie* the fraction collector chromatogram has a temporal resolution of ± 3.2 minutes vs a temporal resolution of 10-30 seconds for the in-line detector).

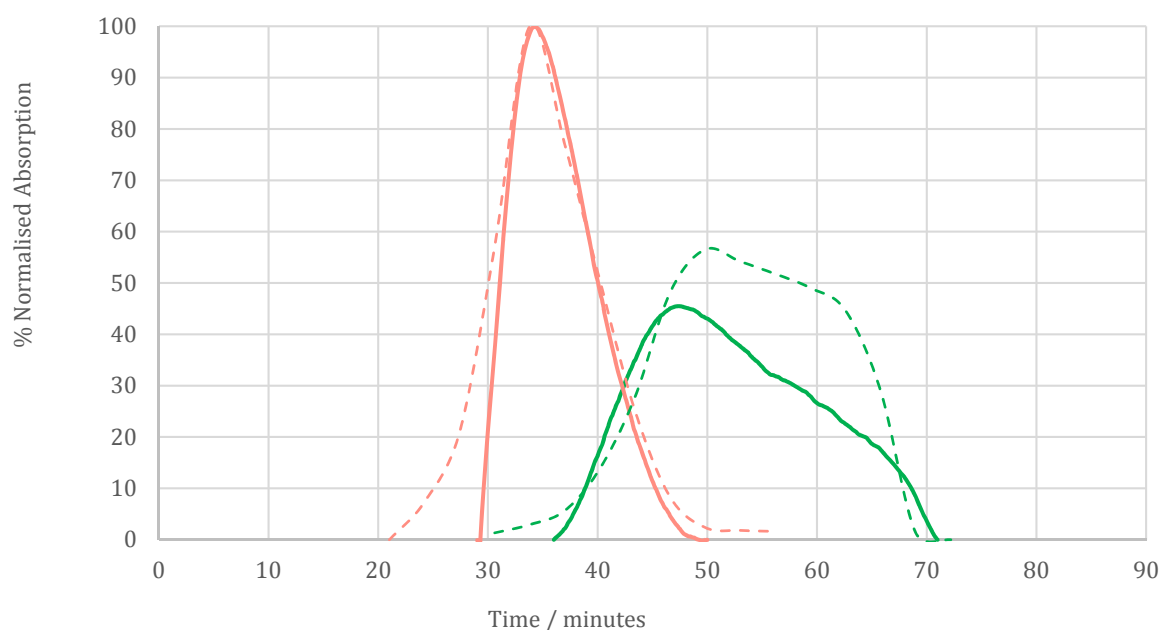


Figure 8. The chromatograms obtained for the separation of aqueous $\text{Pr}(\text{NO}_3)_3 \cdot 6(\text{H}_2\text{O})$ (0.80 g, **green** lines) from $\text{Er}(\text{NO}_3)_3 \cdot 5(\text{H}_2\text{O})$ (0.80 g, **pink** line) using a water (1000 cm^3) / $[\text{P}_{66614}]\text{Cl}$ (200 cm^3) + hexane (270 cm^3) + 3-pentanone (30 cm^3) solvent system containing 5 wt% TBPO dissolved in the stationary phase. This was carried out using Coil 2 at 890 r.p.m., at $1.00 \text{ cm}^3 \text{ min}^{-1}$ flow rate, and 50°C . The solid lines are from the online spectrometer measurements



(Figure 2) (Error = $\pm 5.0\%$) and the dashed lines are based on the offline measurement of the absorption values of the samples collected in the fraction collector (3.2 cm^3 samples per tube) and $\pm 10\%$ error.



Table 1. Table 2. The % of $\text{Pr}(\text{NO}_3)_3 \cdot 6(\text{H}_2\text{O})$ completely separated from $\text{Er}(\text{NO}_3)_3 \cdot 5(\text{H}_2\text{O})$ as determined by integration of the non-overlapping $\text{Ln}(\text{NO}_3)_3$ peaks in ILLC separations at 50 °C, 890 r.p.m. on coil 2 at various flow rates and sample loadings. The numbers in bold show the best separation obtained for the solvent system employed. Error = $\pm 5.0\%$ in integration values.

Entry	Solvent System	Mass of each $\text{Ln}(\text{NO}_3)_3 \cdot n(\text{H}_2\text{O})$ $n = 5 \text{ or } 6$	Flow Rate in $\text{cm}^3 \text{ min}^{-1}$	% Integration of completely separated salts			
				$\text{Er}(\text{NO}_3)_3$ Eluted in a Pure Form	Volume of MP Pumped for the $\text{Er}(\text{NO}_3)_3$ Peak / cm^3	$\text{Pr}(\text{NO}_3)_3$ Eluted in a Pure Form	Volume of MP Pumped for the $\text{Pr}(\text{NO}_3)_3$ Peak / cm^3
01	A1	0.80	0.5	0	38.2	32	42.1
02	A1	0.80	1.0	0	36.8	15	42.7
03	A2	0.80	1.5	0	45.5	7	47.0
04	A2	0.80	2.0	0	48.5	10	51.2
05	B1	0.80	0.5	0		3	
06	B1	0.80	1.0	0		1.5	
07	B1	0.80	2.0	0		4.0	
08	B1	0.80	3.0	0		3	
09	B1	0.80	4.0	0		44	
10	B2	0.80	1.0	9	48.9	78	59.7
11	B2	0.80	2.0	12	42.6	54	49.2
12	B2	0.80	3.0	41	54.8	88	70.7
13	B2	0.80	4.0	50	70.7	48	102.5
14	C1	0.80	0.5	0.1	33.7	2	37.9
15	C1	0.80	1.0	0.01	32.2	4	34.3
16	C1	0.80	2.0	0	36.1	41	45.5
17	C1	0.80	3.0	2		42	
18	C1	0.80	4.0	55		61	
19	C1	0.35	2.0	0		41	
20	C1	0.50	2.0	0		41	
21	C1	1.40	2.0	0		77	
22	C1	2.00	2.0	69		84	
23	C2	0.35	1.5	58		52	
24	C2	0.50	1.5	74		61	
25	C2	0.80	1.5	77		52	
26	C2	1.40	1.5	78		81	
27	C2	2.00	1.5	85		96	
28	C2	0.80	0.5	0.4		61	
29	C2 (Fig. 8)	0.80	1.0	52		58	
30	C2	0.80	2.0	78		87	
31	C2	0.80	3.0	73		85	
32	C2	0.80	4.0	68		90	
33	C2	0.80	5.0	56		82	

A1 Chromatograms

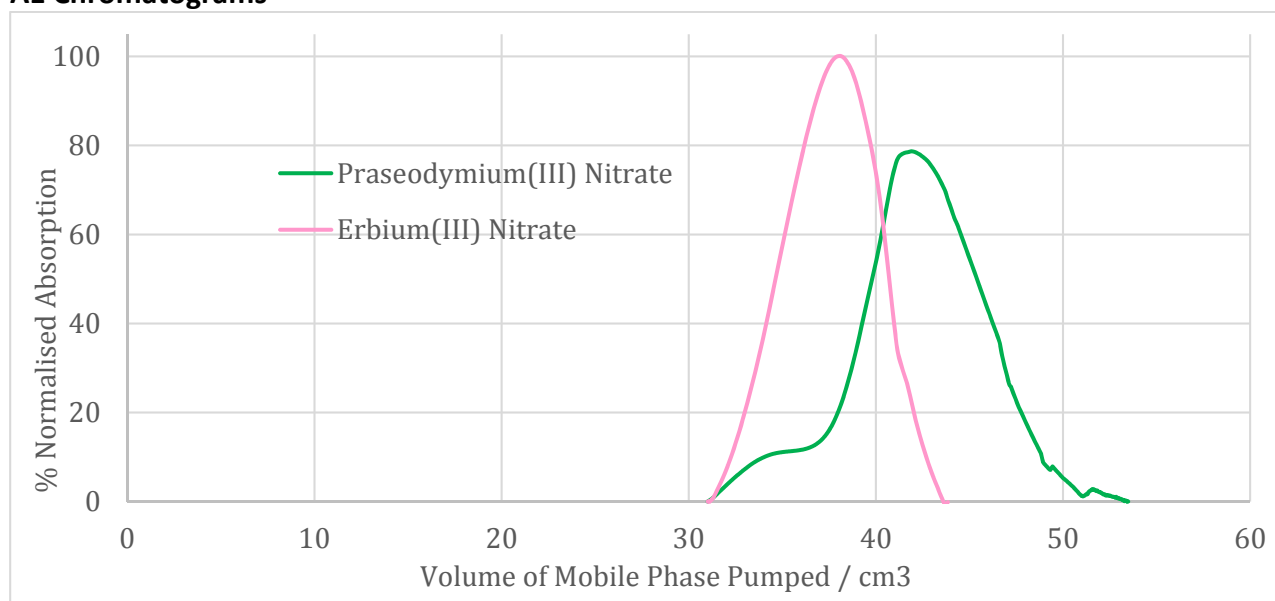


Figure A1-Entry 01, Solvent System = A1, 0.50 cm³ min⁻¹, 0.80g (Pr(NO₃)₃·6(H₂O) + 0.80g Er(NO₃)₃·5(H₂O).

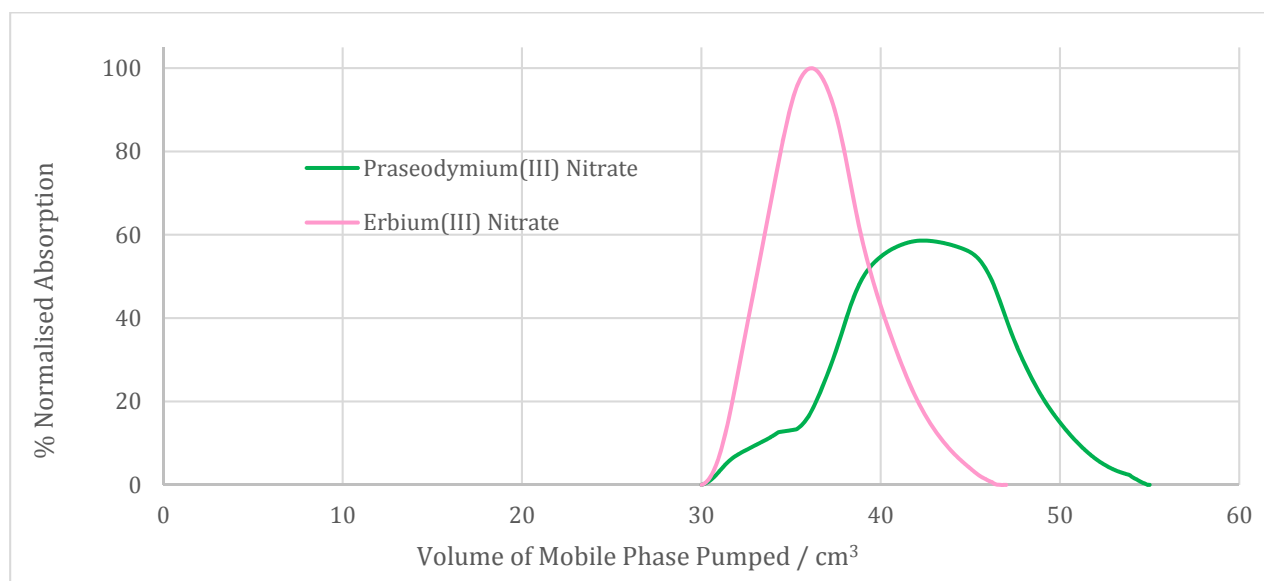


Figure A1-Entry 02, Solvent System = A1, 1.00 cm³ min⁻¹, 0.80g (Pr(NO₃)₃·6(H₂O) + 0.80g Er(NO₃)₃·5(H₂O).

A2 Chromatograms

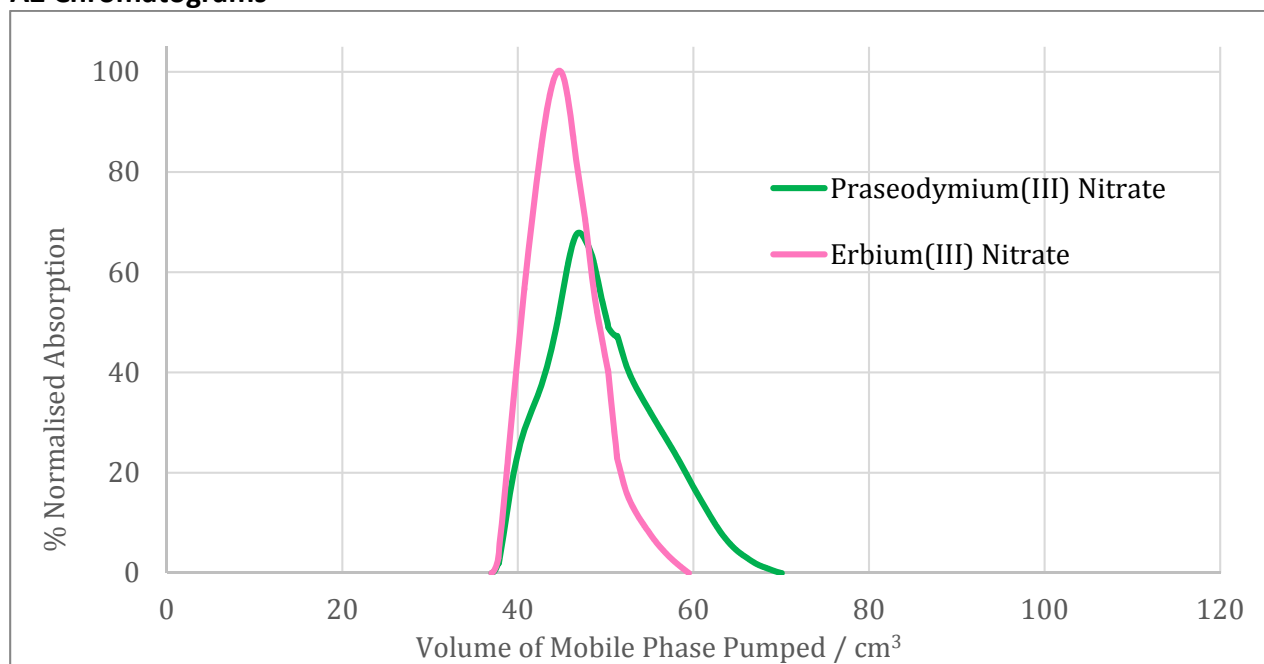


Figure A2-Entry 03, Solvent System = A2, $1.50 \text{ cm}^3 \text{ min}^{-1}$, $0.80\text{g Pr(NO}_3)_3 \cdot 6(\text{H}_2\text{O}) + 0.80\text{g Er(NO}_3)_3 \cdot 5(\text{H}_2\text{O})$.

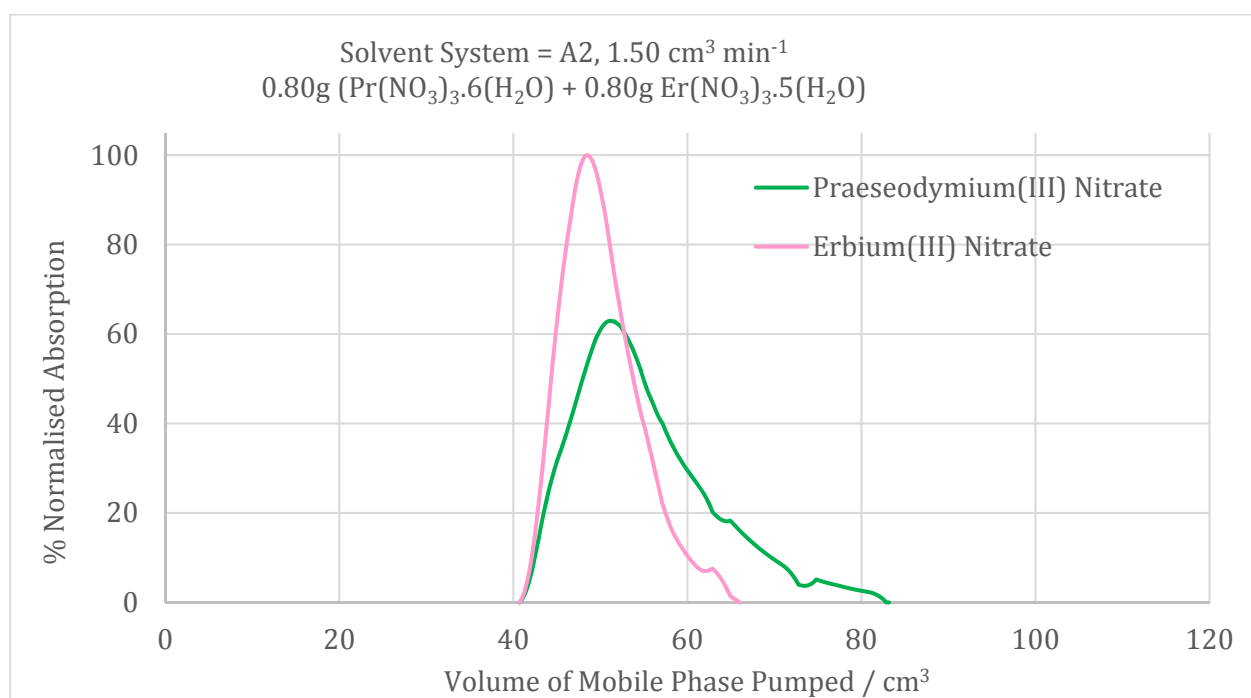


Figure A2-Entry 04, Solvent System = A2, $2.0 \text{ cm}^3 \text{ min}^{-1}$, $0.80\text{g Pr(NO}_3)_3 \cdot 6(\text{H}_2\text{O}) + 0.80\text{g Er(NO}_3)_3 \cdot 5(\text{H}_2\text{O})$.

B1 Chromatograms

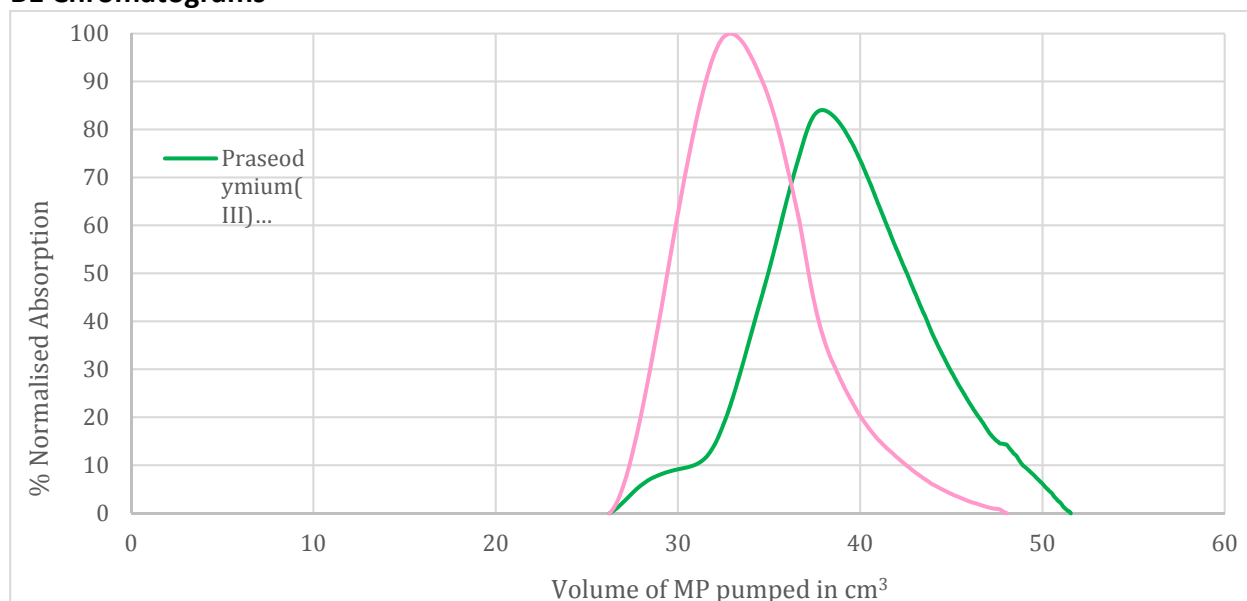


Figure B1-Entry 05, Solvent System = B1, 0.5 cm³ min⁻¹, 0.80g (Pr(NO₃)₃·6(H₂O) + 0.80g Er(NO₃)₃·5(H₂O).

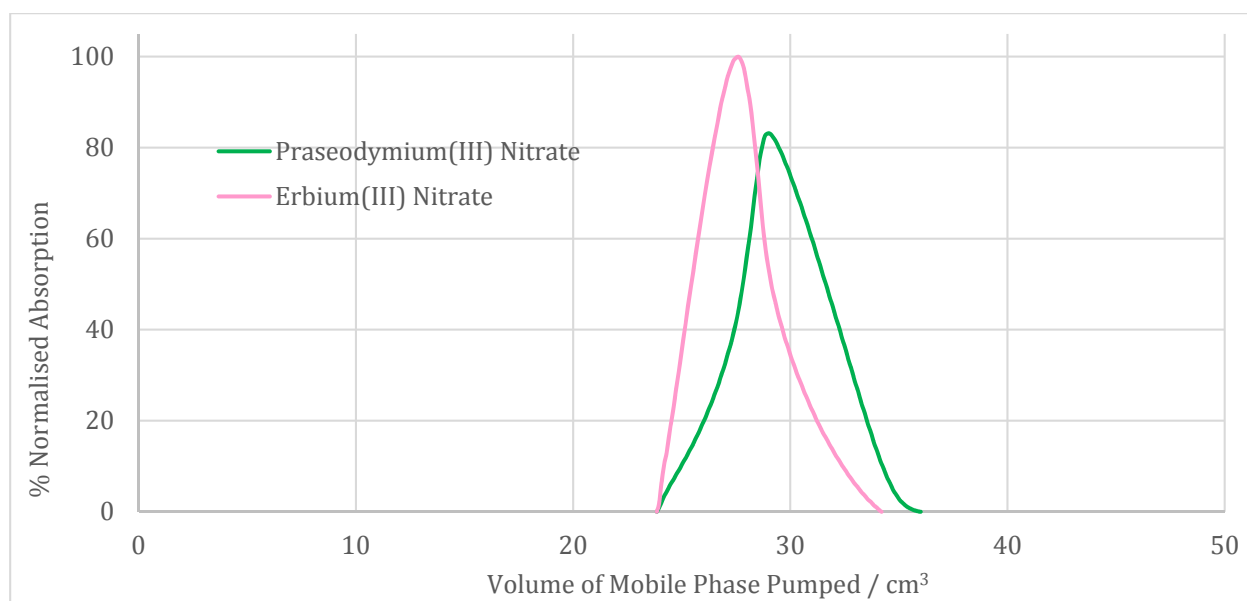


Figure B1-Entry 06, Solvent System = B1, 1.0 cm³ min⁻¹, 0.80g (Pr(NO₃)₃·6(H₂O) + 0.80g Er(NO₃)₃·5(H₂O).

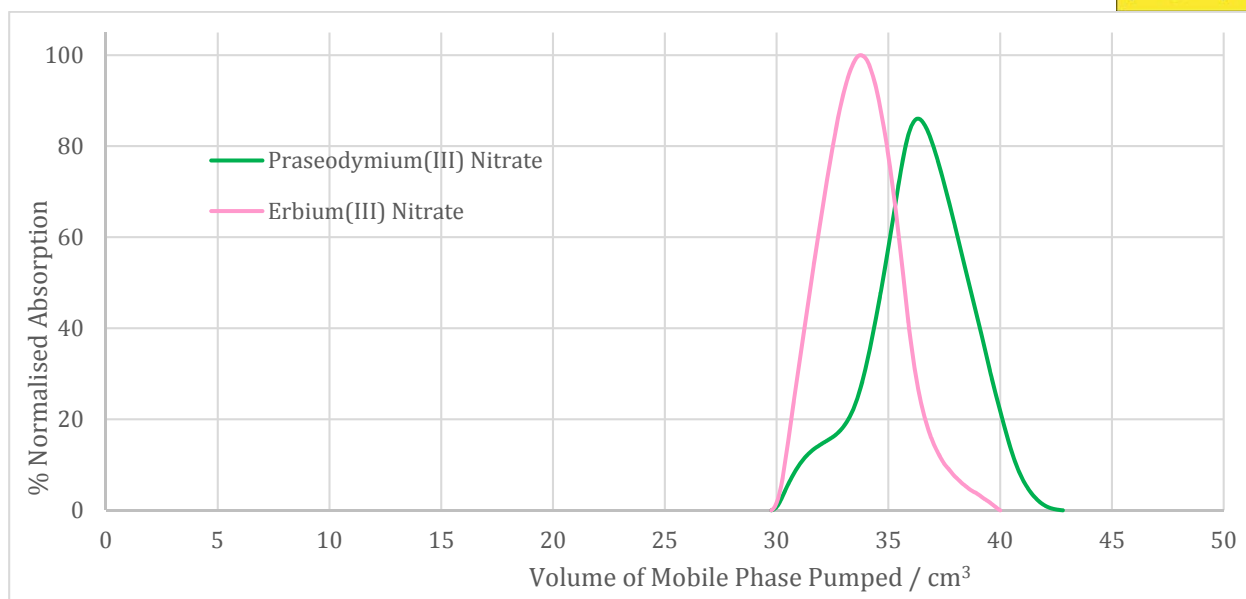


Figure B1-Entry 07, Solvent System = B1, $2.0 \text{ cm}^3 \text{ min}^{-1}$, $0.80\text{g (Pr(NO}_3)_3 \cdot 6\text{(H}_2\text{O)} + 0.80\text{g Er(NO}_3)_3 \cdot 5\text{(H}_2\text{O))}$.

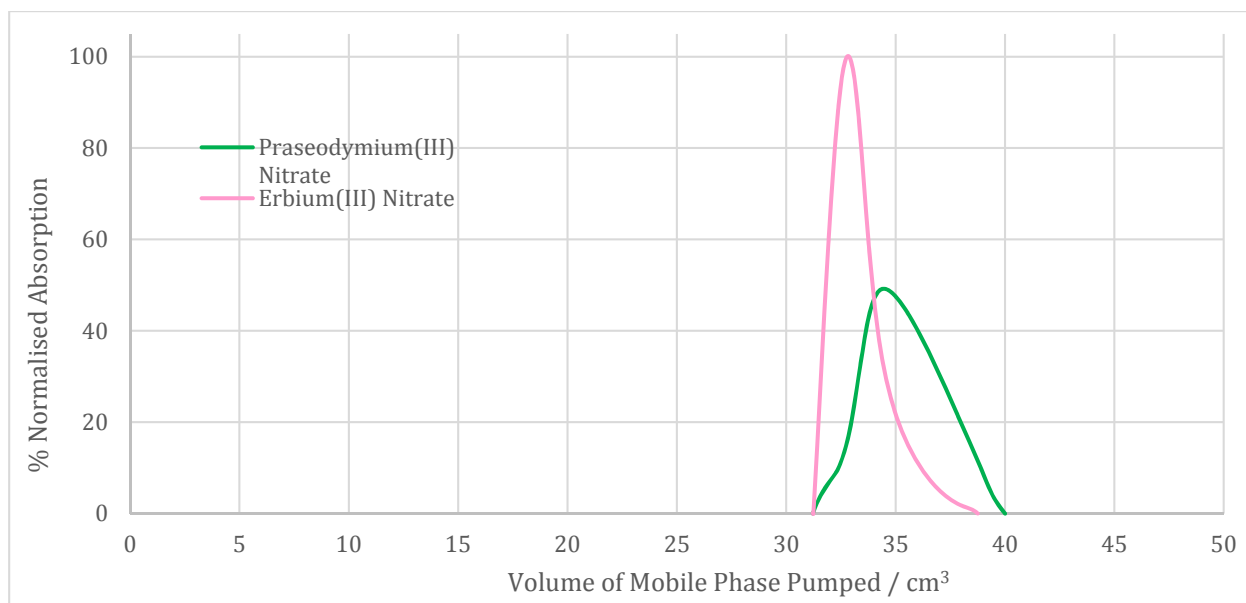


Figure B1-Entry 08, Solvent System = B1, $3.0 \text{ cm}^3 \text{ min}^{-1}$, $0.80\text{g (Pr(NO}_3)_3 \cdot 6\text{(H}_2\text{O)} + 0.80\text{g Er(NO}_3)_3 \cdot 5\text{(H}_2\text{O))}$.

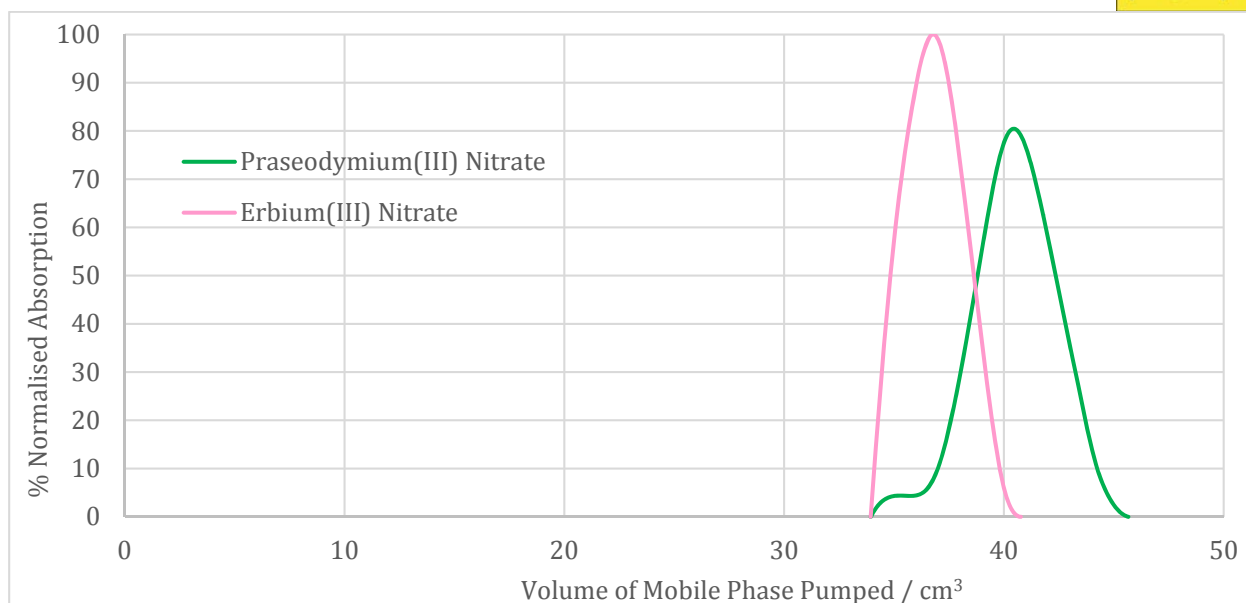


Figure B1-Entry 09, Solvent System = B1, $4.0 \text{ cm}^3 \text{ min}^{-1}$, $0.80\text{g } (\text{Pr}(\text{NO}_3)_3 \cdot 6(\text{H}_2\text{O}) + 0.80\text{g } \text{Er}(\text{NO}_3)_3 \cdot 5(\text{H}_2\text{O})$.

B2 Chromatograms

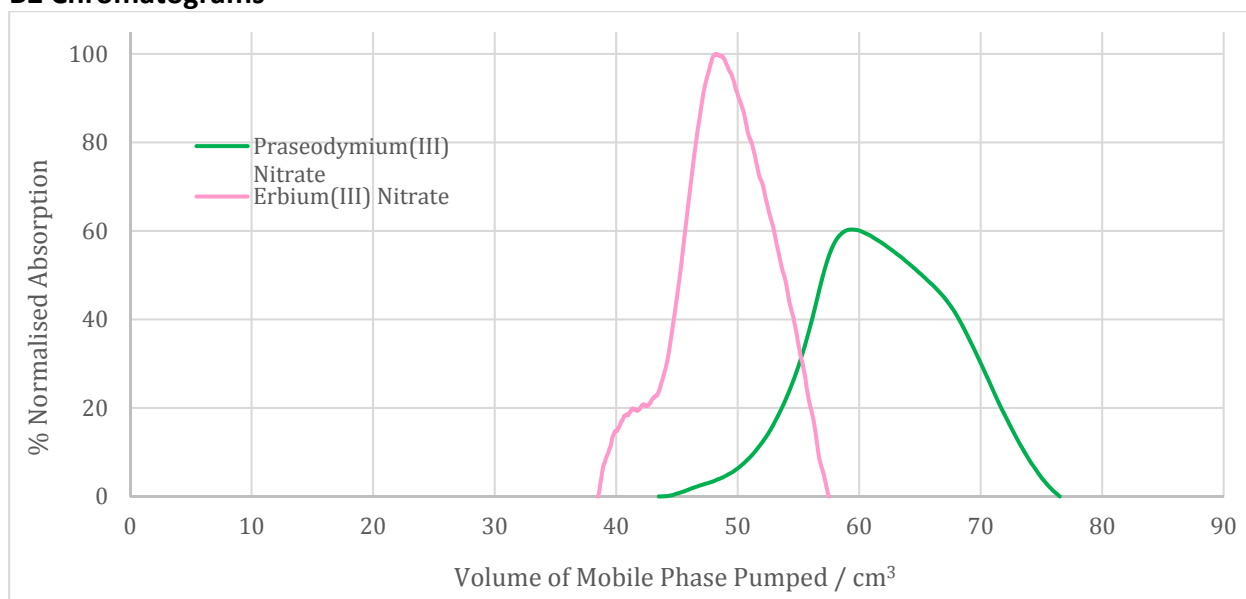


Figure B2-Entry 10, Solvent System = B2, $1.0 \text{ cm}^3 \text{ min}^{-1}$, $0.80\text{g } (\text{Pr}(\text{NO}_3)_3 \cdot 6(\text{H}_2\text{O}) + 0.80\text{g } \text{Er}(\text{NO}_3)_3 \cdot 5(\text{H}_2\text{O})$.

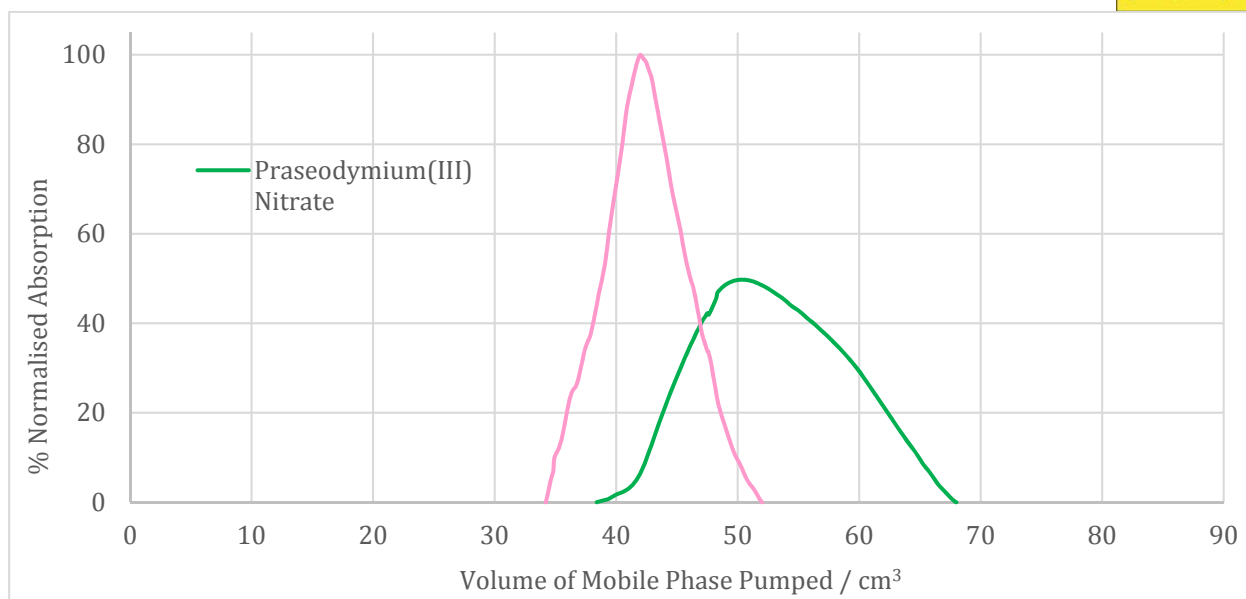


Figure B2-Entry 11, Solvent System = B2, 2.0 cm³ min⁻¹, 0.80g (Pr(NO₃)₃.6(H₂O) + 0.80g Er(NO₃)₃.5(H₂O).

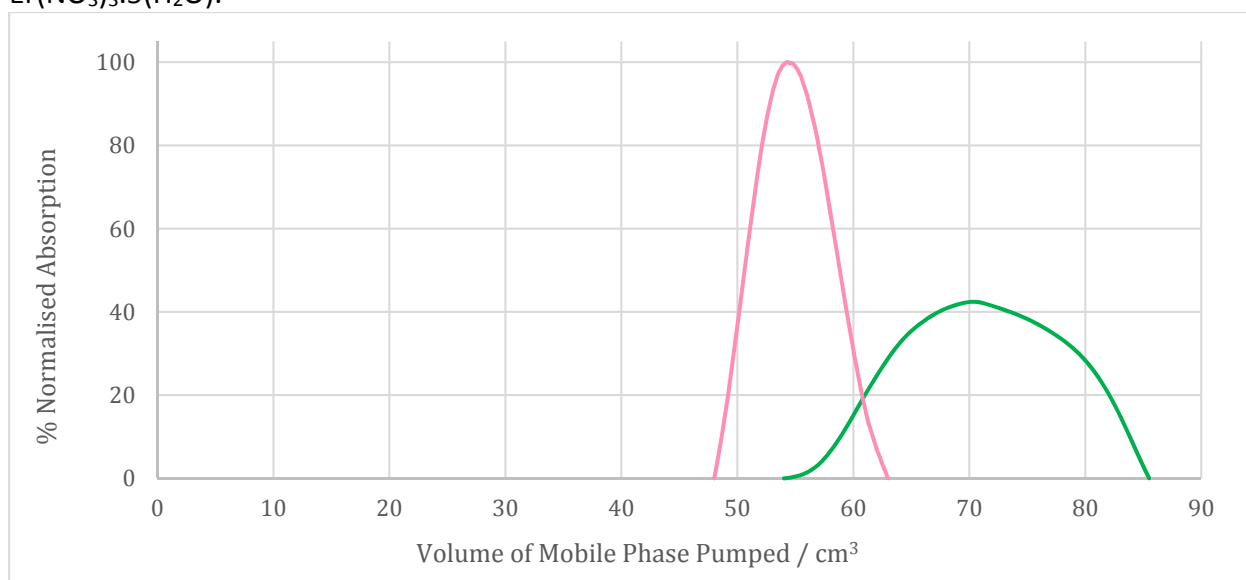


Figure B2-Entry 12, Solvent System = B2, 0.5 cm³ min⁻¹, 0.80g (Pr(NO₃)₃.6(H₂O) + 0.80g Er(NO₃)₃.5(H₂O).

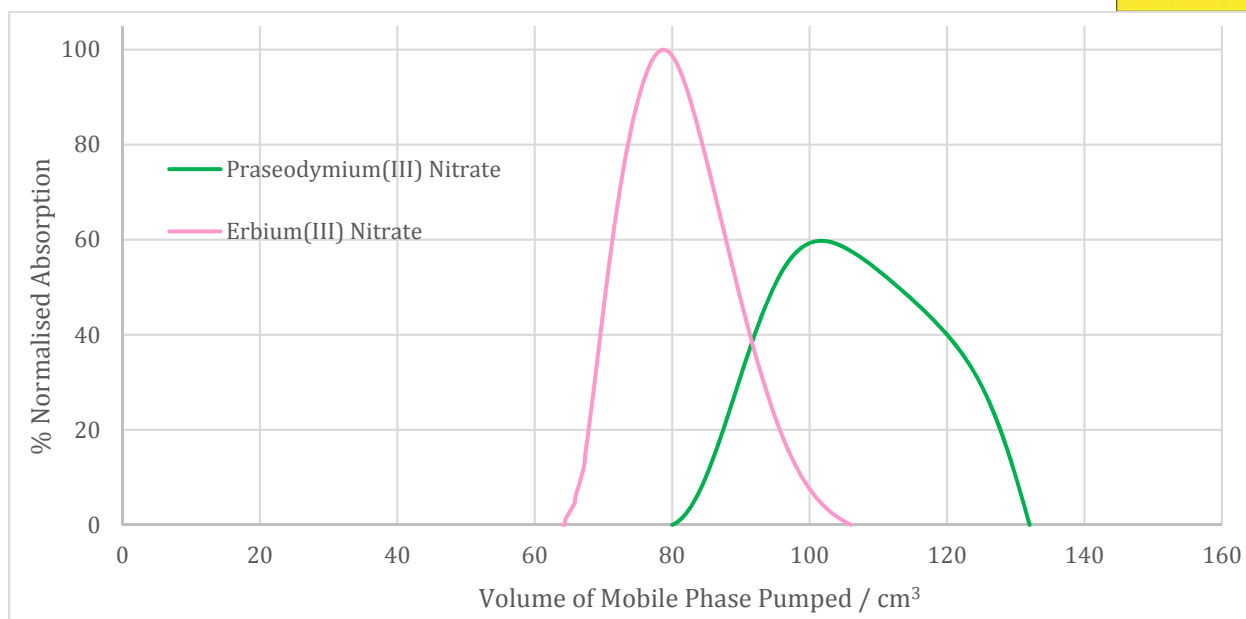


Figure B2-Entry 13, Solvent System = B2, $4.0 \text{ cm}^3 \text{ min}^{-1}$, $0.80\text{g (Pr(NO}_3)_3 \cdot 6\text{(H}_2\text{O)} + 0.80\text{g Er(NO}_3)_3 \cdot 5\text{(H}_2\text{O))}$.

C1 Chromatograms

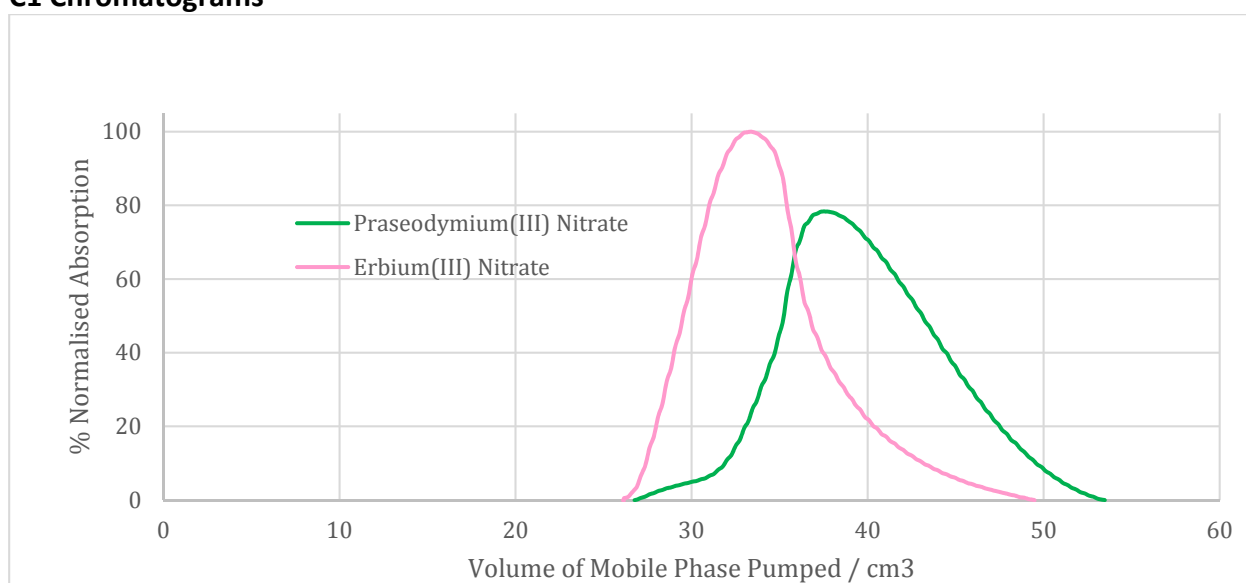


Figure C1-Entry 14, Solvent System = C1, $0.5 \text{ cm}^3 \text{ min}^{-1}$, $0.80\text{g (Pr(NO}_3)_3 \cdot 6\text{(H}_2\text{O)} + 0.80\text{g Er(NO}_3)_3 \cdot 5\text{(H}_2\text{O))}$.

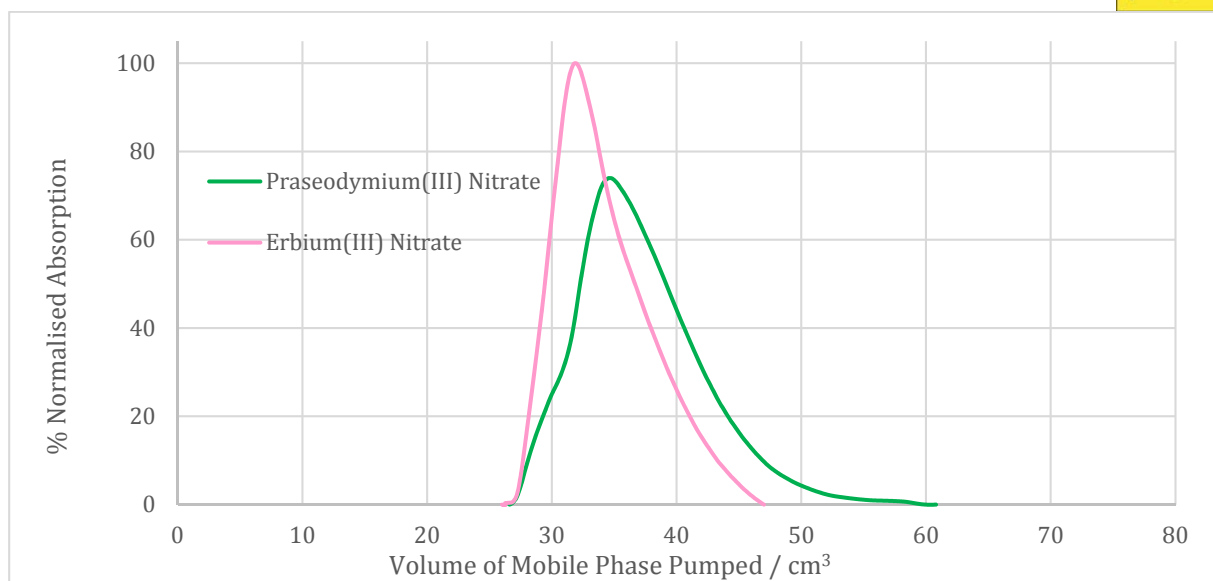


Figure C1-Entry 15, Solvent System = C1, 1.0 cm³ min⁻¹, 0.80g (Pr(NO₃)₃.6(H₂O) + 0.80g Er(NO₃)₃.5(H₂O).

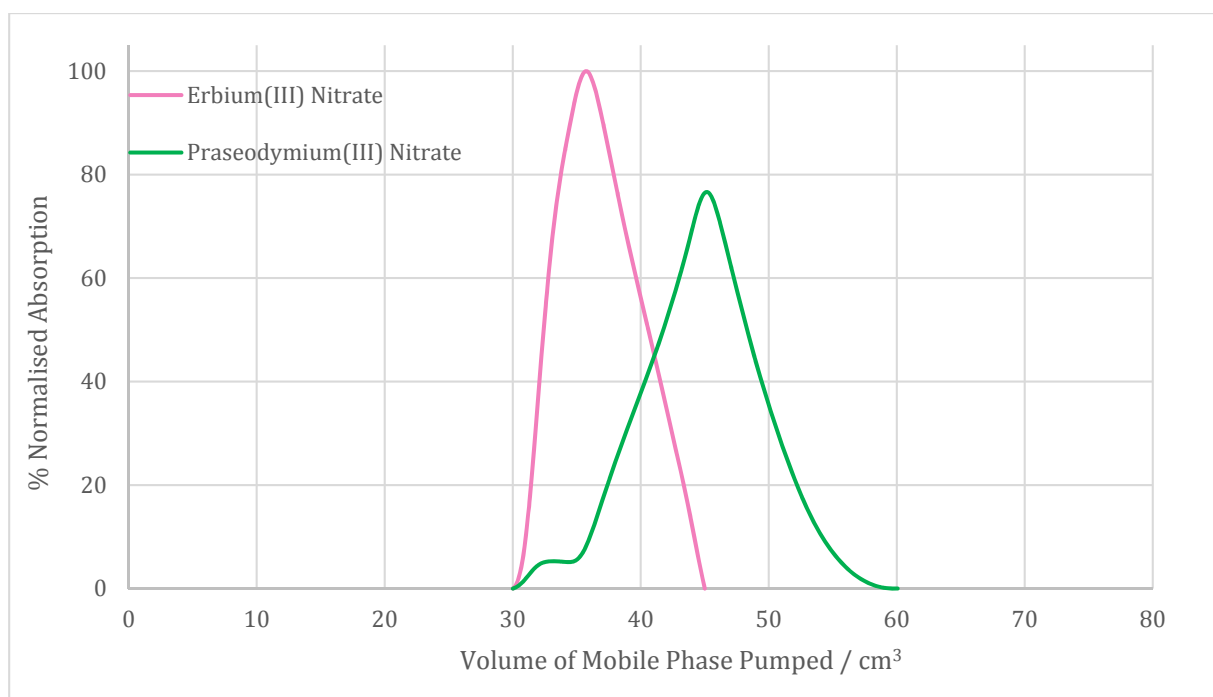


Figure C1-Entry 16, Solvent System = C1, 2.0 cm³ min⁻¹, 0.80g (Pr(NO₃)₃.6(H₂O) + 0.80g Er(NO₃)₃.5(H₂O).



QUILL Quarterly Report

November 18 - January 2019

Name:	Martin Gillespie		
Supervisor(s):	Dr P Nockemann, Dr Malgorzata Swadsba-Kwasny, Dr Stephen Glover		
Position:	PhD Student		
Start date:	01/10/2018	Anticipated end date:	30/09/21
Funding body:			

Hybrid Electrolytes for Solid-State Batteries in Electric Vehicles

Background

Petrol and diesel engines in vehicles are likely to soon become a thing of the past. Declining amounts of fossil fuels, rising atmospheric carbon dioxide levels, worsening air quality in cities and out of control climate change demand significant changes to global human behaviour.

Transitioning from fossil fuel powered transport to electric vehicles (EVs) represents a huge step in humanity taking responsibility for caused environmental deterioration and a striving to correct past poor practices.

Electric vehicles provide transport without any of the noxious exhaust emissions from traditional combustion engines. Presently the build-up of combustion fumes in traffic dense areas causes a localised reduction in life quality, an increase in respiratory diseases, numerous deaths each year as well as adding to already elevated greenhouse gas levels globally. Much of the electricity needed to charge EVs will presently be generated from burning fossil fuels at existing power plants but this energy generation can be over ten times more efficient than within a combustion engine and of course electricity for EVs can be generated from renewable energy sources resulting in very little or no detrimental effects to the environment. Due to having vastly less quantities of individual moving parts when compared to combustion engines EVs require significantly fewer the consumable components. Noise pollution is also reduced by using EVs,

The electrolyte is a vital component in secondary batteries for EVs. A poor-quality electrolyte results in a poor-quality EV. The electrolyte facilitates the transport of metal cations between electrodes during charge/discharge cycles. A highly functioning electrolyte must display some vital characteristics, these are mentioned below and the presence of these qualities within electrolytes will be the focus of this work.

Objective of this work

To improve on the current state-of-the-art electrolytes with respect to ionic conductivity, ionic transference number, electrode compatibility, stability (electrochemical, chemical and thermal), recyclability, integrity under stress and environmental impact from non-intentional cell rupture. The goal is to optimise an electrolyte formulation which can be scaled up and used directly in EVs and possibly in other energy storage entities.



Progress to date

Following on from my initial work, I have synthesised a range of electrolytes. Each electrolyte differs on its mole ratio of oligoether species and lithium bistriflimide salt ($\text{Li}[\text{TFSA}]$). Oligoether components vary both structurally and in chain length. The majority of these electrolytes are composed of a $[\text{O}]/[\text{Li}] = 4$ ratio. This ratio mimics the literature best performing electrolyte composition between the electron donating oxygen content of the organic moiety and the Lewis acidic metal cation number. There have been issues with the potentiostat so testing in a 2 /3 electrode containing glass cell system could not be done; these issues are being dealt with presently. Coin cells have been assembled containing 2 different electrolyte compositions, these have been tested and results will be reported. The oligoether and electrolytes have been tested for thermal stability by thermogravimetric analysis, results from these tests showed much lower stability than expected values. Following interpretation of ^1H and ^{13}C NMR (CD_3OD and CDCl_3) spectra and a gas chromatography mass spectrometry report impurities have been found to be present in the building blocks of the electrolytes. Highly pure electrolytes are essential for good battery function; the presence of impurities vastly reduces stabilities and cell performance due to unwanted and possibly dangerous side reactions occurring within the mixture.

My present reading is into synthesis of structural isomers of glyme oligoether molecules from a bio-derived starting material and the purification methods best suited for each electrolyte component. I am awaiting delivery of apparatus and chemicals with which to begin exploring the potential along this avenue of study.

Conclusions and future work

The importance of high purity materials in this system has been proven to be of utmost importance; to this end all electrolyte building blocks will be as pure as possible before use. My present work is on the purification of any oligoethers supplied and on the conversion of bio-derived starting materials into highly pure structural isomers of straight chain glyme molecules. Extensive testing will then be carried out on electrolytes built in this manner and the potential of each evaluated. Coin cell composition and build sequence will be varied to investigate optimum arrangement. It is hoped that various metal salts will be available for testing within the new systems and the effects of their use observed and reported.

QUILL Quarterly Report

November 2018 – January 2019

Name:	Oliver Hammond		
Supervisor(s):	Marijana Blesic		
Position:	Postdoctoral Research Fellow		
Start date:	1/11/18	Anticipated end date:	31/10/19
Funding body:	EPSRC		

Exploring the potential of zwitterionic salts

Background

One of the biggest problems encountered at any interface with biological substances is the undesired and uncontrolled adsorption of protein, which is known as fouling.¹ The properties of zwitterionic materials, principally their superhydrophilicity, makes them ideally-suited to be used as interfacial coatings to form ultralow-fouling surfaces which selectively resist the formation of these protein coatings.² Zwitterionic materials have accordingly found myriad applications where this is advantageous such as hydrogels for cell culture, and protein-resistant coatings for nanoparticles and biomedical devices such as catheters, notwithstanding their widespread application in contact lenses, and even as zwitterionic liquids.³ In all of these applications the unique properties of zwitterions means that they are far more effective than traditional non-zwitterionic polymers such as PEG.⁴ As well as the selective resistance of zwitterionic surfaces towards nonspecific aggregation of proteins, it is possible to design preferable interactions towards certain substrates, creating a surface which repels all but the object of desire, which have been dubbed ‘romantic surfaces’.⁵

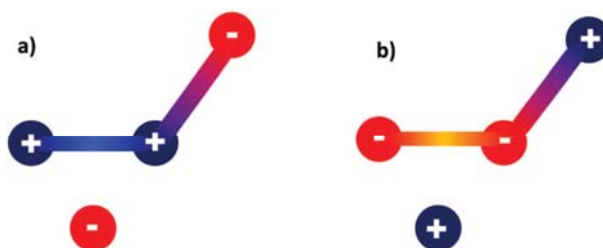


Figure 1. Cartoon examples of the structure of ‘Zwitterionic Salts’ (ZWS). A ZWS is formed when either the cation (a) or anion (b) of a binary salt contains an odd number of formal charges, leaving one unit of charge effectively unpaired. This makes them distinct from traditional salts, zwitterions, and polyelectrolytes.

This work is concerned with the so-called ‘Zwitterionic Salts’ (ZWS), which are a category of asymmetrically-charged compounds containing a formal cation and anion, where one of these units has an embedded zwitterion, shown in Figure 1.⁶ As a relatively recent discovery, the scope, properties and potential applications of ZWS has not been explored.⁷ This project therefore integrates several goals with the overall aim of developing further the fundamental understanding



of ZWS and establishing their potential for future applications. Firstly, it is intended to synthesise some novel zwitterionic materials, and expand the current library of known compounds to further understand structure-property relationships. Then, the physical properties of the synthesised ZWS will be measured, with emphasis on solution-phase interactions. This analysis will primarily focus on interpretation of neutron diffraction data using atomistic modelling, for alkyl-diammonium-bromide-sulfonate ZWS and novel dizwitterionic bolaforms (see Figure 2) with different alkyl spacer lengths, giving insight into properties and interactions of these different zwitterionic species with biomolecules. These advanced measurement techniques will be complemented by measurements of solution physical properties (ie. viscosity, surface tension and excess molar volume measurements) and *ab initio* computational chemistry methods. Following this, methodology will be developed for the preparation of new surfaces coated with ZWS-based materials, and the hypothesis that ZWS will form effective protein-resistant coatings will be tested using techniques such as AFM and QCM.

Objectives of this work

- Devise preparations for new zwitterionic materials and determine their bulk solution properties, particularly ZW-water interactions (ie. H-bonding), with neutron scattering and modelling techniques and measurements of physical properties and phase behaviour.
- Develop methodology for ZWS-coated surfaces to assess whether more efficient protein-resistant surfaces can be prepared, for potential applications in biomedical devices or antifouling marine coatings.

Progress to date

In my first few months I have explored the synthesis of new zwitterionic materials. Current examples are based on a two-step synthesis, with a first alkylation of *N,N,N',N'*-tetramethylethylenediamine (TMEDA) with an alkyl bromide, and subsequent alkylation with either 1,3-propanesultone or acrylic acid to form a cationic ZWS with 1° ethyl, butyl or hexyl chains, a sulfonate or carboxylate headgroup, and a bromide counterion. Therefore, new syntheses are being designed to prepare analogous examples with a chloride counterion to obtain lower-toxicity materials. A series is also being prepared with different lengths of alkyl chain between the ammonium ions. Previous examples using TMEDA showed selective monoalkylation in the first step, but the longer alkyl chains in TMPDA or TMHDA (propyl and hexyl spacers) have been found to preferentially form the dialkylated product. It is hypothesised that this is because the N lone pair in the monoalkylated TMEDA product becomes less available due to inductive effects after the initial alkylation which forms an ammonium cation, but this does not occur in TMPDA or TMHDA due to the alkyl chain length, and selectivity is lost. Additionally, the dialkylated product appears to become favoured in alkyl chloride reactions, even for TMEDA, seemingly due to the long reaction time and high temperature necessitated by the lower alkylation activity of chloroalkanes. Therefore, these syntheses are still subject to further optimisation.

A new family of bolaform dizwitterions based on TMEDA, TMPDA and TMHDA di-sulfonates have been successfully synthesised, shown in Figure 2, and characterisation shows very high purity; these will be taken for neutron measurements in the SANDALS instrument in March. Some physical property measurements have been conducted of the prepared materials, following the expected trends (eg. viscosity-concentration dependence), though to some extent this exploration has been limited by lack of access to suitable analytical equipment in the group, which will hopefully be resolved in the coming weeks with the arrival of new instrumentation for surface tension and viscosity measurements. Significant progress has also been made on analysis of neutron scattering data for a zwitterionic salt, which was measured last year, prior to my arrival in QUILL. The models were re-parameterised to improve quality-of-fit which was insufficient at first pass; these models are now accumulating statistics to ultimately extract atomistic data on the interactions of zwitterionic salts in aqueous solution. We have also commenced quantum chemical modelling of the zwitterionic materials to provide complementary information on eg. solvation to enhance fundamental insights from experiments.

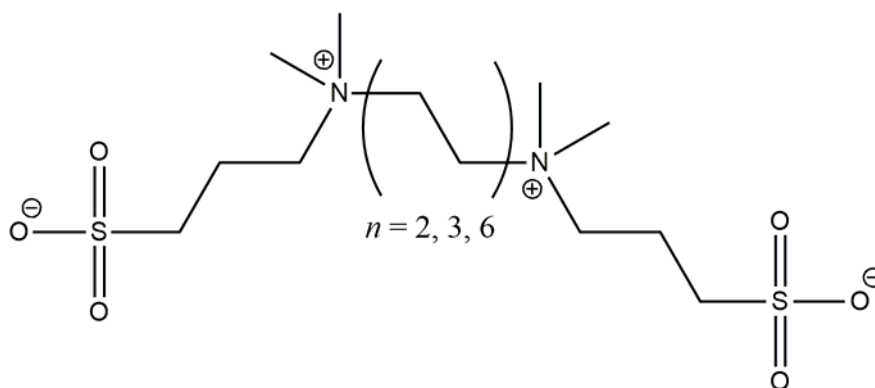


Figure 2. Structure of the bolaform dizwitterionic species synthesised for neutron scattering measurements to take place in March. The synthesis is a diquaternisation of either TMEDA, TMPDA or TMHDA using 1,3-propanesultone.

Conclusions and future work

The successful synthesis of a new family of bolaform dizwitterions based on TMEDA, TMPDA and TMHDA di-sulfonates is important as these will be taken to ISIS Neutron & Muon Source in March for neutron scattering measurements of their solution-state structure. This will provide valuable information on the solvation and interactions of these interesting biomimetic zwitterionic species with biomolecules. While attempted synthesis of ZWS with new structures has been unexpectedly unsuccessful, the optimisation of these new syntheses will continue. Once new equipment has been set up in our lab (surface tension and viscometer) physical properties of these solutions can be measured. Then, the next logical step is to begin the preparation of ZWS-based surfaces and assess the performance of these materials as protein-resistant surfaces.



References

- (1) Blaszykowski, C.; Sheikh, S.; Thompson, M. Surface Chemistry to Minimize Fouling from Blood-Based Fluids. *Chem. Soc. Rev.* **2012**, *41* (17), 5599–5612. <https://doi.org/10.1039/c2cs35170f>.
- (2) Kane, R. S.; Deschatelets, P.; Whitesides, G. M. Kosmotropes Form the Basis of Protein-Resistant Surfaces. *Langmuir* **2003**, *19* (6), 2388–2391. <https://doi.org/10.1021/la020737x>.
- (3) Wu, B.; Kuroda, K.; Takahashi, K.; Castner, E. W. Structural Analysis of Zwitterionic Liquids vs. Homologous Ionic Liquids. *J. Chem. Phys.* **2018**, *148* (19), 193807. <https://doi.org/10.1063/1.5010983>.
- (4) Callow, J. A.; Callow, M. E. Trends in the Development of Environmentally Friendly Fouling-Resistant Marine Coatings. *Nat. Commun.* **2011**, *2* (1), 210–244. <https://doi.org/10.1038/ncomms1251>.
- (5) Baggerman, J.; Smulders, M. M. J.; Zuilhof, H. Romantic Surfaces: A Systematic Overview of Stable, Biospecific, and Antifouling Zwitterionic Surfaces. *Langmuir* **2019**, *35* (5), 1072–1084. <https://doi.org/10.1021/acs.langmuir.8b03360>.
- (6) Blesic, M.; Gilmore, B. F.; Holbrey, J. D.; Jacquemin, J.; Level, G.; Nockemann, P.; Stella, L. An Introduction to Zwitterionic Salts. *Green Chem.* **2017**, *19* (17), 4007–4011. <https://doi.org/10.1039/c7gc01523b>.
- (7) Level, G.; Vieira Fadul, M.; Blesic, M. Solubility-Modifying Power of Zwitterionic Salts. *ChemPhysChem* **2018**, *19* (5), 575–580. <https://doi.org/10.1002/cphc.201701229>.



QUILL Quarterly Report

November 2018 – January 2019

Name:	John Keogh		
Supervisor(s):	Haresh Manyar, Peter Robertson		
Position:	PhD Student		
Start date:	08/01/2018	Anticipated end date:	08/01/2021
Funding body:	Bryden Centre		

Adding Value to Waste Glycerol to produce Renewable Fuels and Chemicals

Background

Glycerol is a 10 wt % by-product from the production of biodiesel. It is important for the economic viability of the biodiesel industry to find ways to add value to this waste by-product, to generate renewable fuels and chemicals and promote a circular economy. One potential route of value addition is through the esterification of glycerol with acetic acid to give glycerol esters. The di- and tri- substituted glycerol esters being of particular interest due to their use as oxygenated fuel additives. These products can then be blended back in with the biodiesel to improve its fuel qualities.

Objective of this work

The objective of this work was to investigate the ability of a number of Bronsted acidic ionic liquids to catalyse the esterification reaction. With a view of producing higher yields of di- and triacetin.

Progress to date

A number of ionic liquids based on alkylpyrrolidone and trialkylamine cations with hydrogen sulfate anions were synthesised. The length of the alkyl chain length was varied on the cations. It was found that [H-NMP]HSO₄ was the most active catalyst. Catalysts based on the alkylpyrrolidone cation were more effective than those based on the trialkylamine cations. DoE was used to optimise the reaction conditions in order to maximise the yield of the di and tri substituted products.

Conclusions and future work

Using [H-NMP]HSO₄ as a catalyst a combined yield of di- and tri-acetin greater than 95 % was achieved after 1 hour, with glycerol conversion of 99 %. The catalyst was recycled 3 times, without significant loss of activity and slight difference in product distribution, possible due to slight loss of the catalyst during separation. Following this my work will diverge away from ionic liquids and will investigate the use of supported heteropolyacids in catalysing this reaction.



QUILL Quarterly Report

November 2018 – January 2019

Name:	Yongdi Lou (Dean)		
Supervisor(s):	Dr. John Holbrey		
Position:	MPhil of Chemical Engineering		
Start date:	01-10-2018	Anticipated end date:	31-12-2019
Funding body:	-		

IL as Dissolution System for Preparing Graphene/Cellulose Based Materials

Background

Cellulose is considered to be environmental-friendly polymers, it is extremely easy to obtain in most plants and the total amount is abundant. It has excellent properties such as mechanical robustness, hydrophilicity, biocompatibility, and biodegradability. More importantly, because of dense hydrogen bonding, it has a severe problem of difficult-to-process. Recently, room-temperature ionic liquids, which are considered as desirable green solvents, have been reported to be effective and promising cellulose solvents. Owing to their advantages, such as excellent dissolving capability, negligible vapour pressure, recyclability, and variety of structure, this class of new cellulose solvents has attracted considerable attention and has been used to prepare different regenerated cellulose materials and cellulose composites. Meanwhile, graphene continues to play an important role in many fields such as carbon nano-materials because of its unique optical, electrical, mechanical, and structural properties. The large delocalized π -electron system and high theoretical specific surface area of graphene make the material suitable for electronic composites or adsorbent/thermal conduction materials. Therefore, our research on such composites with an advanced solvent system has a very broad prospect.

Objective of this work

The solubility characteristics of cellulose in different ionic liquids should be studied and summarized. Combined with the characterization of the prepared materials, one or several ionic liquids should be screened out as an excellent dissolution system for preparing cellulose materials. Find the most promising application direction by studying the properties and characterization of cellulose composites. After the application direction is determined, the synthetic route of the cellulose composites should be optimized to improve the material properties.

Progress to date

1. IL preparation and synthesis

- Preparation of general ionic liquids including $[C_4mim]Cl$, $[C_4mim][OAc]$ according to literature steps.
- Preparation of Dialkyl-phosphate anion ionic liquids using microwave reactor *Monowave 400*. Constant power with multiple times heating is used in the program setting which ensures that the



reaction proceeds quickly in selected temperature ranges and moderate pressure conditions, greatly reducing reaction time compared to conventional heating methods. Synthetic IL: [C₄mim][DMP] (DMP: Dimethyl-phosphate), [C₂mim][DMP], [C₁mim][DMP], [C₄mim][DBP] (DBP: Dibutyl-phosphate).

2. Preparation of Graphene Oxide (GO) according to Hummer's method.

3. Cellulose, Cellulose/GO composite dissolve in different solvent systems and regenerate in distillation water, the obtained hydrogel is dried into aerogel by different drying methods.

i). Dissolution rate compares: [C₁mim][DMP] shows the fastest rate, [C₂mim]Cl & [C₂mim][DMP] in the middle range, [C₄mim]Cl takes a long period till dissolve completely. [C₄mim][DBP] can hardly dissolve cellulose. All dissolution processes take place in 90-100°C, normal pressure condition. Repeated literature experiment, non-IL dissolution system NaOH/urea (aq.) can dissolve cellulose at a temperature of -12°C, but regenerated hydrogel is shapeless.

ii). Tried different regeneration methods, obtained different shapes of hydrogel.

iii). Adjusted GO mass presents in GO/cellulose composite from 0.5% to 5%.

iv). Solvent regeneration with water evaporation and vacuum distillation.

4. Preparation of composite film by using coating machine *RK K Control Coater* and immerse in distillation water to regenerate.

5. Tests conducted so far.

i). NMR tests for Dialkyl-phosphate anion ionic liquids structural presumption.

ii). FT-IR tests for composition and functional group determination of Cellulose and Cellulose/GO aerogels.

iii). SEM tests for synthesized composites morphology display.

iv). Auxiliary tests (eg: Chloride contents tests) submitted to and finished by ASEP.

Conclusions and future work

1-Alkyl-3-Methylimidazolium Dialkyl-phosphate with short alkyl chain (C₁~C₂) has great solubility to cellulose, and the use of microwave-assisted reaction can greatly reduce the time required to synthesize such ILs.

Future work

1. Reduction of Cellulose/GO composite by using ascorbic acid and L(+)-Cysteine to determine the best materials reduction method.

2. Further process hydrogel materials by freeze-drying, compare the difference with the materials processed by the aforementioned drying method.

3. Further testing including but not limited to BET, TGA to explore materials characterization.

4. Determine the main application route for composites.

QUILL Quarterly Report

November- January 2019

Name:	Peter McNeice		
Supervisor(s):	Dr Andrew Marr, Dr Patricia Marr		
Position:	PhD student		
Start date:	October 2016	Anticipated end date:	July 2020
Funding body:	QUILL IAB		

Base Stable and Basic Ionic Liquids

Background

The imidazolium cation is the most common cation in ionic liquids due to its acid stability, thermal stability and oxidative stability.¹ Unfortunately, it can be extremely sensitive to base. The most acidic position is the C2 proton which deprotonates to form a carbene (Figure 1). The instability of the C2 position in base was demonstrated in 1964 with heavy water buffers causing deuteration at the C2 position.² The acidity of this proton limits the use in base catalysed reactions. This has been investigated by Aggarwal *et. al.*³ who found that [BMIM][Cl] was deprotonated to form a carbene which went on to attack the aldehyde component of a Baylis-Hillman reaction, reducing the yield. They found that bases with pK_a as low as 8 or 9 could generate a carbene.

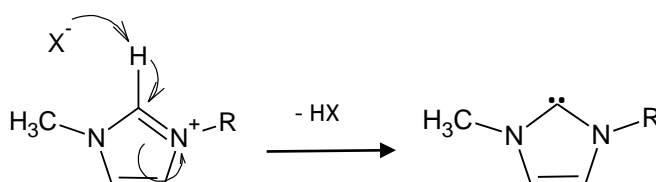


Figure 1: Deprotonation of an imidazolium cation to form a carbene. X^- can be the anion or a base.

When an ionic liquid is able to catalyse a reaction, it is called a functionalised ionic liquid (FIL), previously known as task specific ionic liquids (TSIL).⁴ These materials can be created due to the tuneable properties of ionic liquids and have the potential to cut down on auxiliary stoichiometric catalysts and prevent the formation of salts.

Ionic liquids can be basic due to the presence of a Brønsted basic (proton accepting) anion. Examples include ionic liquids with OH^- ,⁵ imidazolate ([Im]⁻),⁶ carboxylate,^{7,8} amino acids⁹ and dicyanamide ([DCA]⁻)¹⁰ as anions (Figure 2).

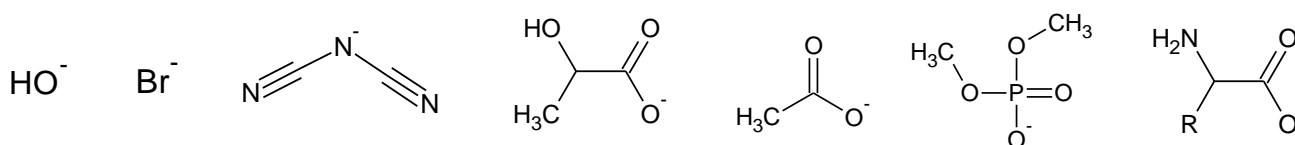


Figure 2: Some Brønsted basic anions for ionic liquids.

Ionic

liquids with basic anions often suffer from instability. The anion is able to attack the cation to form two neutral species as shown in Figure 1. Strong bases such as halide ions and OH^- in particular suffer from this effect.

Heterogenising ionic liquids can increase their stability and allows for simple separation of the ionic liquid catalyst from the reaction mixture. Hydrotalcites (layered double hydroxides) are clay-like materials with the general formula $[M^{II}_{1-x}M^{III}_x(OH)_2]^{x+}(A^{n-})_{x/n} \cdot mH_2O$ where M^{II} and M^{III} are di and tri-valent metal ions which form the outer layers. A^- is an inter-layer ion such as Cl^- , $(CO_3)^{2-}$, $(NO_3)^-$ or $(SO_4)^{2-}$ (Figure 3).¹¹ Hydrotalcites have found use in catalysis,¹² polymer science¹³ and electrochemistry,¹⁴ amongst other applications.¹⁵ The interlayer anions can be exchanged by ion exchange which allows them to be intercalated by ionic liquid anions, immobilising the ionic liquid within the clay structure.¹⁶

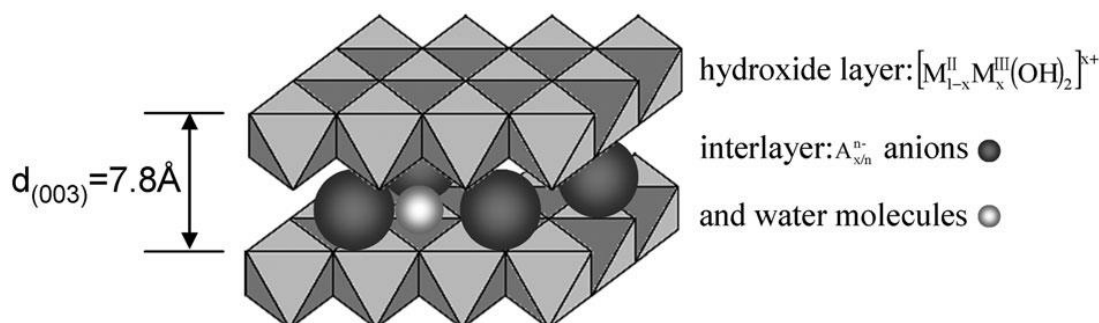


Figure 3: Structure of hydrotalcite, reproduced from Zhao *et. al.*¹⁷

Objective of this work

The overall aim of this project is to synthesise functionalised ionic liquids which are base stable and basic. Basic ionic liquids will be able to act as both solvent and catalyst for reactions, which will eliminate waste. Stability is key for catalysis as well as recovery of the ionic liquid.

Progress to date

A previous report showed that $[P_{66614}][O^iPr]$ was stable in solution but when combined with $[P_{66614}][C_8SO_3]$ and isolated the ionic liquid began to decompose.¹⁸ Combinations of these ionic liquids in solution were used to make a series of ionic liquid supported Mg-Al hydrotalcites (IL-HT). The aim was to improve the stability of the basic phosphonium ionic liquids and to allow for their easy recycle. $[P_{66614}][O^iPr]$ solution and $[P_{66614}][C_8SO_3]$ were combined in to give different ratios of $[C_8SO_3]^-$ and $[O^iPr]^-$ anions. The solution was added to hydrotalcite (20 wt. % IL), suspended in MeOH and refluxed for 18 hours. The suspension was then filtered under suction and washed with MeOH to leave white flakes. XRD analysis (Figure 4) indicates that the ionic liquid has become intercalated within the hydrotalcite layers. The IL-HT have increased crystallinity moving from unmodified hydrotalcite to $[P_{66614}][C_8SO_3]$ -HT, shown by the sharpening of the peak at 24° for hydrotalcite. There is also a slight increase in basal (layer) spacing seen by the shift to a lower angle. This is due to incorporation of the long-chain $[C_8SO_3]^-$ anion between the layers and is consistent with literature.¹⁶ Interestingly, incorporating both $[C_8SO_3]^-$ and $[O^iPr]^-$ anions further increases the basal spacing to a similar value with the peak shifting from 24° to $22-23^\circ$. The crystallinity of these IL-HT appears to increase from $[P_{66614}][C_8SO_3]_{0.9}[O^iPr]_{0.1}$ -HT to $[P_{66614}][C_8SO_3]_{0.74}[O^iPr]_{0.26}$ -HT and then decreases from $[P_{66614}][C_8SO_3]_{0.74}[O^iPr]_{0.26}$ -HT to $[P_{66614}][C_8SO_3]_{0.48}[O^iPr]_{0.52}$ -HT. This is seen from the decrease in intensity and sharpness of XRD peaks which tends to indicate a decrease in crystallinity.¹⁹

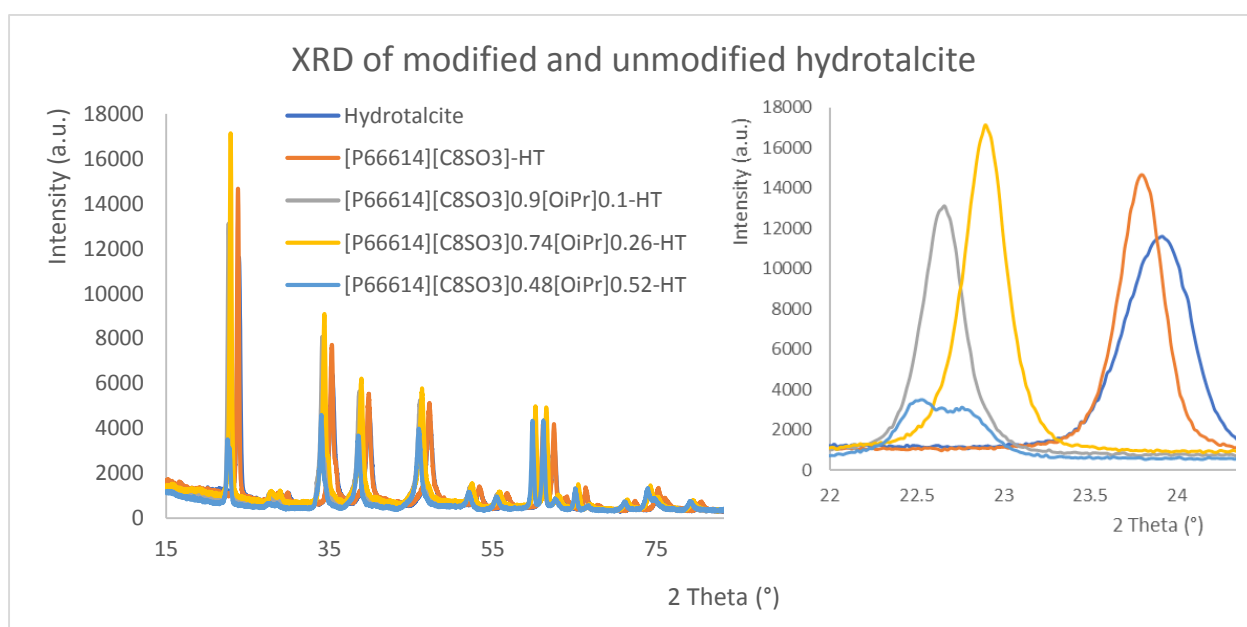


Figure 4: XRD diffraction pattern of modified and unmodified hydrotalcites between $15-90^\circ$, and inset $22-25^\circ$.

TGA and BET data (Table 1) show some correlation with XRD data. The IL-HTs with greater basal spacing ([P₆₆₆₁₄][C₈SO₃]_{0.9}[OⁱPr]_{0.1}-HT, [P₆₆₆₁₄][C₈SO₃]_{0.74}[OⁱPr]_{0.26}-HT and [P₆₆₆₁₄][C₈SO₃]_{0.48}[OⁱPr]_{0.52}-HT) display a larger pore size (Table 1 entries 3, 4, 5) than [P₆₆₆₁₄][C₈SO₃]-HT and hydrotalcite (Table 1 entries 1, 2) which had a lower basal spacing. The greater pore size of [P₆₆₆₁₄][C₈SO₃]_{0.9}[OⁱPr]_{0.1}-HT and [P₆₆₆₁₄][C₈SO₃]_{0.74}[OⁱPr]_{0.26}-HT (Table 1 entries 3, 4) may be the reason for the lower surface area of these catalysts. [P₆₆₆₁₄][C₈SO₃]_{0.48}[OⁱPr]_{0.52}-HT (Table 1 entry 5) has both high surface area and large pore size which may be as a result of the low crystallinity as discussed above. Intercalated sulfonate ions decompose between 400 and 500 °C.¹⁶ The high decomposition temperature of the IL-HTs is as a result of the intercalated [P₆₆₆₁₄][C₈SO₃] which has a T_d of 398 °C. The solid structure of hydrotalcite may provide the extra stability of [P₆₆₆₁₄][C₈SO₃]-HT (Table 1 entry 2). All IL-HTs containing [OⁱPr]⁻ anions have been stabilised, decomposing above 390 °C. Isolated ionic liquids with the same composition decomposed between 300 and 360 °C.¹⁸ This may be due to protection of the basic ionic liquid which has been shown to occur in gel systems.²⁰

Table 1: BET surface area and pore size alongside decomposition temperature of intercalated ions.

Entry	Catalyst	Surface Area (m ² /g) ^a	Pore Size (Å) ^b	T _d -Intercalated (°C) ^c
1	Hydrotalcite	9.86	41.64	390
2	[P ₆₆₆₁₄][C ₈ SO ₃]-HT	9.79	32.84	402
3	[P ₆₆₆₁₄][C ₈ SO ₃] _{0.9} [O ⁱ Pr] _{0.1} -HT	9.64	73.22	400
4	[P ₆₆₆₁₄][C ₈ SO ₃] _{0.74} [O ⁱ Pr] _{0.26} -HT	9.56	72.44	393
5	[P ₆₆₆₁₄][C ₈ SO ₃] _{0.48} [O ⁱ Pr] _{0.52} -HT	10.57	71.08	400

^a) BET surface area. ^b) BJH adsorption average. ^c) Onset degradation temperature analysed by TGA.

The IL-HTs were applied to the Aldol condensation between benzaldehyde and acetophenone (Figure 5). The reaction was carried out at 140 °C for 1 hour without solvent. After this time the product was extracted into CDCl₃, combined with ethyl trifluoroacetate as an internal standard and a sample removed and analysed by ¹H NMR and ³¹P NMR. The remaining reaction mixture was filtered, the catalyst washed with MeOH, recovered and reused.

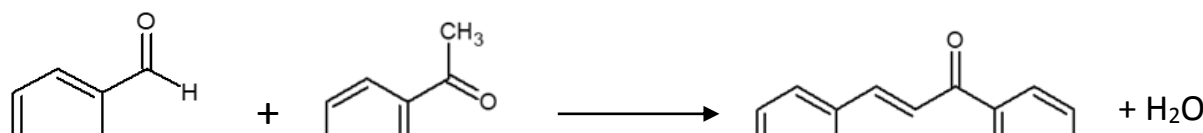


Figure 5: Aldol condensation between benzaldehyde and acetophenone.

Table 2: Catalyst and yield from Aldol condensation between benzaldehyde and acetophenone.

Entry	Catalyst	1 ST Run (±, SD)	Crude Yield ^a	
			2 ND Run	3 RD Run
1	None	0 (0)	NA	NA
2	Hydrotalcite	43 (8)	13	0
3	[P ₆₆₆₁₄][C ₈ SO ₃]-HT	36 (3)	7	0
4	[P ₆₆₆₁₄][C ₈ SO ₃] _{0.9} [O ⁱ Pr] _{0.1} -HT	55 (5)	13	0
5	[P ₆₆₆₁₄][C ₈ SO ₃] _{0.74} [O ⁱ Pr] _{0.26} -HT	75 (7)	29	0
6	[P ₆₆₆₁₄][C ₈ SO ₃] _{0.48} [O ⁱ Pr] _{0.52} -HT	46 (5)	15	0

Conditions: Benzaldehyde (0.037 g, 0.34 mmol), acetophenone (0.105 g, 0.87 mmol, 2.5 eq.), IL-HT (0.0037, 10 wt. % of benzaldehyde), (25 °C, stir rate 500 RPM and time 1 h). ^a) % Obtained from ¹H NMR against a known mass of ethyl trifluoroacetate.

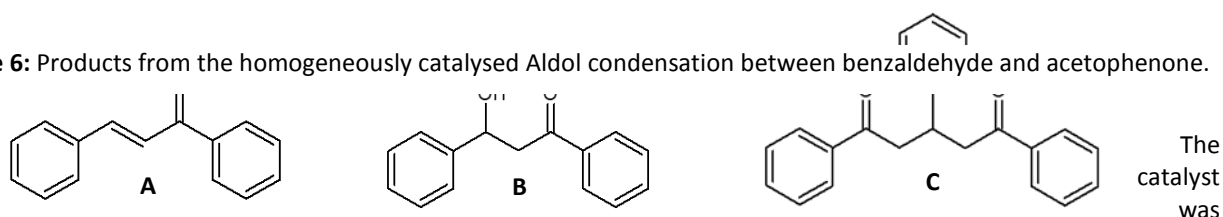
Upon moving from hydrotalcite to [P₆₆₆₁₄][C₈SO₃]-HT the yield decreases from 43 to 36 % (Table 2, entries 2 and 3). Despite the increased spacing between the layers the ionic liquid may be coating the basic site of hydrotalcite preventing them from catalysing the reaction. Moving to ILs with [OⁱPr]⁻ anion there is an increased yield compared to the sole [C₈SO₃]⁻ anion. The yield increases from 55 % for [P₆₆₆₁₄][C₈SO₃]_{0.9}[OⁱPr]_{0.1}-HT to 75 % for [P₆₆₆₁₄][C₈SO₃]_{0.74}[OⁱPr]_{0.26}-HT (Table 2 entries 4, 5). This is probably due to the higher proportion of basic anion more effectively catalysing the reaction. The yield decreases from 75 to 46 % moving from [P₆₆₆₁₄][C₈SO₃]_{0.74}[OⁱPr]_{0.26}-HT to [P₆₆₆₁₄][C₈SO₃]_{0.48}[OⁱPr]_{0.52}-HT (Table 2 entries 5, 6). The increased proportion of [OⁱPr]⁻ anion has not increased the yield. This may be due to the alteration of the hydrotalcite support. The XRD pattern (Figure 4) shows a similar basal spacing of the hydrotalcite layers but the crystallinity of [P₆₆₆₁₄][C₈SO₃]_{0.48}[OⁱPr]_{0.52}-HT is much reduced. This may prevent access of the substrates to the basic ionic liquid and therefore reduce the yield of the reaction. When standard deviation is taken into account hydrotalcite, (Table 2, entry 2) [P₆₆₆₁₄][C₈SO₃]_{0.9}[OⁱPr]_{0.1}-HT (Table 2, entry 4) and [P₆₆₆₁₄][C₈SO₃]_{0.48}[OⁱPr]_{0.52}-HT (Table 2, entry 6) may have similar values. However [P₆₆₆₁₄][C₈SO₃]_{0.74}[OⁱPr]_{0.26}-HT (Table 2, entry 5) is still the best performing

catalyst. The relatively large errors may be due to evaporation of reagents. The use of solvent or lower reaction temperatures may allow for more uniform results.

A similar reaction between benzaldehyde and 2-hydroxyacetophenone to produce chalcone and flavanone was catalysed by Zn-Al hydrotalcite supported ionic liquid.²¹ The catalyst was hydrotalcite which had 35 wt. % 1-(tri-ethoxy-silyl-propyl)-3-methylimidazolium chloride (TES-MimCl) grafted/impregnated onto it. The reaction was performed without solvent for 6 hours at 140 °C producing a total flavanone/chalcone yield of 99 %. The catalyst in the reaction is solely the hydrotalcite, the ionic liquid acts as a structural modifier only. The authors claim that the high IL loading change the structure of the catalyst to free up more Al³⁺ sites for catalysis. While this system produces higher a yield than the IL-HT systems of this study there is a longer reaction time, the OH group on the acetophenone makes it a more activated reagent and the IL loading is higher, 35 wt. % compared to 20 wt. %.

The previously reported homogeneous binary alkoxide ionic liquid produced three products from the Aldol condensation between benzaldehyde and acetophenone (Figure 6).²² The IL-HT system produces only the dehydrated ketone product **A**. The IL-HT catalyst must promote the dehydration step of the reaction to prevent formation of hydroxy ketone **B**. The Michael addition product **C** is bulky. The heterogeneous catalyst may restrict the size of the potential products which may prevent formation of the Michael product. The homogeneous system produced a total yield of 78 % at 25 °C, slightly higher than 75 % of the best performing IL-HT ([P₆₆₆₁₄][C₈SO₃]_{0.74}[OⁱPr]_{0.26}-HT, Table 2 entry 5) at 140 °C. However the homogeneous system produced a mixture of products which would need to be separated whereas the ketone product **A** was the only product from the IL-HT system.

Figure 6: Products from the homogeneously catalysed Aldol condensation between benzaldehyde and acetophenone.



recovered by filtration and retested. On the second run the activity of all catalysts dropped significantly and on the 3rd run no product was formed. Analysis of the ³¹P NMR of the reaction mixture did not show any peaks. This indicates that if leaching of the phosphonium ionic liquid occurred it is below the limits of detection, 50-70 µg/g in a 300 MHz NMR.²³ However the catalyst has become deactivated. The [OⁱPr]⁻ anion may not be regenerated and at the high reaction temperature may be lost as ⁱPrOH. The problem of catalyst reuse may be solved by using alternate conditions such as lower reaction temperature or by utilising a solvent.

Conclusions and Future work

A series of binary basic phosphonium ionic liquids have been successfully supported upon Mg-Al hydrotalcite. The ionic liquids alter both the basal spacing and crystallinity of the hydrotalcite as seen by XRD. Significantly, TGA analysis of the materials shows that the ionic liquids are more thermally stable when supported on hydrotalcite than the liquid equivalent.

The catalysts were successfully applied to the Aldol condensation between benzaldehyde and acetophenone, with the best performing catalyst providing a yield of 75 %, higher than unmodified hydrotalcite. The catalysts are able to be recovered by filtration after the reaction. Whilst ³¹P NMR does show that any ionic liquid leaching is below the level of detection the catalyst has become deactivated. Hot filtration tests²⁴ should be performed to confirm there is no leaching and alternate reaction conditions should be employed to determine whether the catalyst can be recycled.

Another reason to alter the reaction conditions such as time and solvent is to try to improve the consistency and yield of the reaction as the literature shows yields of up to 99 % are possible.²¹ If the catalysts can be successfully reused, further modifications of the catalyst will be performed. Hydrotalcites are known to support nanoparticles for hydrogenation,²⁵ transamination²⁶ and C-C bond coupling reactions²⁷ amongst others. Our group has recently published a hydrogen transfer system where a basic ionic liquid gel and homogeneous catalyst acted in tandem but could not be combined in one material.²⁸ The IL-HT materials could be modified with catalyst or nanoparticles in order to contain all catalytic materials for this reaction in one material, stabilising both the base and catalyst.

References

- ¹ S. T. Handy, *Curr. Org. Chem.*, 2005, **9**, 959-988.
- ² R. A. Olofson, W. R. Thompson, J. S. Michelman, *J. Am. Chem. Soc.*, 1964, **86**, 1865-1866.
- ³ V. K. Aggarwal, I. Emme, A. Mereu, *Chem. Commun.*, 2002, 1612-1613.
- ⁴ A. C. Cole, J. L. Jensen, I. Ntai, K. Loan, T. Tran, J. K. Weaver, D. C. Forbes, J. H. J. Davis, *J. Am. Chem. Soc.*, 2002, **124**, 5962-5963.
- ⁵ J.-M. Xu, Q. Wu, Q.-Y. Zhang, F. Zhang, X.-F. Lin, *Eur. J. Org. Chem.*, 2007, 1798-1802.
- ⁶ H. Luo, Z. Zhai, W. Fan, W. Cui, G. Nan, Z. Li, *Ind. Eng. Chem. Res.*, 2015, **54**, 4923-4928.
- ⁷ Y. Liu, Y. Huang, P.-O. Boamah, L. Cao, Q. Zhang, Z. Lu, H. Li, *J. Appl. Polym. Sci.*, 2015, **132**, 41727.
- ⁸ A. Cieniecka-Rostiewicz, K. Kita, A. Fojutowski, J. Nawrot, K. Materna, J. Pernak, *Chem. Eur. J.*, 2008, **14**, 9305-9311.
- ⁹ H. Peng, Y. Zhou, J. Liu, H. Zhang, C. Xia, X. Zhou, *RSC Adv.*, 2013, **3**, 6859-6864.
- ¹⁰ D. R. MacFarlane, S. A. Forsyth, J. Golding, G. B. Deacon, *Green Chem.*, 2002, **4**, 444-448.
- ¹¹ W. T. Reichle, *Solid State Ionics*, 1986, **22**, 135-141.
- ¹² S. Nagasaki, M. Halma, A. Bail, G. G. C. Arízaga, F. Wypych, *Colloid Interface. Sci.*, 2005, **281**, 417-423.
- ¹³ S. O'Leary, D. O'Hare, G. Seeley, *Chem. Commun.*, 2002, **0**, 1506-1507.
- ¹⁴ Y. Wang, W. Yang, J. Yang, *Electrochem. Solid-State Lett.*, 2007, **10**, A233-A236.
- ¹⁵ Q. Wang, D. O'Hare, *Chem Rev.*, 2012, **112**, 4124-4155.
- ¹⁶ S. Livi, V. Bugatti, L. Estevez, J. Duchet-Rumeau, E. P. Giannelis, *J. Colloid Interface Sci.*, 2012, **388**, 123-129.
- ¹⁷ B. Zhao, C. Li, C. Xu, *Catal. Sci. Technol.*, 2012, **2**, 1985-1994.
- ¹⁸ P. McNeice, *Base Stable and Basic Ionic Liquids*, QUILL Quarterly Report December-March 2018, Unpublished, March 2018.
- ¹⁹ S. Kannan, A. Narayanan, C. S. Swamy, *J. Mater. Sci.*, 1996, **31**, 2353-2360.
- ²⁰ K. M. Bothwell, P. C. Marr, *ACS Sustainable Chem. Eng.*, 2017, **5**, 1260-1263.
- ²¹ L. B. Kunde, S. M. Gade, V. S. Kalvani, S. P. Gupte, *Catal. Commun.*, 2009, **10**, 1881-1888.
- ²² P. McNeice, *Base Stable and Basic Ionic Liquids*, QUILL Quarterly Report August-October 2018, Unpublished, November 2018.
- ²³ W. R. Creasy, D. J. McGarvey, J. S. Rice, R. O'Connor, H. D. Durst, *Study Of Detection Limits And Quantitation Accuracy Using 300 Mhz NMR*, EAI Corporation, Abingdon MD, 2003.
- ²⁴ J. E. Hamilton, K. Hirai, A. Millan, P. M. Maitlis, *J. Mol. Catal.*, 1980, **7**, 543-544.
- ²⁵ Á Mastalir, Z. Kirá, *J. Catal.*, 2003, **2**, 372-381.
- ²⁶ D. Ainembabazi, N. An, J. C. Manayil, K. Wilson, A. F. Lee, A. M. Voutchkova-Kostal, *ACS Catal.*, 2019, **9**, 1055-1065.
- ²⁷ M. L. Kantam, S. Roy, M. Roy, B. Sreedhar, B. M. Choudary, R. L. De, *J. Mol. Catal. A: Chem.*, 2007, **273**, 26-31.
- ²⁸ K. M. Bothwell, F. Lorenzini, E. Mathers, P. C. Marr, A. C. Marr, *ACS Sustainable Chem. Eng.*, 2019, **7**, 2686-2690.



QUILL Quarterly Report

November 2018 – January 2019

Name:	Keith Moore		
Supervisor(s):	Gosia Swadźba-Kwaśny		
Position:	Research Assistant (Grants)		
Start date:	July 2018	Anticipated end date:	Feb 2019
Funding body:	QUILL		

Grant Writing

Objective of this work

To assist with the preparation of grant applications within QUILL. Supplementary role in managing the QUILL webpages.

Progress to date

Assisted with the resubmission of a MSCA Horizon2020 ITN application for a doctoral training program involving 5 QUILL academics and a range of close academic partners in the ionic liquids field across Europe. We are hopeful for success in the upcoming review of submissions.

Additional work has been put into the completion of an EPSRC application on new battery electrolyte production, which should be ready for submission shortly.

Maintenance of the QUILL website has continued, including the formation of a secure access section for members of the IAB. This provides a consistent route for obtaining key QUILL documentation as well as a selection of recently published QUILL academic papers.

Conclusions and future work

Continued grant applications will proceed, with upcoming submissions expected for the ISCF Faraday Battery Challenge and several calls from the Horizon2020 program concerning energy storage materials (both metal ion and redox flow). I am also coordinating a workshop at the upcoming March QUILL meeting to engage both academic and industrial parties to make ambitious collaborative bids for funding.



QUILL Quarterly Report

November 2018 – January 2019

Name:	Gareth Nelson		
Supervisor(s):	Dr John Holbrey, Dr Małgorzata Swadźba-Kwaśny		
Position:	PhD student		
Start date:	13/09/16	Anticipated end date:	13/09/19
Funding body:	DEL		

Ionic Liquid Catalysts for the Glycolysis of PET

Background

There are 4 broad types of PET recycling, primary recycling is pre-consumer scrap recycling. Secondary recycling is physical recycling, this approach first grinds the PET, then melts it before reforming it. The heat and force exerted in this process degrades the polymer leaving it unsuitable for many uses. Tertiary recycling is chemical recycling, the PET is recycled through chemical action, generally through depolymerisation of PET into constituent monomers. These monomers are re-polymerised to regenerate virgin PET. Quaternary recycling is the recovery of energy from the material, this is usually through incineration. This project focuses on chemical recycling of PET as it gives high quality polymers as a product. There are several methods for the depolymerisation of PET, these methods attack the ester linkage to break down the polymer. The focus of this project is glycolysis; this occurs through a transesterification reaction between PET and ethylene glycol (EG), commonly catalysed by a metal acetate, carbonate or sulfate. This reaction is attractive because the product, bis(2-hydroxyethyl)terephthalate (BHET), requires no additional processing before being converted to PET thus is easy to incorporate into PET production. Work utilising ionic liquids as a catalysts was investigated by H, Wang et al.^{1,2} Initially their work utilised imidazolium halide and several acidic ionic liquids, poor yields were achieved but this showed a new approach to the glycolysis reaction.² Q, Wang also utilised ionic liquids as catalysts, previously H, Wang had performed this reaction using [bmim][FeCl₄], the logical extension of this was to test other transition metal salt containing ionic liquids.^{3,4} Q, Wang found that while [bmim][FeCl₄] was effective, [bmim]₂[ZnCl₄] and [bmim]₂[CoCl₄] were more effective, achieving similar conversion of PET (almost 100%) but greater yields of BHET with an increase of almost 20% over [bmim][FeCl₄] for both ionic liquids. Work in literature had previously used acetate ionic liquids, however the results reported were lower and required higher temperatures and more catalyst than those reported by H, Wang using halometallate ionic liquids.⁵

1. H. Wang, Y. Lui, Z. Li, X. Zhang, S. Zhang, and Y. Zhang, **Eur. Polym. J.**, 2009, **45**, 1535–1544
2. H. Wang, Z. Li, Y. Liu, X. Zhang, and S. Zhang, *Green Chem.*, 2009, **11**, 1568-1575.
3. H. Wang, R. Yan, Z. Li, X. Zhang, and S. Zhang, *Catal. Commun.*, 2010, **11**, 763–767.
4. Q. Wang, Y. Geng, X. Lu, and S. Zhang, *ACS Sustain. Chem. Eng.* 2015, **3**, 340–348
5. A.M. Al-Sabagh, F.Z. Yehia, A.M.M.F. Eissa, M.E. Moustafa, G. Eshaq, A.R.M. Rabie, and A.E. El-Metwally *Ind. Eng. Chem. Res.*, 2014, **53**, 18443–18451

Objective of this work

The objective of this work is the production of bis(2-hydroxyethyl)terephthalate (BHET), a monomeric intermediate in PET production, from the glycolysis of waste PET. To achieve this, the applications of novel ionic liquids as catalysts for the glycolysis of PET in particular halometallate ionic liquids and acetate containing ionic liquids.

Progress to date

It was previously reported that after testing a range of ionic liquids the yields were found to be tremendously under reasonable expectations based on the degree of conversion. A new calibration curve was made and the experiments were repeated and analysed by HPLC.

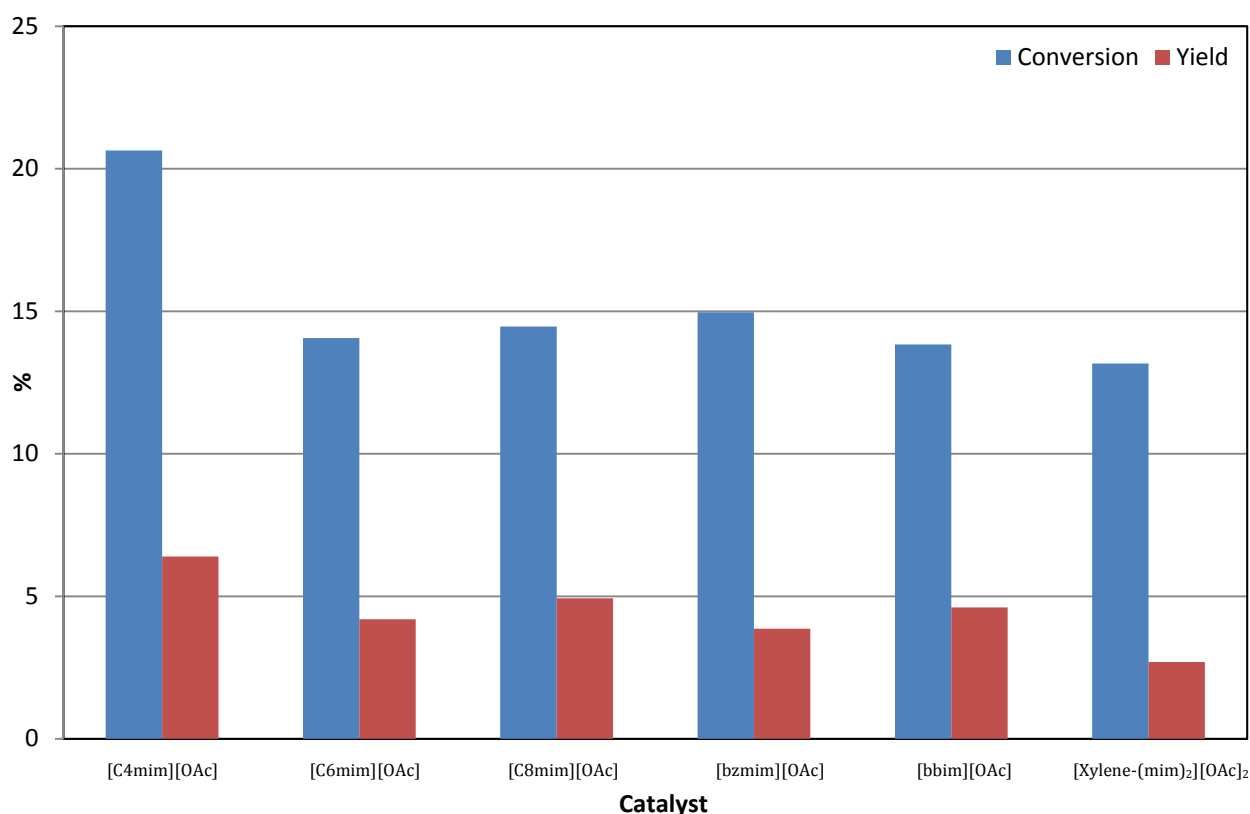


Fig. 1 Graph to compare conversion and yield for ionic liquid catalysts in the glycolysis of PET, reaction time 3 hours, temperature 180 °C, 0.01 mol catalyst (0.005 mol for [Xylene-(mim)₂][OAc]₂), 2 g PET and 20 g ethylene glycol.

The corrected results are better, however the yield is lower than previous experiments, this is likely due to large inaccuracies in measuring the reaction temperature of the previous reactions. This has impacted both the conversion and the yield, but to different extents. The reduction in the conversion shows the general reduction in reaction speed, as expected of a temperature decrease. However the reduction in yield shows that the decrease has had a far larger impact than the conversion would suggest. BHET yield is far reduced because there are far more dimers and trimers left in these reactions than previously. To counter this the temperature could be increased or an increase in the reaction time would suffice.

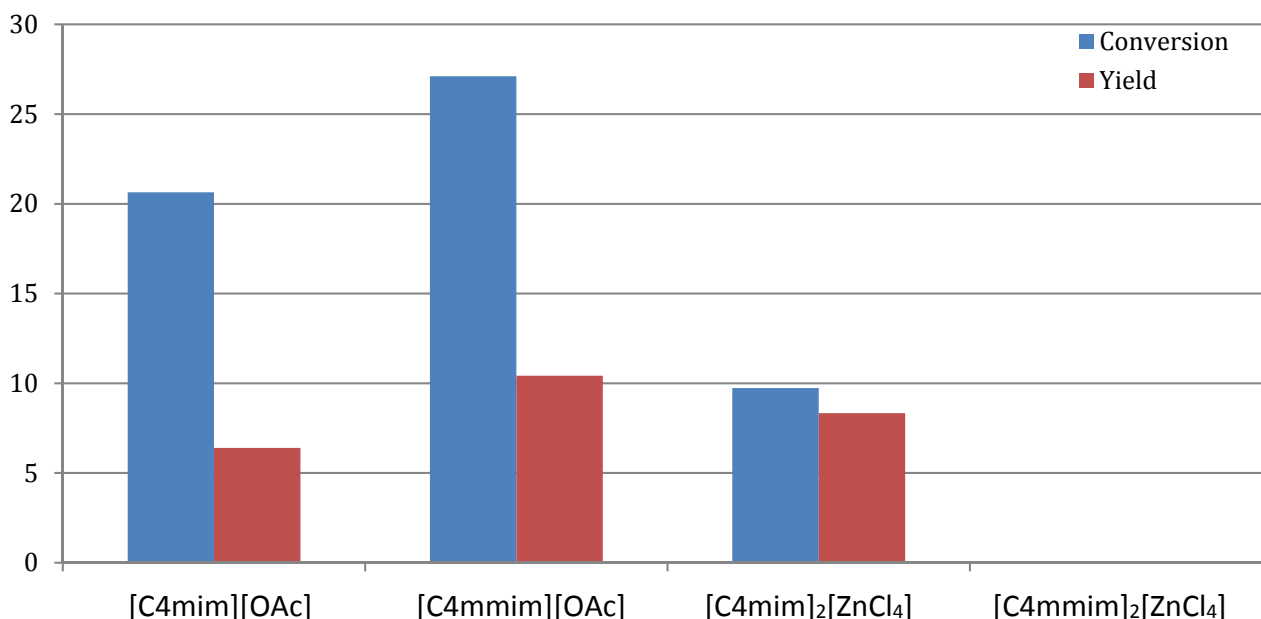


Fig. 2 Graph to compare conversion and yield for ionic liquid catalysts in the glycolysis of PET, reaction time 3 hours, temperature 180 °C, 0.01 mol catalyst, 2 g PET and 20 g ethylene glycol.

The impact of C2 methylation was investigated. The difference between the [C4mim][OAc] and [C4mmim][OAc] while noticeable is not extremely concerning as it is a consistent difference and overall not too far outside of expected experimental error, the difference could simply be improved solubility. However when the chlorozincate ionic liquids are considered the difference is much more obvious. The presence of the acetate ion is the driving force for the acetate ionic liquids catalytic ability, however the chlorozincate ionic liquids require a proton in the C2 position. The ionic liquid [C4mim]₂[ZnCl₄] has similar catalytic activity as both the acetate ionic liquids however it is clearly much more selective towards the BHET monomer.

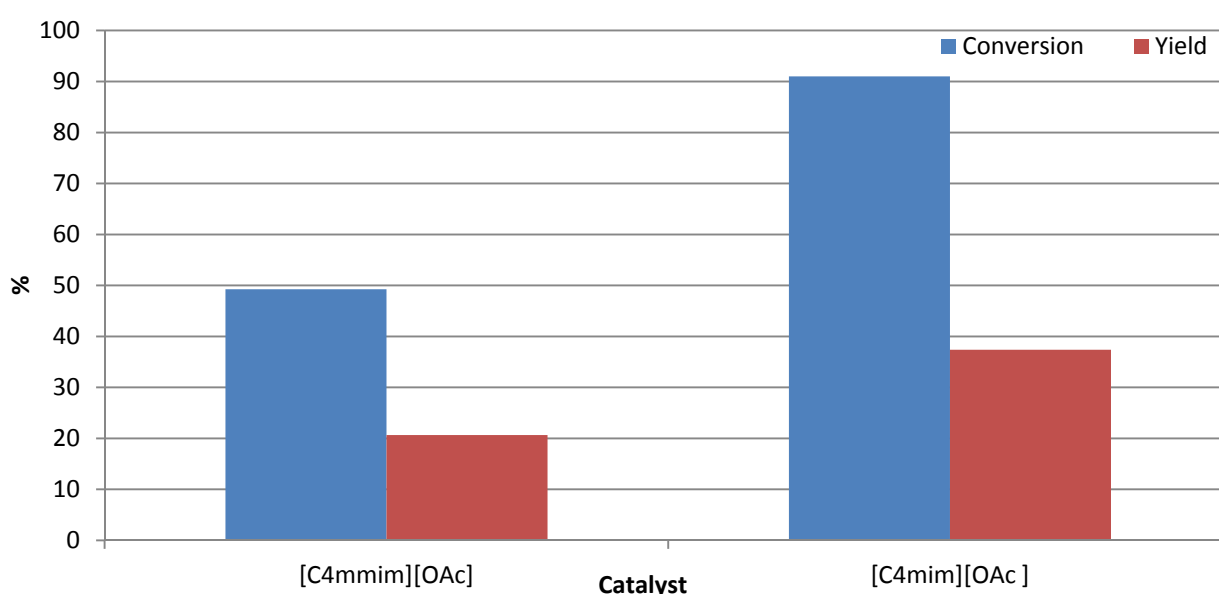


Fig. 3 Graph to compare conversion and yield for ionic liquid catalysts in the glycolysis of PET, reaction time 3 hours, temperature 190 °C, 0.01 mol catalyst, 2 g PET and 20 g ethylene glycol.

When the temperature is increased to 190 °C the catalytic activity of [C4mim][OAc] is seen to increase beyond that of [C4mmim][OAc]. This could potentially be due to a change in mechanism for [C4mim][OAc], from being acetate driven to the acetate abstracting the C2 proton to form an in situ carbene. This would explain why there was no marked increase for [C4mmim][OAc] above what would be seen from just increasing the reaction temperature.

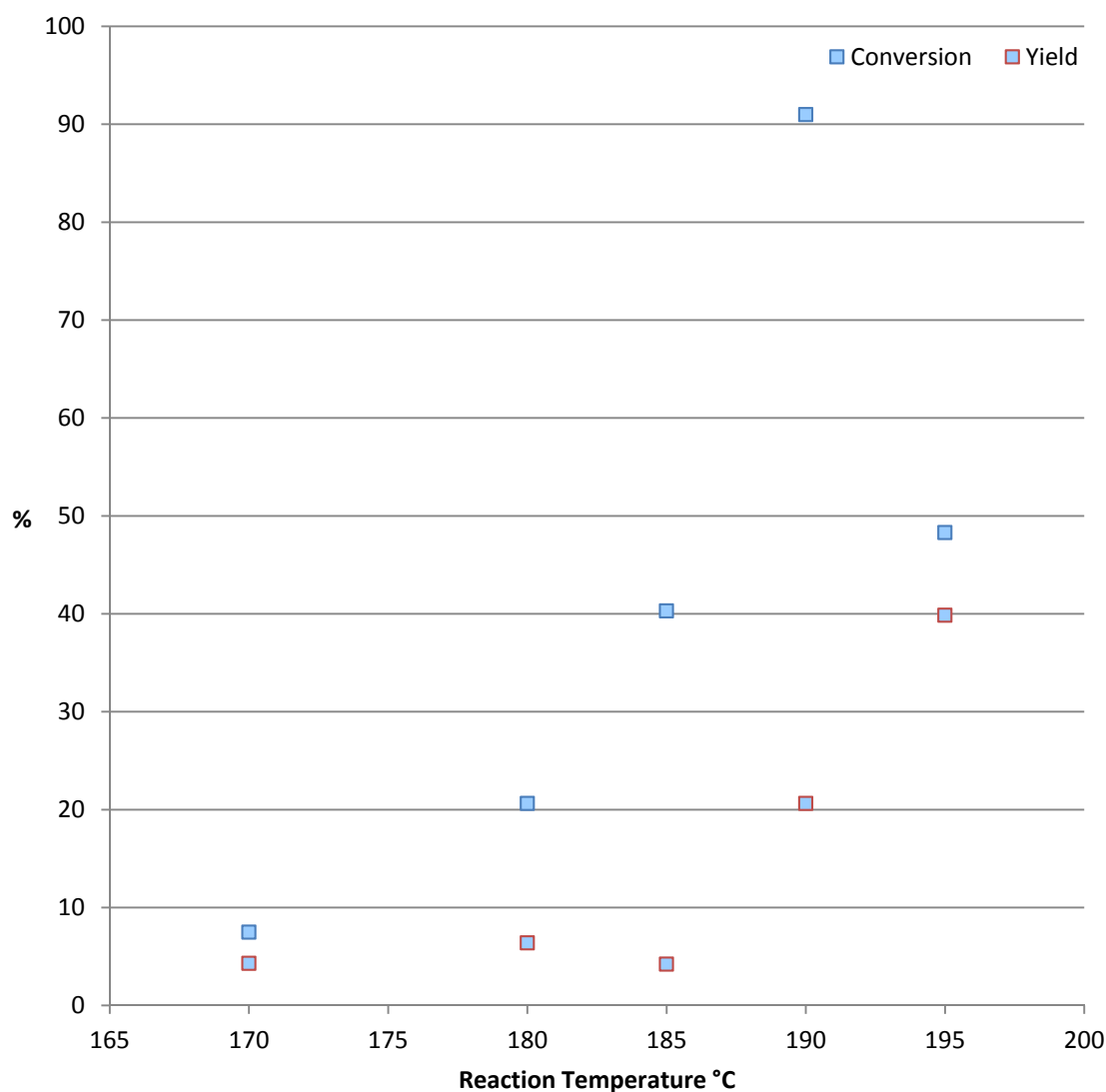


Fig. 4 Graph to compare conversion and yield for [bmim][OAc] as a catalyst in the glycolysis of PET, reaction time 3 hours, 0.01 mol [bmim][OAc], 2 g PET and 20 g ethylene glycol.

A set of experiments were performed in which [bmim][OAc] was used as a catalyst while the temperature was varied. From this it can be seen that increasing the temperature correlates to an increase in conversion. The conversion increases in an almost exponential manner, however the 195 °C result is much lower than the result at 190 °C and would be more suggestive of a linear relationship. There are several results that appear egregious when compared to the other results as well as changes in the selectivity, as such 185 °C, 190 °C, and 195 °C have been repeated and are currently awaiting analysis by HPLC, this has been held up by numerous mechanical issues with the HPLC, as well as the machine being required by multiple research groups who needed different columns.



Following the work at ISIS a series of experiments using choline phosphate as a catalyst were performed. The method of production of the choline phosphate was varied, the use of choline chloride and phosphoric acid to form choline phosphate resulted in an inactive catalyst. The use of choline carbonate and phosphoric acid to form choline phosphate has shown some potential, however this requires HPLC and I am currently awaiting CHNS results.

Conclusions and future work

To conclude, the difference in catalytic activity between [C4mim][OAc] and [C4mmim][OAc] with increasing temperature is very interesting as it gives insight into the potential reaction mechanism. The difference in activity between choline phosphate produced by different methods requires additional investigation to better understand the purity of the catalyst as well as what is present that facilitates the reaction. The production of 4,5-dichloroimidazole ionic liquids suffered multiple setbacks due to the initial synthesis of 4,5-dichloroimidazole and when synthesised the 4,5-dichloroimidazole was highly impure. Pure 4,5-dichloroimidazole has been obtained in a limited quantity, with more to be ordered, as such the production of 4,5-dichloroimidazole ionic liquids has resumed with testing to begin soon.



QUILL Quarterly Report

November 2018 – January 2019

Name:	Helene Raabjerg		
Supervisor(s):	Nimal Gunaratne		
Position:	Chemical Research Apprentice		
Start date:	01.11.2018	Anticipated end date:	31.08.2019
Funding body:			

Reactive ionic liquid esters for perfume release in neutral water

Background

This is a continuation of the work of Nimal Gunaratne (<https://daro.qub.ac.uk/quill-perfume>)

Normal carboxylic esters cannot be hydrolysed in neutral water without any aid such as an enzyme. These are generally hydrolysed, swiftly, in basic water where strongly nucleophilic HO^- plays a mediator role. Strong aqueous acids are also capable of their effective hydrolysis. We explore here the possibility of activating esters with aid of ionic liquid chemistry, having the ester group integrated into the cation. The purpose of this project is to activate the ester to such an extent that it is hydrolysed by weakly nucleophilic neutral water thereby avoiding the use of undesirable strong acids and bases. We will try to hydrolyse ionic liquid ester in water, which is activated because of the positive charge in the cation. If this hypothesis is realised, Ionic liquid esters tagged with perfume alcohols can be utilised as pro-fragrances for slow release of perfumes in water. The results obtained in a model study that was carried out with 'methyl ester' ionic liquids are presented below.

Progress to date

We have made a model study to prove that we can hydrolyse ionic liquid esters in neutral water. Three model compounds that were synthesised for this project is shown in figure 1.

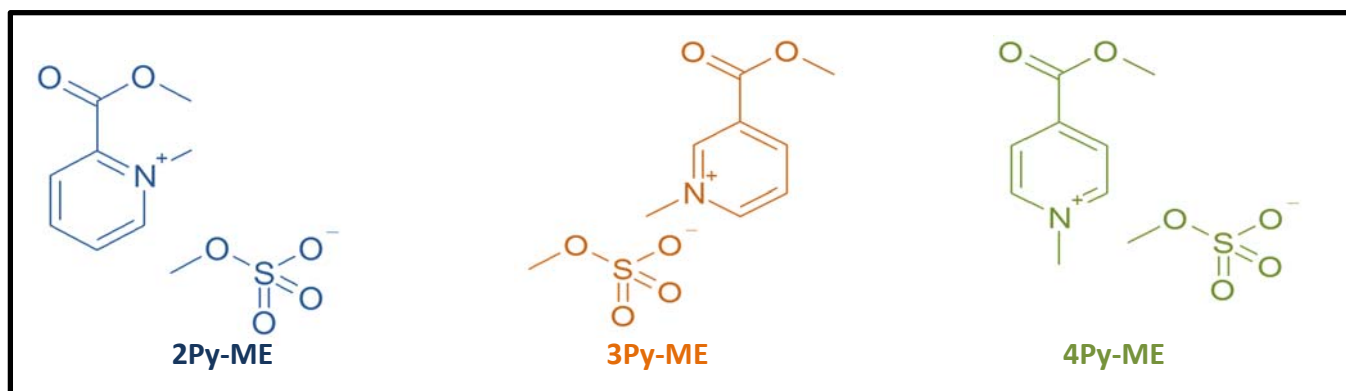


Figure 1: Our three methyl ester ionic liquids. They are named after the position of the ester group with respect to quaternary nitrogen atom in the pyridine. So with methyl picolinate, the positive charge is in the second position and therefore we get the name 2Py-ME which means 2-pyridine-methyl ester and the same system is used to name the two other compounds.

To assess their reactivity towards water, we ran kinetic runs, heating these compounds in D₂O solutions (identical concentrations) at 80°C in NMR tubes. These reactions were monitored by running NMRs at different time intervals to observe the release of product, in these cases methanol.

In Figure 2, the case for the kinetic profile for hydrolysis of 2PyME in neutral D₂O is presented. The complete hydrolysis of the 2PyME occurred in approximately in 250 hours.

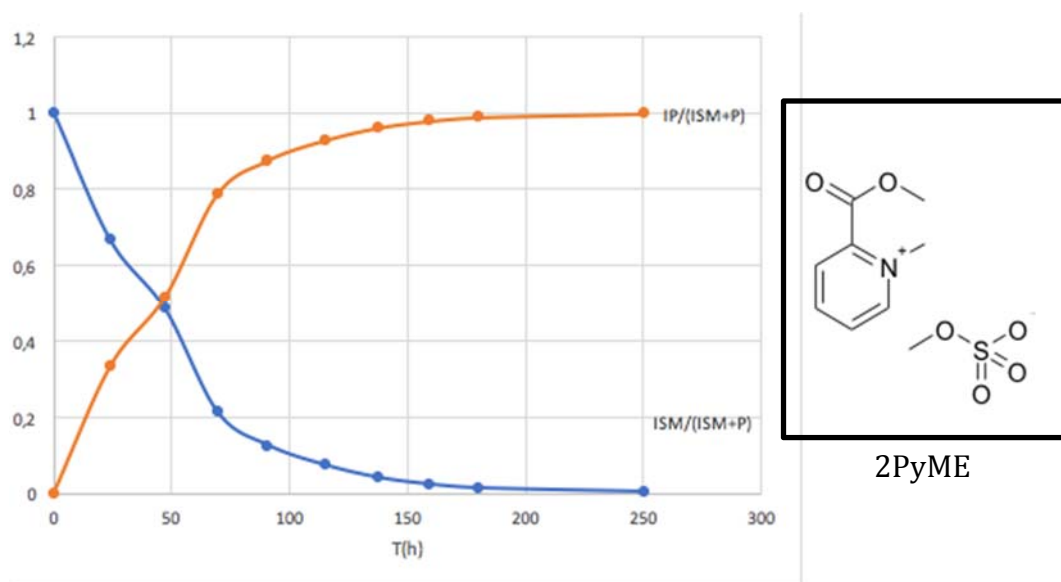


Figure 2: The Kinetic profile of hydrolysis of 2PyME in neutral water, at 80°C. The reaction was monitored by ¹H NMR spectroscopy.

The orange graph represents product (P) formation where integrals for product and starting material (SM) were used to compute $P/SM+P$ plotted against time. and the blue graph shows $SM/SM+P$ NB: $P/SM+P = \text{Product}/(\text{Starting Material} + \text{Product})$ and $SM/SM+P = \text{Starting Material}/(\text{Starting Material} + \text{Product})$

A similar study was carried out on for 3PyME and the results are shown in figure 3 below. This clearly indicates the hydrolysis was considerably slower than the case for 2PyME.

This is expected due to electronic effects operating from the positive charge on the nitrogen atom being unable to relay closer to the ester group. Whereas in 2PyME the positive charge can be relayed closer to the ester group.

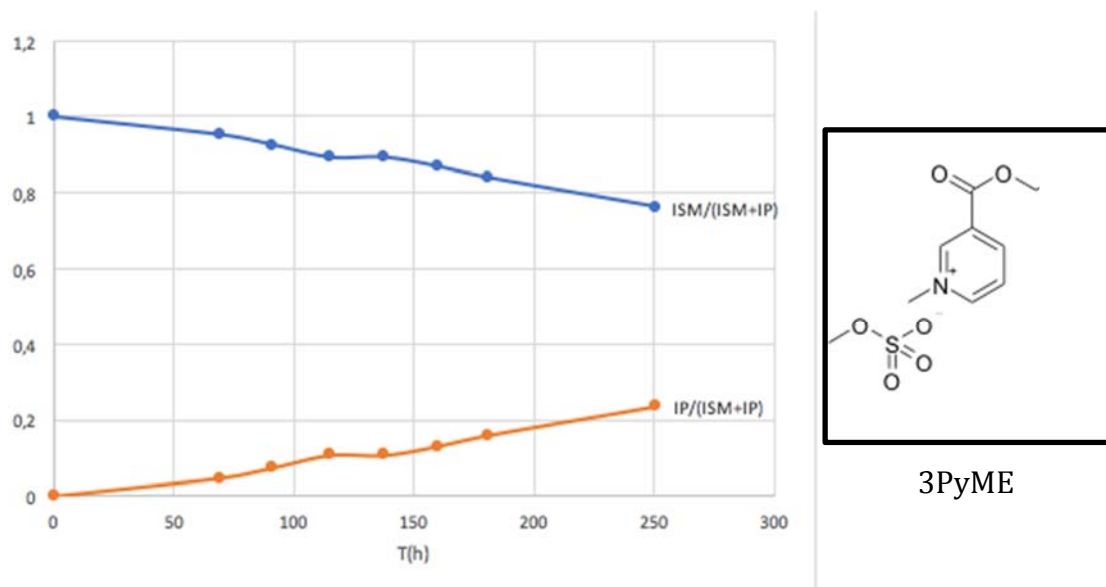


Figure 3: As with figure 3 this figure shows the hydrolysis of 3PyME in neutral water at 80°C

The reaction was monitored by ^1H NMR spectroscopy.

NB: $P/SM+P = \text{Product}/(\text{Starting Material} + \text{Product})$ and $SM/SM+P = \text{Starting Material}/(\text{Starting Material} + \text{Product})$

As expected 4PyME hydrolysed at a reasonable rate, albeit little slower than the case of 2PyME. Nevertheless, the rate was much higher than that of the case of 3PyME.

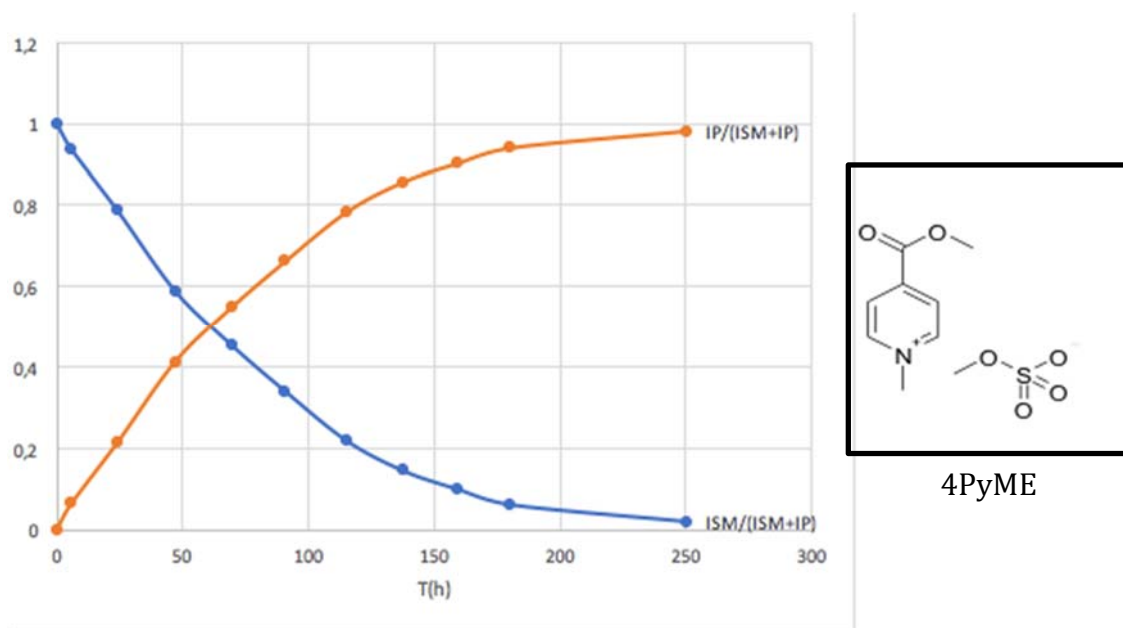


Figure 4: In this figure the kinetic profile of 4PyME is represented by a graph like in figure 2-3.

NB: $P/SM+P = \text{Product}/(\text{Starting Material} + \text{Product})$ and $SM/SM+P = \text{Starting Material}/(\text{Starting Material} + \text{Product})$

For direct comparison, kinetic profiles for hydrolysis of all three cases, 2PyME, 3PyME and 4PyME, in neutral D₂O is depicted in figure 5 below.

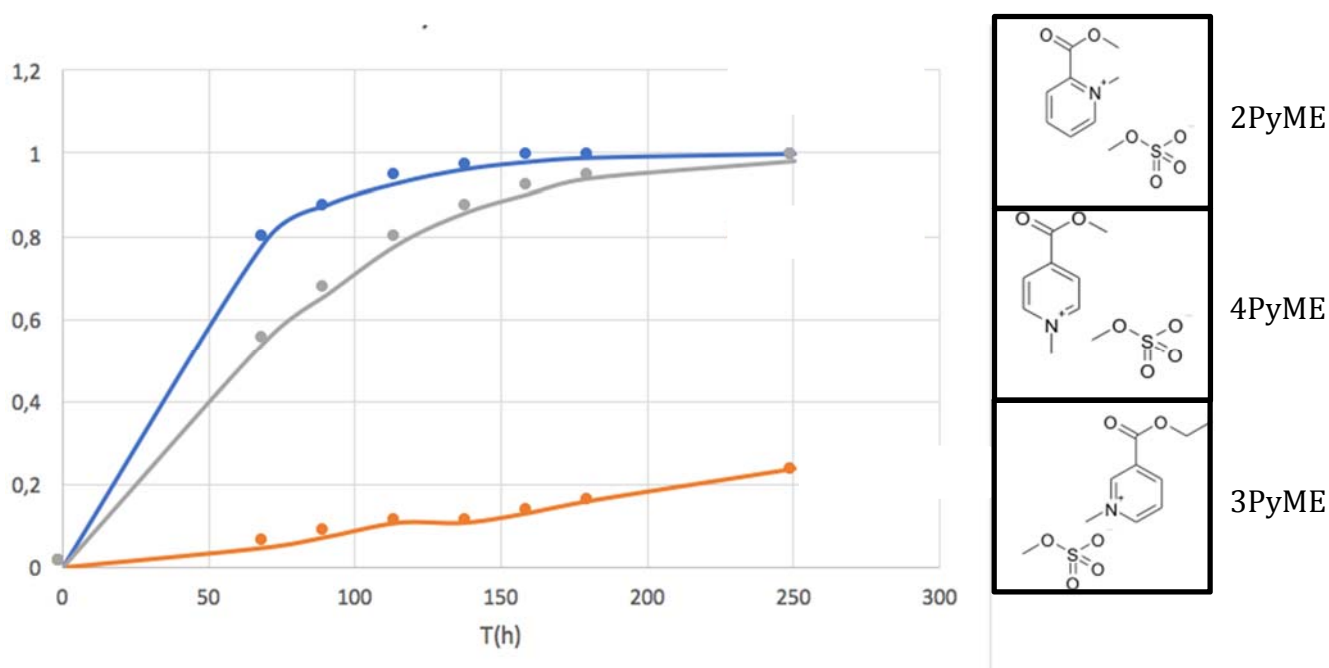


Figure 5: Here in the graph you can see the comparison of the three compounds 2PyME (blue line), 3PyME (orange line) and 4PyE (grey line) and that the position of the N makes a difference in how fast the product is released.

The unquarternised esters were difficult to hydrolyse in neutral water due to the lack of positive charge on the nitrogen atom leading to no activation originating from it.

We have clearly demonstrated here with the correct choice of pyridinium ester the hydrolysis kinetics can be controlled.

We were able to produce three pyridinium salts with a perfume alcohol tagged, as shown in figure 6 below.

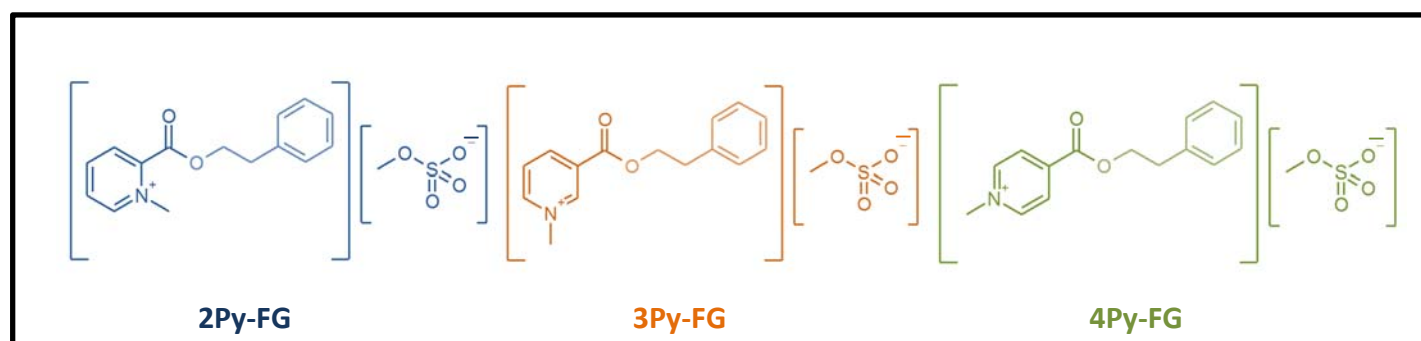


Figure 6: Our three esters tagged with perfume alcohol 2-phenylethanol. They are named after the position of the positive charge in the pyridine.

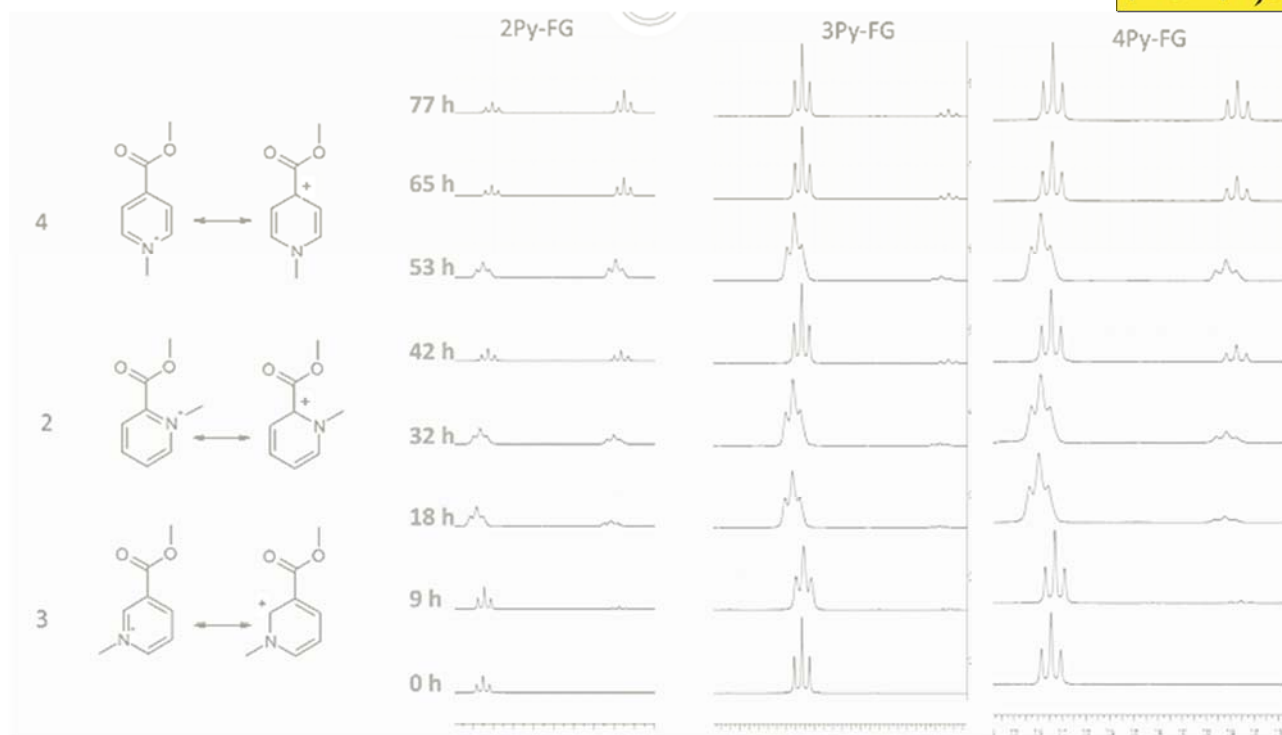


Figure 7: Preliminary results on the hydrolysis of perfume tagged ionic liquid esters at 80°C in neutral water.

2Py-FG, which has the ester group at the two-position in respect to nitrogen is the one which reacts the fastest. 4Py-FG reacts relatively fast with water, but it is a little slower than the case with 2Py-FG, but 2Py-FG has gone 50% of the way at 53h and in comparison, the case of 4PyME has only gone approximately 30% at 77h.

On the left hand side in figure 7 it shows how the positive charge on the nitrogen atom can be relayed towards the ester group. In the cases of 2Py-FG and 4Py-FG the positive charge is relayed closest to the ester group whereas in the case of 3Py-FG the positive charge cannot be relayed as close to the ester group due to well established electronic effects.

Conclusions and future work

The reaction monitoring process is still ongoing. Similar compounds will be made with other perfume alcohols and kinetic study will be undertaken. We also hope to use binary and ternary ester ionic liquid systems for multiple perfume delivery. We also plan to run further analysis including TGA, MS and possibly FTIR among other analysis.